



ALMA MATER STUDIORUM
UNIVERSITÀ DI BOLOGNA

**DOTTORATO DI RICERCA IN
CHIMICA**

Ciclo XXXVI

Settore Concorsuale: 03/A1 – CHIMICA ANALITICA

Settore Scientifico Disciplinare: CHIM/01 – CHIMICA ANALITICA

**CHEMILUMINESCENCE – BASED BIOANALYTICAL DEVICES FOR
ASTROBIOLOGICAL, FOOD SAFETY AND CLINICAL APPLICATIONS**

Presentata da: Ilaria Trozzi

Coordinatore Dottorato:

Prof. Luca Prodi

Supervisore:

Prof.ssa Mara Mirasoli

Co – supervisori:

Prof.ssa Martina Zangheri

Dott. Donato Calabria

CONTENTS

1. INTRODUCTION TO BIOSENSORS.....	1
1.1 Enzymes in biosensors.....	5
1.1.1 An outline of enzyme kinetics.....	5
1.1.2 Enzyme based biosensors.....	8
1.2 Immunosensors.....	11
1.2.1 Labelled – biosensors	13
1.2.2 Label – free biosensors	15
1.3 Paper and hydrogel: ideal materials for bioassays	16
1.3.1 Paper in biosensing.....	16
1.3.2 Hydrogels in biosensing.....	18
1.4 Chemical Luminescence System	20
References.....	24
2. PROPOSAL FOR THE THESIS.....	38
3. PAPER – BASED IMMUNOSENSORS WITH BIO- CHEMILUMINESCENCE DETECTION.....	40
3.1 Introduction.....	41
3.2 Nanomaterials for signal enhancement of chemiluminescence	45
3.3 Fluid control and fluid handling	50
3.4 Progress in reagents storage and self – contained devices for POC application	53
3.5 Light detection technologies integrated with CL paper – based immunoassay devices.....	56
3.6 Conclusions.....	61
Funding.....	62

References.....	63
-----------------	----

4. ASTROBIO – CUBESAT: A LAB – IN – SPACE FOR CHEMILUMINESCENCE – EXPERIMENTS..... 76

4.1 Introduction.....	77
-----------------------	----

4.2 Materials and methods	80
---------------------------------	----

4.2.1 Chemicals.....	80
----------------------	----

4.2.2 Fabrication of the origami device	80
---	----

4.2.3 Optimization of the experimental conditions	82
---	----

4.2.4 Mission scenario and protocol of experiments	82
--	----

4.3 Results and discussion	84
----------------------------------	----

4.3.1 Rationale of experiment design.....	84
---	----

4.3.2 The AstroBio CubeSat and the subsystems for bioanalytical experiments	86
---	----

4.3.2.1 Bioanalytical payload requirements and implementation solutions	86
---	----

4.3.2.2 ABCS subsystems for bioanalytical experiments.....	87
--	----

4.3.3 Optimization of origami μ PAD and experimental protocols	90
--	----

4.3.4 Stability requirements and testing.....	94
---	----

4.3.5 Test experiments performed on the ground model of ABCS.....	96
---	----

4.4 Conclusions.....	98
----------------------	----

Acknowledgements	98
------------------------	----

References.....	99
-----------------	----

5. AN ORIGAMI PAPER – BASED BIOSENSOR FOR ALLERGEN DETECTION BY CHEMILUMINESCENCE IMMUNOASSAY ON MAGNETIC MICROBEADS 105

5.1 Introduction.....	106
-----------------------	-----

5.2 Materials and methods	109
---------------------------------	-----

5.2.1 Chemicals.....	109
----------------------	-----

5.2.2 Fabrication of the origami μ PAD device	110
---	-----

5.2.3 Assay procedure	111
-----------------------------	-----

5.2.4 Data elaboration and statistics	113
---	-----

5.2.5 Real sample processing	113
------------------------------------	-----

5.2.6 In silico simulations.....	114
----------------------------------	-----

5.3 Results	114
5.3.1 Synthesis of OVA – MBs	114
5.3.2 Design of the origami μ PAD	116
5.3.3 Optimization of the origami μ PAD and assay procedure	119
5.3.4 Measurement of OVA with the origami μ PAD.....	121
5.3.5 Assay specificity	123
5.3.6 Accuracy and quantification of Ovalbumin in real samples.....	126
5.3.7 Stability of the origami μ PAD.....	128
5.4 Conclusions	129
Supplementary materials	129
Funding	129
References	130
6. SMARTPHONE – BASED CHEMILUMINESCENCE GLUCOSE BIOSENSOR EMPLOYING A PEROXIDASE – MIMICKING, GUANOSINE – BASED SELF – ASSEMBLED HYDROGEL	139
6.1 Introduction	140
6.2 Materials and methods	143
6.2.1 Reagents	143
6.2.2 Preparation of the Guanosine/Hemin CL hydrogel.....	144
6.2.3 Measurement of H ₂ O ₂ and glucose in the microtiter plate format.....	144
6.2.4 Smartphone – based CL detection with 3D printed device	145
6.2.5 Real sample analysis.....	146
6.2.6 Data analysis	146
6.3 Results and discussion	146
6.3.1 Design of the G-quadruplex hydrogel – based biosensor	146
6.3.2 G-quadruplex hydrogel performance for H ₂ O ₂ quantitative detection	147
6.3.3 G-quadruplex hydrogel performance for glucose quantitative detection	150
6.3.4 Smartphone – based glucose biosensing device	150
6.3.5 Assay selectivity.....	154
6.3.6 Application to real samples.....	154
6.3.7 Stability of the glucose biosensor	155
6.3.8 Hydrogel 3D printing.....	156
6.4 Conclusions	157

Funding.....158

References.....159

7. CONCLUSIONS AND FUTURE PERSPECTIVES..... 167

References.....169

ABSTRACT

At the intersection of biology, chemistry, and engineering, biosensors are a multidisciplinary innovation that provide a cost-effective alternative to traditional laboratory techniques. They have transformed various fields by incorporating innovative materials, transducing devices, and immobilization techniques. Their simplicity, accuracy, and portability make them accessible to non-experts and allow them to be used on-site, eliminating the problems of sample transport and storage. Due to their versatility and advantages, biosensors are used in medical diagnostics, environmental monitoring, food safety, wearable technology and in the industrial and pharmaceutical sectors.

The first part of this thesis is concerned with learning the state of the art of paper-based immunosensors with bioluminescent (BL) and chemiluminescent (CL) detection. The use of biospecific assays combined with (CL) detection and paper-based technology offers an optimal approach to creating portable analytical tools for on-site applications, but the translation of scientific advances into everyday use of such devices is lagging behind. Therefore, we have focused on the specific areas that are responsible for this disparity and need to be considered more in order to ensure a future practical implementation of these methods in routine analyses.

The subsequent part of this thesis addresses the development of a fully autonomous lab – on – chip platform for performing chemiluminescent – based bioassays in space environment, exploiting a CubeSat platform for astrobiological investigations. An origami-inspired microfluidic paper-based analytical device (μ PAD) has been developed to preload all reagents in a dry form onto the paper substrate, simplifying both device construction and analytical processes. The primary purpose of this device is twofold: first, to assess its performance in space by integrating it into the AstroBio CubeSat (ABCS) nanosatellite, and second, to evaluate the device's functionality and the resilience of the (bio)molecules used in the assays when exposed to a radiation-rich environment. Subsequently, we designed a paper – based assay to detect traces of ovalbumin (OVA) in food samples. To this purpose, we developed an origami paper-based device that

exploits a competitive immunoassay coupled with chemiluminescence detection. Magnetic microbeads have been used to easily immobilize ovalbumin on paper. Immobilized ovalbumin competes with the OVA present in the sample for a limited amount of enzyme (HRP)-labelled anti-OVA antibody. Using the origami design, a series of analytical steps can be performed using reagents preloaded on different paper layers, creating a user-friendly and immediately deployable immunosensing platform. Finally, with the aim of exploring the use of biomimetic materials in biosensors development, an hydrogel – based chemiluminescence (CL) biosensor for the detection of H₂O₂ and glucose was developed. A guanosine hydrogel was prepared and loaded with a CL reagent (luminol) and a catalytic cofactor (hemin), miming a DNAzyme activity. Subsequently, the hydrogel was modified by incorporating glucose oxidase (GOD) enzyme to enable glucose biosensing. To enable point-of-care (POC) applications, the emitted photons were detected using a portable device equipped with a smartphone's CMOS (complementary metal oxide semiconductor) camera for CL emission detection.

Introduction to biosensors

Biosensors, at the captivating crossroads of biology, chemistry, and engineering, have revolutionized diverse fields through their fabrication, materials, transducing devices, and immobilization techniques, symbolizing the essence of multidisciplinary innovation [1]. These innovative devices have been developed to meet the need for alternatives to standard laboratory analytical methods based mainly on instrumental techniques such as spectrophotometry and chromatography, and are in fact an inexpensive solution for solving qualitative and quantitative analytical questions without the use of complex instrumentation [2], [3].

Broadly speaking, a sensor can be described as a device or component that helps to identify changes in various physical properties, including pressure, temperature, humidity, motion, strength, and even electrical properties such as current. It does this by converting these changes into signals that can be detected and analyzed [3], [4]. Sensors are commonly classified into different groups, as shown in *Figure 1*, based on the specific physical attribute or substance they are intended to measure. These categories include distinctions such as their power source (active and passive sensors), their mode of physical interaction (contact and non-contact sensors), their comparability of measurement (absolute and relative sensors), their type of signal output (analogue and digital sensors), and their method of signal detection [5], [6]. Within this diverse range of sensors there is a subset known as biological sensors, often referred to as biosensors for brevity. This term was coined by Cammann [7] and its definition was introduced by

The biological recognition element has a specific affinity for the target molecule and triggers the generation of a measurable signal via the transducer, which is subsequently converted into a quantifiable output by the electronic component. This operating sequence enables biosensors to identify extremely small amounts of both chemical and biological substances, making them indispensable in a wide range of applications [11].

Furthermore, in order to develop highly effective, reliable and high-performance devices, special requirements are needed, such as:

- Selectivity in determine and differentiate a specific target molecule (the analyte) in a complex sample without interference derived from matrix components [12] .
- Sensitivity, which can be defined as the relationship between the intensity of the transmitted and the analytes concentration. This characteristic is also defined by upper and lower detection limits, which are the highest and lowest measurable concentrations within a sample, with acceptable accuracy (the capability of a sensor to produce a measured value with a degree of closeness as high as possible to the known true value under established conditions) and precision (the closeness of agreement among a series of measurements) [8], [13], [14].
- Specificity, that is the ability to reveal and differentiate the target molecule from other analytes, including substances that are structurally similar to the target, metabolites, isomers, impurities or concomitant medications [14].
- Short response time, to ensure quick and easy use especially in the field of screening analysis.
- Reproducibility, defined as the ability to consistently obtain identical results when an experiment is repeated [14].
- The last but not the least property is the stability, that is a measure of the intactness an analyte in a given matrix under specific storage and use conditions relative to the starting material for given time intervals [12] . Ensuring stability is very important especially when continuous monitoring is required, because it is an indication of how vulnerable the biosensor is to variation in factors external or internal to the device. In particular, the aspects that affect stability are the affinity

of the bioreceptor (the extent of binding of the analyte to the bioreceptor) and the degradation of the bioreceptor over time [11].

One of the main advantages of biosensors is their versatility: thanks to their simplicity, accuracy and portability, they can also be used by inexperienced personnel or those without an equipped analytical laboratory, and can be used directly in the field, avoiding possible inconveniences related to the transport and storage of samples. Given their considerable advantages, they find applications in various fields, such as medical diagnostics, environmental monitoring, food safety assessment, wearable technology, but also in industrial and pharmaceutical sectors [15]. For example, in medical diagnostics, biosensors have transformed patient care by enabling rapid and accurate detection of diseases, monitoring of glucose levels for diabetics, and identification of specific biomarkers indicative of health conditions [16]. This not only enhances the efficiency of healthcare but also empowers individuals to take charge of their well-being. Environmental monitoring benefits significantly from biosensors as well. These devices can detect pollutants, heavy metals, and toxins in air, water, and soil, facilitating timely intervention to mitigate potential hazards [17]. In the food industry, biosensors play a crucial role in ensuring food safety by identifying contaminants or spoilage indicators [18]. This safeguards both consumers and producers from health risks and financial losses.

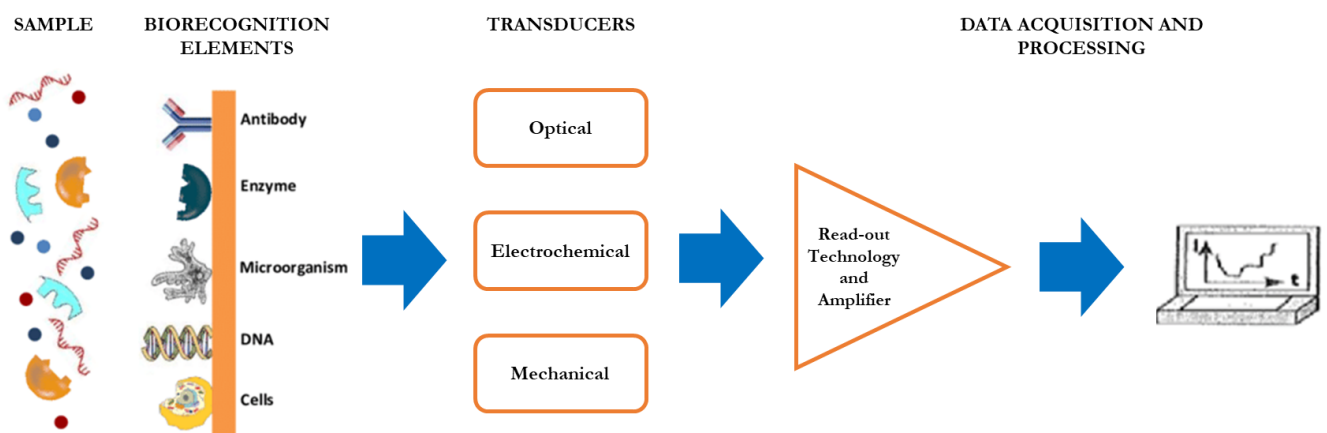


Figure 2. The basic configuration of a biosensor, that is represented by its primary constituents: the biorecognition element, the transducer, and the output system.

Moreover, the integration of biosensors with smartphones has led to a remarkable convergence of healthcare and technology, enabling individuals to access quick and convenient diagnostic information right from their mobile devices. These smartphone-based biosensors capitalize on the ubiquity and computational power of smartphones to create portable, affordable, and user-friendly platforms for various diagnostic applications [19–21], quantifying the signal provided by the transducer element. The principal advantages of this implementation include [22], [23]:

- accessibility to a larger population;
- portability, allowing users to carry them anywhere, which is especially beneficial for point-of-care testing and on-the-go monitoring;
- affordability and user-friendly, in fact the interface of smartphones is familiar to most people, making these biosensors intuitive and easy to use without requiring specialized training;
- connectivity, enabling data sharing with healthcare professionals or central databases for remote monitoring and analysis.

1.1 Enzymes in biosensors

1.1.1 An outline of enzyme kinetics

Enzymes, which are proteins found in all tissues and fluids of living organisms, can act as biocatalysts. Their primary function is to increase the rate of thermodynamically favoured reactions, by reducing the activation energy required to form the reactants complex essential for the generation of reaction products. Enzymes exhibit exceptional stability and specificity and can be conveniently isolated once the reaction is complete. They can also be easily immobilised on receptor surfaces and re – used after a reaction [24], [25]. From a structural point of view, all enzymes are characterized by an active or catalytic site, which is the region in which the catalytic events takes place: the reacting chemical species called substrates bind in a specific way and are converted into the

product, passing through a transition state [26], according to the scheme shown in *Figure 3*.

a)



b)

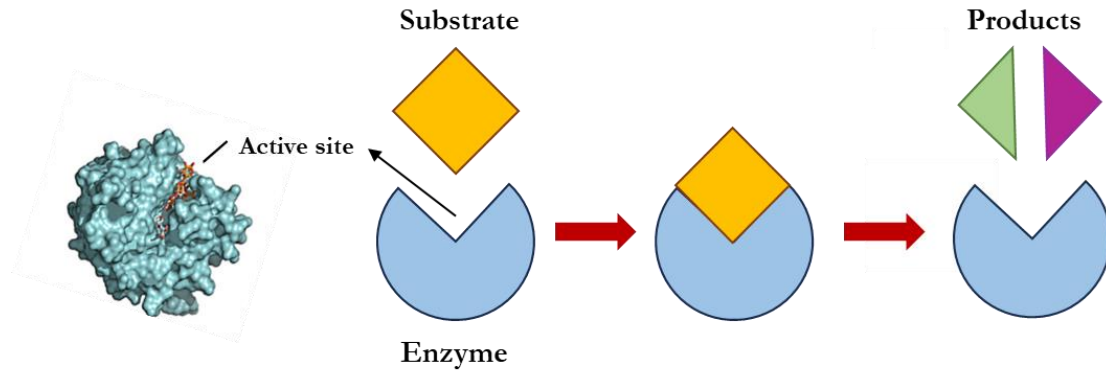


Figure 3. a) Scheme of the steps that take place during an enzymatic reaction. First of all, an enzyme substrate (ES) complex must be formed; then, this complex passes to the transition state (ES*); finally, the transition state complex advances to an enzyme product complex (EP), that dissociates to product and free enzyme. **b)** Graphical representation of a classic enzymatic reaction.

Among the first to outline kinetic models to describe these types of reactions were the biochemists Michaelis and Menten, to whom we owe the following equation:

$$V = \frac{V_{MAX} \cdot [S]}{K_M + [S]}$$

Where V is the reaction rate of an enzyme - catalyzed reaction; V_{max} is the maximum reaction rate; [S] is the substrate concentration; K_M is the Michaelis – Menten constant, which is a measure of the affinity between the enzyme active site and its specific substrate [27]. The purpose of the Michaelis-Menten equation is to provide quantitative information on the concentration of substrate and/or enzyme starting from the

measurement of the reaction rate. Graphing the reaction rate (V) as a function of the substrate concentration $[S]$, the typical Michaelis - Menten plot is obtained [Figure 4], from which it is evident that at the substrate concentration that produces exactly half of the maximum reaction rate, i.e., $1/2 V_{\max}$, the substrate concentration is numerically equal to K_M . Moreover, it can be noticed that at high concentrations of substrate the rate of the reaction is almost equal to V_{\max} .

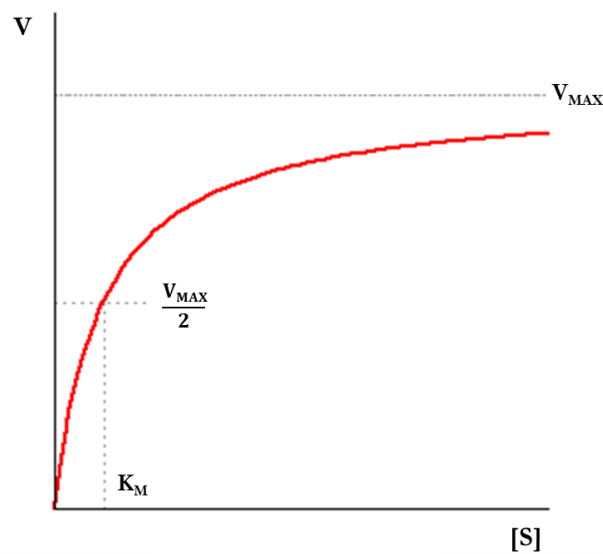


Figure 4. Michaelis – Menten plot.

It is also important to consider two areas in the Michaelis-Menten curve. The first zone refers to the condition in which the substrate concentration falls short of the Michaelis-Menten constant ($[S] \ll K_M$). In this case, the previously described equation can be rearranged in this way:

$$V \approx \frac{V_{\max} \cdot [S]}{K_M}$$

The following equation describes a first order kinetics in which the reaction rate exhibits a linear correlation from $[S]$, i.e. it varies proportionally as $[S]$ increases. These conditions

are therefore of interest for the determination of the substrate concentration of an enzymatic reaction by measuring the reaction rate [28]. Instead in the second zone, the concentration of the substrate is in excess ($[S] \gg K_M$), causing the saturation of the enzyme. Therefore the concentration of the enzyme becomes equal to that of the substrate which has bound and the reaction rate becomes maximum. In conclusion, for high values of $[S]$, the term K_M in the denominator becomes irrelevant and the Michaelis-Menten equation is greatly simplified:

$$V \approx V_{MAX}$$

This equation describes a zero-order kinetics in which the reaction rate is independent of the substrate concentration $[S]$, but is directly proportional to the total enzyme concentration $[E_t]$ [28]. This area of the curve is therefore interesting to evaluate the enzymatic activity starting from the measurement of the reaction rate.

1.1.2 Enzyme based biosensors

Enzymes used as biocatalysts are employed in a wide variety of fields to derive analytical information. They are found in the diagnostic-clinical field as they enable the assessment of organ function or serve as markers of specific diseases. They can also be used in forensic science as a method of detecting body fluids or as markers of a subject's genetic individuality. They are also widely used as biospecific probes with applications in immunological methods. Still, in the food industry, thanks to enzymes it is possible to evaluate the proper performance of operations such as pasteurization and sterilization. Finally, in the field of environmental chemistry enzymes are exploited to monitor the presence of specific pollutants (e.g., pesticides) or in the pharmaceutical field to assess the quality of certain formulations [29], [30].

From an analytical point of view, the use of enzymes in biosensing is extremely advantageous because it allows rapid and accurate chemical analyses, due to their specificity toward substrates, and with detection limits so low that the use of very small volumes of sample is sufficient, resulting in reagent savings. The use of enzymes also makes it possible to increase the selectivity of chemiluminescent (CL) and electrochemiluminescent (ECL) detection reactions. To broaden the utility of the enzyme-based biosensors and extend their ability to measure a wider range of molecules, it is possible to construct a cascade system of coupled enzymes. In this setup, the primary product resulting from the analyte conversion undergoes subsequent enzymatic transformations, ultimately yielding a secondary product that can be measured [31], [25]. Oxidase enzymes that generate H_2O_2 , such as xanthine oxidase or glucose oxidase, are most commonly used for this purpose [32].

An enzyme-based biosensor operates on the basis of several factors, including the catalytic reaction and the binding affinity for the target analyte [33]. The mechanisms underlying analyte recognition can take several forms:

- the enzyme may metabolize the analyte and this catalytic conversion is used to measure the concentration of the analyte;
- the analyte can inhibit or activate an enzyme, linking its concentration to a reduction in the enzyme product formation;
- Monitoring the enzyme characteristics and their variations. [34–37]

Furthermore, it is very important that the biosensor be stable to ensure its safe and effective long-term use, and this skill is achievable if the stability of the enzyme used to fabricate it can be guaranteed. For this purpose, many different techniques have been employed, such as protein engineering [38], the use of enzymes from naturally thermostable microorganisms [39], [40], immobilized enzymes [41], [42] and by addition of stabilizing agents to the enzymes [43], [44].

One of the most studied systems, which also led to the development of the first biosensor, is one that exploits glucose oxidase, whose reaction mechanism is shown in *Figure 5*.

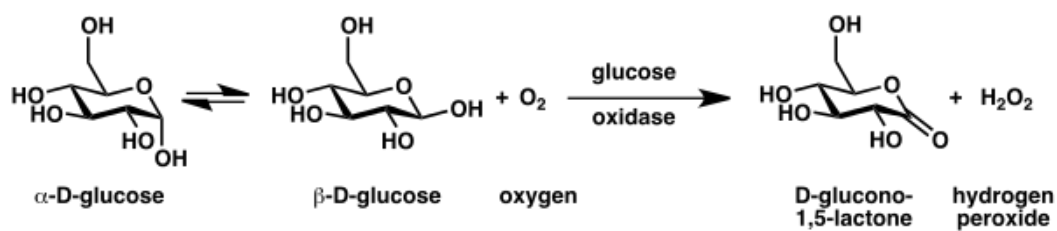


Figure 5. Oxidation reaction of glucose catalyzed by glucose oxidase.

The beginnings of glucose biosensors can be traced back to a pioneering experiment by Leland C. Clark, shown in *Figure 6*.

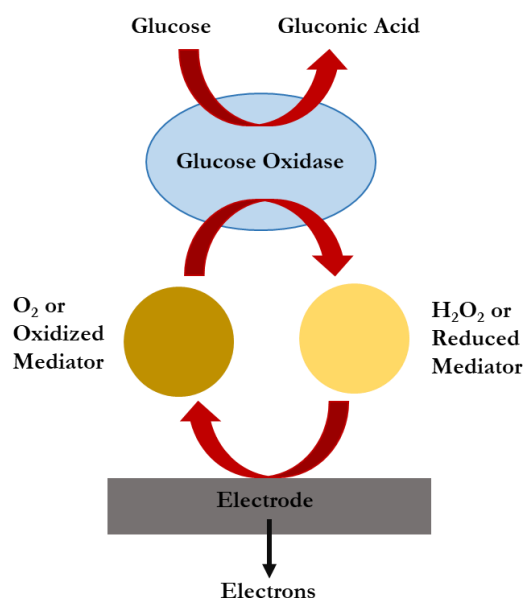


Figure 6. Schematization of the Clark's experiment.

In this experiment, platinum (Pt) electrodes were used to detect oxygen. The enzyme glucose oxidase (GOD) was strategically positioned in close proximity to the platinum surface, secured in place by a piece of dialysis membrane. When glucose interacts with

GOD, it led to the formation of gluconic acid, producing two electrons and two protons, effectively reducing GOD. The reduced GOD, together with the surrounding oxygen, electrons, and protons underwent a reaction that results in the production of hydrogen peroxide and the regeneration of oxidized GOD. This rejuvenated GOD could then participate in further glucose reactions. Notably, a higher glucose concentration leads to increased oxygen consumption, while lower glucose levels produce more hydrogen peroxide. Consequently, the platinum electrodes could detect either the depletion of oxygen or the generation of hydrogen peroxide, making them a reliable indicator of glucose concentration [45]. The most common and commercially available enzymatic biosensors using glucose oxidase are those characterized by electrochemical transduction. Of these, the most common and commercially available are the amperometric and potentiometric ones, which are mainly used in clinical settings to measure blood glucose concentration [46], [47]. The present and future applications of glucose biosensors are broad, driven primarily by their direct utility in self-monitoring capillary blood glucose levels in people with diabetes. These monitoring devices represent one of the most expansive markets for biosensors today, significantly improving the quality of life for people suffering from diabetes [47], [48].

1.2 Immunosensors

Immunosensors are innovative analytical devices that merge the principles of immunology with cutting-edge sensor technology to detect and quantify specific biological molecules, such as proteins, antigens, or antibodies. These biosensors are designed to provide rapid, precise, and sensitive measurements of target analytes, making them invaluable tools in a wide range of applications [49].

At the heart of immunosensors lies the strong interaction between antibodies (the affinity biorecognition elements) and antigens, a fundamental process within the immune system [50]. Antibodies possess the structure of immunoglobulins (Ig) (*Figure 7*) in the form of “Y” shape, which consists of two heavy and two light polypeptidic chains

connected by disulfide bonds. Five classes of antibodies have been defined based on differences in heavy chains: IgG, IgM, IgA, IgD, and IgE [51]. They are highly specific proteins that can bind to specific antigens, and this specificity forms the basis for the remarkable precision of immunosensors. When an antibody recognizes and binds to its corresponding antigen, this event can be related to the generation of a measurable output, typically an electrical or optical signal.

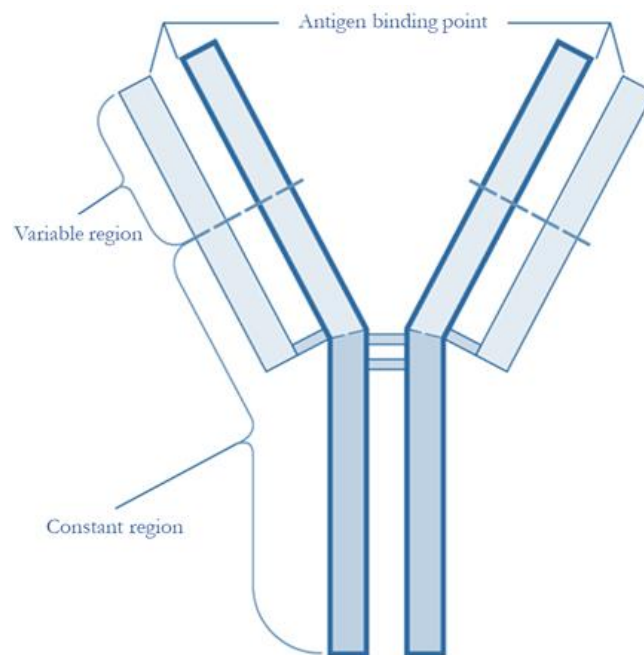


Figure 7. Schematic structure of an immunoglobulin. The two short outer components are called light chains, while the two longer inner portions are called heavy chains.

Immunosensors offer several advantages:

- They can selectively detect and quantify the target molecule in the presence of complex mixtures, reducing the likelihood of false-positive results. The specificity is provided by the binding domains of antibodies, which are located on the arms of their “Y” conformational shape [52], [53].

- Thanks to their sensitivity, immunosensors can detect analytes at very low concentrations, making them suitable for early disease diagnosis and monitoring trace-level substances.
- They provide rapid results, often in minutes, making them valuable for point-of-care testing and on-site analysis.
- Many immunosensors are compact and portable, enabling their use in various settings, including remote or resource-limited areas [54].

In addition, immunosensors can be classified as labelled and non – labelled. The first case derives from immunoassay technology: a sensitively detectable label is introduced and the antigen–antibody complex is assessed through label measurement. Conversely, label – free immunosensors are designed to discern the antigen-antibody complex by assessing the physical alterations induced as the complex forms [55].

1.2.1 Labelled – biosensors

In labelled immunosensor methodologies, antibodies are typically conjugated with a sensitively detectable label, such as fluorophores, nanoparticles, enzymes, or redox probes. These tagged antibodies then bind to the target antigen, facilitating highly sensitive detection. The labels employed can encompass enzymes, such as horseradish peroxidase (HRP) and alkaline phosphatase (ALP), as in enzyme-linked immunosorbent assays (ELISA) [56], [57], as well as fluorescence probes or chemiluminescent markers [58], [59]. Furthermore, there is a growing emphasis on the use of nanomaterials as labels in immunosensors development [60], [61]. Notably, ELISA in its two formats (sandwich assays and competitive assays) has garnered increased attention due to its simplicity [62].

The sandwich immunosensing approach stands as the most widely employed analytical method for detecting and quantifying specific proteins of interest [63]. In this approach, the antigen is trapped between two antibodies: a primary antibody (capture antibody) and a labelled secondary antibody, as depicted in *Figure 8*.

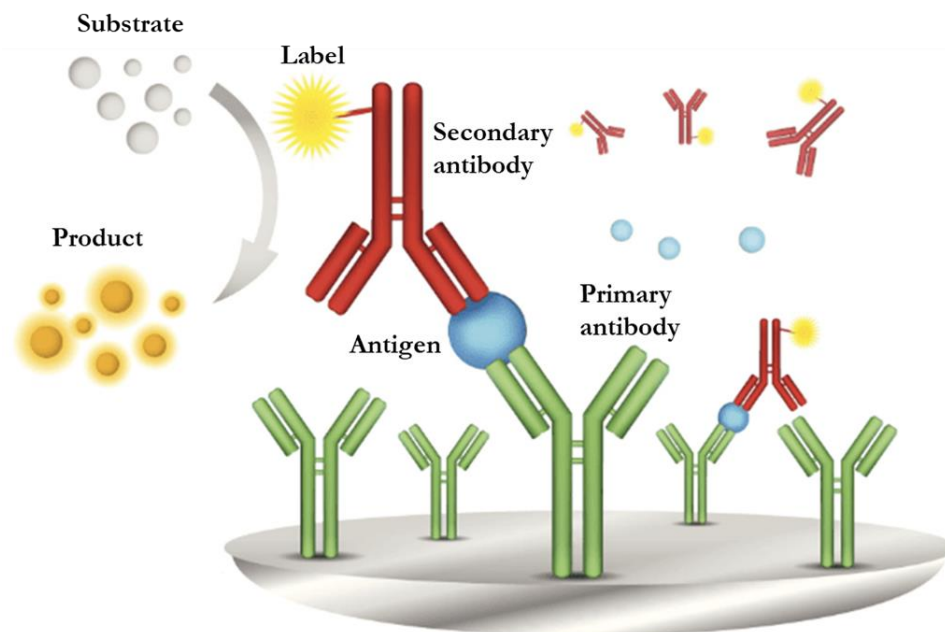


Figure 8. Schematic of a typical sandwich immunoassay.

Initially, a fixed quantity of primary antibody, tailored to the antigens, is immobilized onto the sensor surface. Following this immobilization, various dilutions of the antigens (typically proteins) are introduced and captured by the antibodies affixed to the surface. Any unbound antigens are then removed through washings. Subsequently, an enzyme-linked secondary antibody, specific to the antigens, is applied to the sensor. After another washing step to eliminate any unbound enzyme-labelled secondary antibody, a substrate solution is introduced into the wells, and the signal increases proportionally to the quantity of antigen bound to the antibody [64].

Competitive immunosensors in their direct form, as shown in *Figure 9*, involve the fixing of a specific antibody onto a sensor surface. In this configuration, both unlabelled antigen and enzyme-labelled antigen (typically labelled with enzymes such as HRP or ALP) compete for binding sites on the antibody. Quantification of antibody-bound labelled antigen is achieved by colorimetric or chemiluminescent means, where the intensity of the colour or emission is inversely related to the amount of unbound antigen or unlabelled antigen present in the sample [64].

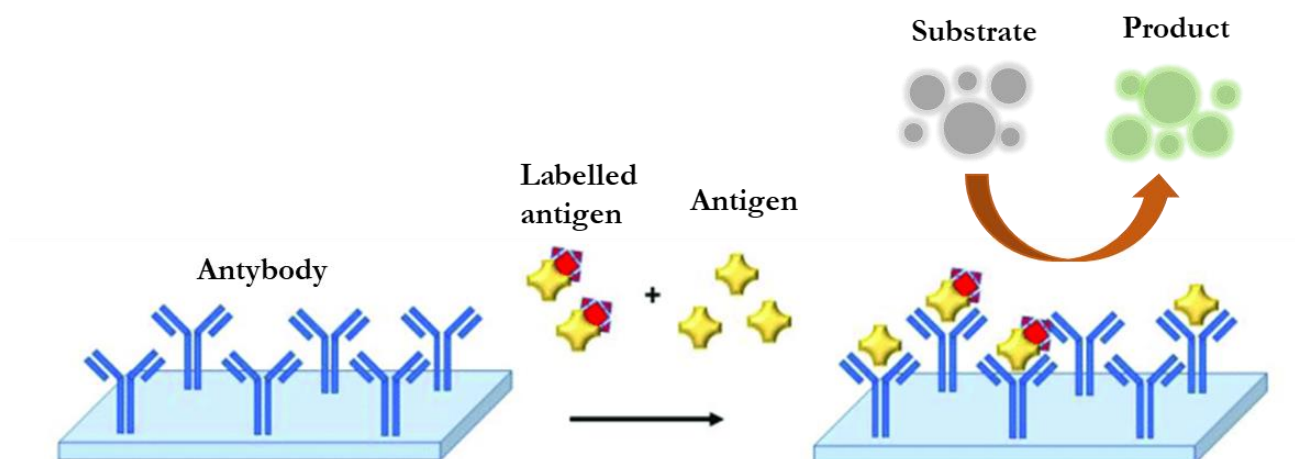


Figure 9. Schematic of a typical competitive immunoassay.

1.2.2 Label – free biosensors

In label-free or direct immunosensors, antibodies are attached to the surface of the sensor, where they form binding interactions with the target antigen. When the capture antibody specifically recognizes the antigen at the molecular level, it induces alterations in the interfacial properties, including charge, current, capacitance, impedance, mass, and thickness at the surface of the immunosensor. These changes directly influence the electron transfer reaction of the probe at the interface between the immunosensor and the electrolyte solution. Consequently, the direct electrochemical immunoassay typically involves the measurement of shifts in impedance, capacitance, current, and potential resulting from the formation of the immunocomplex [65], [66], [67]. In addition, many label – free immunosensors make use of optical detection methods, such as surface plasmon resonance (SPR) e surface – enhanced Raman spectroscopy (SERS). In fact, antibodies, antigens or oligonucleotides can be labelled with metal nanoparticles (i.e. AuNPs, AgNPs), which are therefore widely used for biomolecule detection [68]. The Raman scattering radiation of molecules adsorbed on the nanostructured surface can be measured and amplified through SERS phenomenon [69]. Moreover, metal

nanoparticles shows optical properties due to the SPR effect [70], which gives rise to a well-defined absorption band in the UV-vis spectrum [71].

Label-free measurements of a wide variety of markers are mainly appealing due to their capability for real-time monitoring [64].

1.3 Paper and hydrogel: ideal materials for bioassays

1.3.1 Paper in biosensing

Paper has attracted considerable attention as a promising material for sensors and devices in analytical and clinical chemistry due to its versatility, wide availability and cost-effectiveness [72–74]. These analytical devices can be seamlessly integrated to provide flexibility, portability, disposability, and ease of use. A variety of techniques and processes, involving chemical modification and/or physical deposition, can be used to tailor the properties of paper, making it suitable for subsequent modification or direct application in a wide range of uses [75]. Numerous methods for confining liquids to specific regions on paper have been documented in the literature, including photolithography [76], inkjet printing [77], etching [78], plasma treatment [79], paper cutting [80], wax printing [81], screen printing [82], and laser treatment [83].

Paper-based sensors represent an emerging technology that offers an innovative approach to the development of creating simple, cost-effective, portable, and disposable analytical tools for use in different fields such as clinical diagnostics, food quality assurance, and environmental monitoring. The key advantages of using paper as a sensing platform lie in its special properties, which allow passive liquid transport and compatibility with a wide range of chemicals and biochemicals.

Among the many paper based devices, one of the most important examples is the Lateral Flow Immunoassay (LFIA). LFIA techniques readily find practical use with an high commercial diffusion primarily because they require minimal modifications to function as end-user devices [84], but also because they are simple, rapid, cost-effective and have no requirement of equipment or technical expertise. A typical LFIA device

(Figure 10) comprises several layers, with a thin porous nitrocellulose membrane adhering to a plastic backing support, which provides structural stability to the device. At its ends, there are two cellulose or glass – fiber pads, namely the sample pad and the absorbent pad [85].

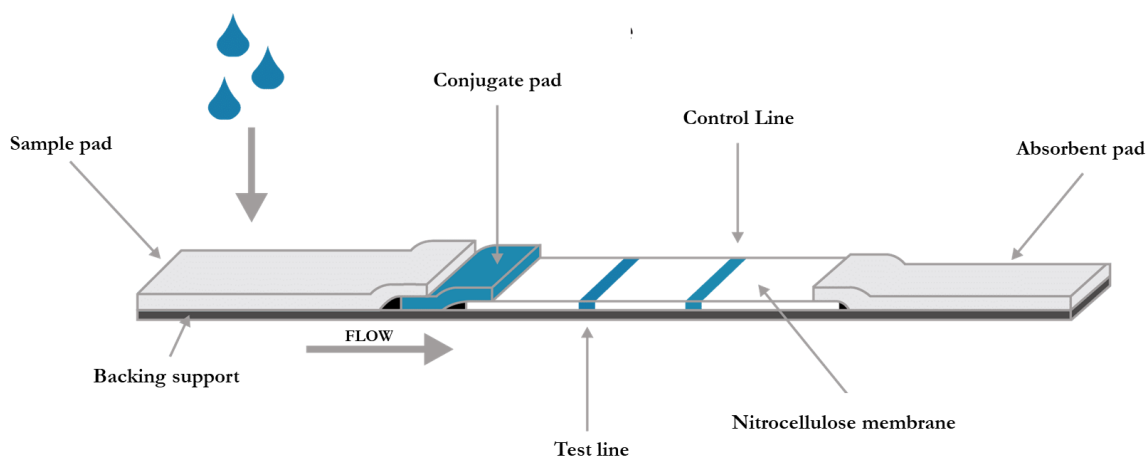


Figure 10. The structural components of a typical LFIA strip.

The sample pad gradually absorbs the liquid sample, pre-treating it to minimize matrix effects, while the absorbent pad facilitates capillary flow and acts as a reservoir for the processed liquid. Another pad, often made of polyester or glass – fiber, is located right after the sample pad: it is called conjugate pad. It is impregnated with a suitable labelled immunoreagent solution and is dried. On the nitrocellulose membrane, specific lines are designated for dispensing solutions containing immunoreagents: these regions are called Test lines and Control line. The Test lines reveal interactions with the target molecule, while the Control line ensures the test's proper functioning by binding with the probe, independent of the presence of the target. The assembled strip is enclosed in a plastic cassette, which includes a reading window covering the reactive regions on the nitrocellulose and a sample well for introducing the sample. The cassette features pressure points to ensure proper contact between the layered components, facilitating the flow of the sample and labelled conjugate mixture along the strip [86]. To perform

an LFIA experiment, the liquid sample is deposited on the sample pad, generating a capillary flow of sample along the membrane. This mechanism allows immunoreaction to occur along the dedicated lines [85].

As one of the most successful analytical platforms for point-of-need testing, LFIA's applications range from the determination of biological markers for clinical purposes, food and feed safety, veterinary medicine, environmental control and even forensic analysis [85], [87], [88].

1.3.2 Hydrogels in biosensing

Over the last few years, hydrogels, a class of materials with a high water content and a three-dimensional network structure, have emerged as a versatile and indispensable tool in the field of biosensing, thanks to their ability to incorporate alien substances while preserving a favourable environment for biosensing events. These remarkable materials offer a unique combination of biocompatibility, tunable physical properties, and the ability to absorb and release water, making them ideal candidates for a wide range of biosensing applications [89], [90], [91]. Hydrogels consist of a hydrophilic polymer network that can retain large amounts of water within their structure, granting them soft and flexible nature, similar to natural tissues. The latter property makes them suitable for various biological applications and preserves the native structure of biomolecules, an essential prerequisite for feasibility, specificity, and sensitivity in biosensing applications [92]. These polymers can be synthetic or natural, such as alginate [93], collagen [94], or hyaluronic acid [95], offering researchers a plethora of options to tailor hydrogels for specific biosensing needs. The fundamental characteristics of hydrogels can be resumed as follow [96], [97]:

- Hydrogels are biocompatible materials, meaning they are well-tolerated by living organisms. This property is vital in biosensing applications, as it minimizes the risk of adverse reactions when hydrogels come into contact with biological samples or tissues.

- The high water content in hydrogels mimics the natural environment of cells and biological fluids, enabling the effective exchange of analytes between the hydrogel and its surroundings. This is particularly valuable in biosensing, where precise control of the microenvironment is often required.
- Thanks to their 3D porous structure, hydrogels can be easily functionalized with various recognition elements, such as antibodies, enzymes, or DNA probes. This functionalization enables the selective detection of specific analytes, making hydrogel-based sensors highly specific and sensitive.

In literature it is possible to find numerous applications in which hydrogels are used, including: hydrogel-based glucose sensors, that use glucose oxidase enzymes embedded in hydrogels to detect changes in glucose concentration [98]; pH and ion concentration monitoring in biological fluids, with sensors that finds applications in environmental and healthcare fields [99]; hydrogel – embedded biosensors, which allow a controlled drug delivery, releasing drugs in response to specific stimuli, such as changes in pH or temperature [100]; sensors for the detection of specific proteins or biomarkers in complex biological samples, realized functionalizing hydrogels with antibodies or aptamers, for diagnostic and biomedical purposes [101]; hydrogel-based wearable sensors, which have gained popularity for the continuous monitoring various physiological parameters, including hydration, lactate levels [102] and many others [103]. In conclusion, hydrogels are excellent functional materials for biosensor development. However, although they have made significant strides in biosensing applications, challenges such as stability, long-term performance, and integration into miniaturized devices remain. Researchers are continually working on improving hydrogel formulations, exploring new functionalization strategies, and developing innovative sensor architectures.

1.4 Chemical Luminescence System

Biosensors can be classified not only by the type of biorecognition element but also by the different types of transducer system, such as electrochemical, optical, thermal, electronic, gravimetric, magnetic, and acoustic. In particular, in optical biosensors the output transduced signal derives from the interaction of matter with an electromagnetic radiation, that is the product of the biospecific recognition event. The most commonly used optical-based biosensors are, colorimetric, fluorescence, chemical luminescence, SPR, and optical fiber-based biosensors [104–107].

Chemical luminescence is a physical phenomenon caused by the production of light via a chemical reaction, in particular by an excited chemical species called the luminophore. Depending on the nature of the stimulus able to trigger the reaction, a further subdivision can be made: chemiluminescence (CL) and bioluminescence (BL) are referred to the production of light started by mixing the reagents, the latter exploiting enzymes and photoproteins isolated from living organisms [108]; electrogenerated chemiluminescence (ECL) is the luminescence generated at the surface of an electrode by relaxation of excited state molecules produced during an electron-transfer reaction [109]; thermo-chemiluminescence (TCL) is the emission of light produced by the thermally-induced decomposition of a molecule [110].

Certain conditions must be met for a chemical reaction to produce light [111]:

1. the reaction must be exergonic so as to populate an electronically excited state (singlet). The free energy requirement can be calculated using the following equation:

$$\Delta G \geq \frac{hc}{\lambda_{\text{ex}}} = \frac{28600}{\lambda_{\text{ex}}}$$

Based on the above, the energy required by a chemiluminescence reaction producing photons in the visible (400 – 700 nm) range is around 40 – 70 kcal mol⁻¹.

1.

2. the electronically excited state must have accessibility on the reaction coordinates.
3. Photon emission from the excited state has to be energetically favored. So, the product of the reaction has to be fluorescent or, through an intra/intermolecular energy transfer, an excited state can be populated.

The chemical luminescence quantum yield, is defined as the number of photons emitted per reacting molecule and can be calculated as follows:

$$\Phi_{\text{CL}} = \Phi_{\text{R}} \cdot \Phi_{\text{ES}} \cdot \Phi_{\text{F}}$$

where Φ_{R} is the chemical yield of the reaction, Φ_{ES} is the fraction of the product entering the excited state and Φ_{F} is the fluorescent quantum yield.

One of the most described and studied CL reactions is certainly that of the oxidation of luminol, a diprotic acid with pKa values of 6 and 13, respectively. Under alkaline conditions and in the presence of H_2O_2 , luminol is oxidized to the corresponding radical anion in its excited state, which releases a photon while decaying to the ground state, as shown in *Figure 11*. A blue light is emitted at 428 nm with a relatively low quantum yield of 1% [112]. The reaction is usually catalyzed by the enzyme horseradish peroxidase (HRP), which is commonly employed as a marker in immunometric assays due to its ability to amplify signals and its high turnover number [113].

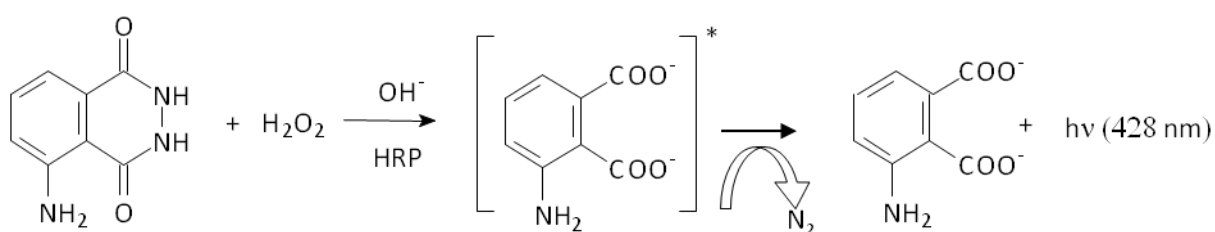


Figure 11. Chemiluminescent HRP-catalyzed oxidation of luminol.

Utilizing an enzyme such as HRP as a label offers the potential to enhance the CL signal, as an abundance of CL substrate leads to the generation of numerous product molecules from a single enzyme molecule [114]. Furthermore, attaining the steady – state of the CL emission enables the establishment of standard experimental parameters and the quantitative measurement of the investigated labeled probe. This is due to the direct correlation between steady-state light intensity and enzyme activity. The analytical performance of the HRP-catalyzed CL oxidation of luminol can be improved through the addition to the CL cocktail of some enhancers like p-iodophenol (PIP), 4- (1-imidazolyl)phenol [115], and other p-phenol derivatives [116], sodium 3-(100-phenothiazinyl)propane-1-sulfonate (SPTZ) [117], p-phenylphenol and sodium tetraphenylborate as synergistic enhancer [58], or $K_3Fe(CN)_6$ as electron mediator [118], or . These enhancers enable the amplification and stabilization of the CL signal, thereby enhancing the sensitivity of the analytical approach [117].

Chemical luminescence detection techniques are of analytical significance primarily due to their ability to generate photons without requiring photoexcitation, unlike fluorescence-based methods. This characteristic allows for the mitigation of issues related to light scattering, background fluorescence, and light source instability. Therefore, instrumentation for chemical luminescence measurements is very simple, since no excitation source, nor wavelength selection systems, are required. Furthermore, when chemical luminescence detection is combined with imaging systems for detection, such as charge-coupled device (CCD) or complementary metal-oxide semiconductor (CMOS) cameras, or arrays of thin-film photosensors, adaptable setups for the reading cell become feasible. This flexibility extends to aspects like the arrangement of microarray spots on a modified surface, given that measures are taken to manage cross-talk phenomena. Finally, chemical luminescence detection exhibits extensive dynamic ranges, simplifying the examination of samples featuring highly disparate analyte concentrations. Conversely, the primary limit of these detection methods arises from the possible influence of the sample matrix on the chemical reaction, potentially enhancing or impeding the light-emitting process. Such impacts are inherently unpredictable and might result in aberrations or erroneous outcomes. Moreover, owing to the heightened

detectability of chemical luminescence labels, meticulous management of non-specific binding is essential to prevent excessive background signals. Consequently, strategies for functionalizing surfaces play a pivotal role in ensuring the assay's success [119]. An additional factor requiring consideration, particularly during signal acquisition within a flow setup, is the reliance on the kinetics of photon emission dictated by the employed chemistry (spanning from flash-type to glow-type). Given that the chemical luminescence signal is temporally unstable, the species emitting light experience diffusion within the solution, leading to a loss in resolution [120].

References

- [1] Mehrotra, P. Biosensors and Their Applications – A Review. *Journal of Oral Biology and Craniofacial Research* **2016**, *6* (2), 153–159. <https://doi.org/10.1016/j.jobcr.2015.12.002>.
- [2] Swager, T. M.; Mirica, K. A. Introduction: Chemical Sensors. *Chem. Rev.* **2019**, *119* (1), 1–2. <https://doi.org/10.1021/acs.chemrev.8b00764>.
- [3] Banica, F.-G. *Chemical Sensors and Biosensors: Fundamentals and Applications*; John Wiley & Sons, 2012.
- [4] Ensafi, A. A. *Electrochemical Biosensors*, 1st Edition.; Elsevier, 2019.
- [5] White, R. M. A Sensor Classification Scheme. *IEEE Trans. Ultrason., Ferroelect., Freq. Contr.* **1987**, *34* (2), 124–126. <https://doi.org/10.1109/T-UFFC.1987.26922>.
- [6] Khanna, V. K. *Nanosensors: Physical, Chemical, and Biological*; CRC Press, 2021.
- [7] Cammann, K. Bio-Sensors Based on Ion-Selective Electrodes. *Z. Anal. Chem.* **1977**, *287* (1), 1–9. <https://doi.org/10.1007/BF00539519>.
- [8] Thevenot, D. R.; Tóth, K.; Durst, R. A.; Wilson, G. S. Electrochemical Biosensors: Recommended Definitions and Classification. *Pure and Applied Chemistry* **1999**, *71* (12), 2333–2348. <https://doi.org/10.1351/pac199971122333>.
- [9] *The IUPAC Compendium of Chemical Terminology: The Gold Book*, 4th ed.; Gold, V., Ed.; International Union of Pure and Applied Chemistry (IUPAC): Research Triangle Park, NC, 2019. <https://doi.org/10.1351/goldbook>.
- [10] Clark Jr., L. C.; Lyons, C. Electrode Systems for Continuous Monitoring in Cardiovascular Surgery. *Annals of the New York Academy of Sciences* **1962**, *102* (1), 29–45. <https://doi.org/10.1111/j.1749-6632.1962.tb13623.x>.
- [11] Naresh, Varnakavi.; Lee, N. A Review on Biosensors and Recent Development of Nanostructured Materials-Enabled Biosensors. *Sensors* **2021**, *21* (4), 1109. <https://doi.org/10.3390/s21041109>.
- [12] Food and Drug Administration (FDA). Bioanalytical Method Validation Guidance for Industry, 2018.

- [13] Turner, A. P. F. Biosensors: Sense and Sensibility. *Chem. Soc. Rev.* **2013**, *42* (8), 3184–3196. <https://doi.org/10.1039/C3CS35528D>.
- [14] European Medicine Agency. ICH M10 on Bioanalytical Method Validation - Scientific Guideline, 2019. <https://www.ema.europa.eu/en/ich-m10-bioanalytical-method-validation-scientific-guideline> (accessed 2023-10-21).
- [15] Song, M.; Lin, X.; Peng, Z.; Xu, S.; Jin, L.; Zheng, X.; Luo, H. Materials and Methods of Biosensor Interfaces With Stability. *Frontiers in Materials* **2021**, *7*. <https://doi.org/10.3389/fmats.2020.583739>.
- [16] Mascini, M.; Tombelli, S. Biosensors for Biomarkers in Medical Diagnostics. *Biomarkers* **2008**, *13* (7–8), 637–657. <https://doi.org/10.1080/13547500802645905>.
- [17] Justino, C. I. L.; Duarte, A. C.; Rocha-Santos, T. A. P. Recent Progress in Biosensors for Environmental Monitoring: A Review. *Sensors* **2017**, *17* (12), 2918. <https://doi.org/10.3390/s17122918>.
- [18] Eyvazi, S.; Baradaran, B.; Mokhtarzadeh, A.; Guardia, M. de la. Recent Advances on Development of Portable Biosensors for Monitoring of Biological Contaminants in Foods. *Trends in Food Science & Technology* **2021**, *114*, 712–721. <https://doi.org/10.1016/j.tifs.2021.06.024>.
- [19] Beduk, T.; Beduk, D.; Hasan, M. R.; Guler Celik, E.; Kosel, J.; Narang, J.; Salama, K. N.; Timur, S. Smartphone-Based Multiplexed Biosensing Tools for Health Monitoring. *Biosensors* **2022**, *12* (8), 583. <https://doi.org/10.3390/bios12080583>.
- [20] Mudanyali, O.; Dimitrov, S.; Sikora, U.; Padmanabhan, S.; Navruz, I.; Ozcan, A. Integrated Rapid-Diagnostic-Test Reader Platform on a Cellphone. *Lab on a Chip* **2012**, *12* (15), 2678–2686. <https://doi.org/10.1039/C2LC40235A>.
- [21] Oncescu, V.; Mancuso, M.; Erickson, D. Cholesterol Testing on a Smartphone. *Lab on a Chip* **2014**, *14* (4), 759–763. <https://doi.org/10.1039/C3LC51194D>.
- [22] Sun, A. C.; Hall, D. A. Point-of-Care Smartphone-Based Electrochemical Biosensing. *Electroanalysis* **2019**, *31* (1), 2–16. <https://doi.org/10.1002/elan.201800474>.

- [23] Roda, A.; Michelini, E.; Zangheri, M.; Di Fusco, M.; Calabria, D.; Simoni, P. Smartphone-Based Biosensors: A Critical Review and Perspectives. *TrAC Trends in Analytical Chemistry* **2016**, *79*, 317–325. <https://doi.org/10.1016/j.trac.2015.10.019>.
- [24] Palmer, T.; Bonner, P. L. *Enzymes: Biochemistry, Biotechnology, Clinical Chemistry*; Elsevier, 2007.
- [25] Copeland, R. A. *Enzymes: A Practical Introduction to Structure, Mechanism, and Data Analysis*; John Wiley & Sons, 2023.
- [26] Bhatia, S. Introduction to Enzymes and Their Applications; 2018; pp 1–29. <https://doi.org/10.1088/978-0-7503-1302-5ch1>.
- [27] Nelson, D. L.; Cox, M. M. *I principi di biochimica di Lehninger*, 7th ed.; Zanichelli, 2018.
- [28] Eggins, B. R. *Chemical Sensors and Biosensors*; John Wiley & Sons, 2008.
- [29] Amine, A.; Mohammadi, H.; Bourais, I.; Palleschi, G. Enzyme Inhibition-Based Biosensors for Food Safety and Environmental Monitoring. *Biosensors and Bioelectronics* **2006**, *21* (8), 1405–1423. <https://doi.org/10.1016/j.bios.2005.07.012>.
- [30] Zhu, Y.-C.; Mei, L.-P.; Ruan, Y.-F.; Zhang, N.; Zhao, W.-W.; Xu, J.-J.; Chen, H.-Y. Chapter 8 - Enzyme-Based Biosensors and Their Applications. In *Advances in Enzyme Technology*; Singh, R. S., Singhania, R. R., Pandey, A., Larroche, C., Eds.; Biomass, Biofuels, Biochemicals; Elsevier, 2019; pp 201–223. <https://doi.org/10.1016/B978-0-444-64114-4.00008-X>.
- [31] Eilertsen, J.; Schnell, S. A Kinetic Analysis of Coupled (or Auxiliary) Enzyme Reactions. *Bull Math Biol* **2018**, *80* (12), 3154–3183. <https://doi.org/10.1007/s11538-018-0513-4>.
- [32] Skoog; Holler; Crouch. *Chimica analitica strumentale*, 2nd ed.; Edises, 2009.
- [33] Gonsalves, K.; Halberstadt, C.; Laurencin, C. T.; Nair, L. *Biomedical Nanostructures*; John Wiley & Sons, 2007.
- [34] Liu, H.; Ge, J.; Ma, E.; Yang, L. 10 - Advanced Biomaterials for Biosensor and Theranostics. In *Biomaterials in Translational Medicine*; Yang, L., Bhaduri, S. B., Webster, T. J., Eds.; Woodhead Publishing Series in Biomaterials; Academic Press, 2019; pp 213–255. <https://doi.org/10.1016/B978-0-12-813477-1.00010-4>.

- [35] Justino, C. I. L.; Freitas, A. C.; Pereira, R.; Duarte, A. C.; Rocha Santos, T. A. P. Recent Developments in Recognition Elements for Chemical Sensors and Biosensors. *TrAC Trends in Analytical Chemistry* **2015**, *68*, 2–17. <https://doi.org/10.1016/j.trac.2015.03.006>.
- [36] Lim, S. A.; Ahmed, M. U. Introduction to Food Biosensors. *Food biosensors* **2017**, 1–21.
- [37] Perumal, V.; Hashim, U. Advances in Biosensors: Principle, Architecture and Applications. *Journal of Applied Biomedicine* **2014**, *12* (1), 1–15. <https://doi.org/10.1016/j.jab.2013.02.001>.
- [38] Victorino da Silva Amatto, I.; Gonsales da Rosa-Garzon, N.; Antônio de Oliveira Simões, F.; Santiago, F.; Pereira da Silva Leite, N.; Raspante Martins, J.; Cabral, H. Enzyme Engineering and Its Industrial Applications. *Biotechnology and Applied Biochemistry* **2022**, *69* (2), 389–409. <https://doi.org/10.1002/bab.2117>.
- [39] E. Ibrahim, N.; Ma, K. Industrial Applications of Thermostable Enzymes from Extremophilic Microorganisms. *Current Biochemical Engineering* **2017**, *4* (2), 75–98. <https://doi.org/10.2174/2212711904666170405123414>.
- [40] Atalah, J.; Cáceres-Moreno, P.; Espina, G.; Blamey, J. M. Thermophiles and the Applications of Their Enzymes as New Biocatalysts. *Bioresource Technology* **2019**, *280*, 478–488. <https://doi.org/10.1016/j.biortech.2019.02.008>.
- [41] Yushkova, E. D.; Nazarova, E. A.; Matyuhina, A. V.; Noskova, A. O.; Shavronskaya, D. O.; Vinogradov, V. V.; Skvortsova, N. N.; Krivoschapkina, E. F. Application of Immobilized Enzymes in Food Industry. *J. Agric. Food Chem.* **2019**, *67* (42), 11553–11567. <https://doi.org/10.1021/acs.jafc.9b04385>.
- [42] Rodrigues, R. C.; Berenguer-Murcia, Á.; Carballares, D.; Morellon-Sterling, R.; Fernandez-Lafuente, R. Stabilization of Enzymes via Immobilization: Multipoint Covalent Attachment and Other Stabilization Strategies. *Biotechnology Advances* **2021**, *52*, 107821. <https://doi.org/10.1016/j.biotechadv.2021.107821>.
- [43] Silva, C.; Martins, M.; Jing, S.; Fu, J.; Cavaco-Paulo, A. Practical Insights on Enzyme Stabilization. *Critical Reviews in Biotechnology* **2018**, *38* (3), 335–350. <https://doi.org/10.1080/07388551.2017.1355294>.

- [44] J. Virgen-Ortíz, J.; Santos, J. C. S. dos; Berenguer-Murcia, Á.; Barbosa, O.; C. Rodrigues, R.; Fernandez-Lafuente, R. Polyethylenimine: A Very Useful Ionic Polymer in the Design of Immobilized Enzyme Biocatalysts. *Journal of Materials Chemistry B* **2017**, *5* (36), 7461–7490. <https://doi.org/10.1039/C7TB01639E>.
- [45] Mohanty, S. P.; Kougiianos, E. Biosensors: A Tutorial Review. *IEEE Potentials* **2006**, *25* (2), 35–40. <https://doi.org/10.1109/MP.2006.1649009>.
- [46] Wang, J. Glucose Biosensors: 40 Years of Advances and Challenges. *Electroanalysis* **2001**, *13* (12), 983–988. [https://doi.org/10.1002/1521-4109\(200108\)13:12<983::AID-ELAN983>3.0.CO;2-#](https://doi.org/10.1002/1521-4109(200108)13:12<983::AID-ELAN983>3.0.CO;2-#).
- [47] Teymourian, H.; Barfidokht, A.; Wang, J. Electrochemical Glucose Sensors in Diabetes Management: An Updated Review (2010–2020). *Chemical Society Reviews* **2020**, *49* (21), 7671–7709. <https://doi.org/10.1039/D0CS00304B>.
- [48] Martinkova, P.; Pohanka, M. Biosensors for Blood Glucose and Diabetes Diagnosis: Evolution, Construction, and Current Status. *Analytical Letters* **2015**, *48* (16), 2509–2532. <https://doi.org/10.1080/00032719.2015.1043661>.
- [49] Lippa, P. B.; Sokoll, L. J.; Chan, D. W. Immunosensors—Principles and Applications to Clinical Chemistry. *Clinica Chimica Acta* **2001**, *314* (1–2), 1–26. [https://doi.org/10.1016/S0009-8981\(01\)00629-5](https://doi.org/10.1016/S0009-8981(01)00629-5).
- [50] Vo-Dinh, T.; Sepaniak, M. J.; Griffin, G. D.; Alarie, J. P. Immunosensors: Principles and Applications. *ImmunoMethods* **1993**, *3* (2), 85–92. <https://doi.org/10.1006/immu.1993.1042>.
- [51] Schroeder, H. W.; Cavacini, L. Structure and Function of Immunoglobulins. *Journal of Allergy and Clinical Immunology* **2010**, *125* (2, Supplement 2), S41–S52. <https://doi.org/10.1016/j.jaci.2009.09.046>.
- [52] *Human Monoclonal Antibodies: Methods and Protocols*; Steinitz, M., Ed.; Methods in Molecular Biology; Springer: New York, NY, 2019; Vol. 1904. <https://doi.org/10.1007/978-1-4939-8958-4>.
- [53] Van Regenmortel, M. H. V. Specificity, Polyspecificity and Heterospecificity of Antibody-Antigen Recognition. In *HIV/AIDS: Immunochemistry, Reductionism and Vaccine Design: A Review of 20 Years of Research*; Van Regenmortel, M. H. V., Ed.;

- Springer International Publishing: Cham, 2019; pp 39–56.
https://doi.org/10.1007/978-3-030-32459-9_4.
- [54] Cristea, C.; Florea, A.; Tertiş, M.; Săndulescu, R.; Cristea, C.; Florea, A.; Tertiş, M.; Săndulescu, R. Immunosensors. In *Biosensors - Micro and Nanoscale Applications*; IntechOpen, 2015. <https://doi.org/10.5772/60524>.
- [55] Lim, S. A.; Ahmed, M. U. Introduction to Immunosensors. **2019**.
<https://doi.org/10.1039/9781788016162-00001>.
- [56] Yan, X.; Wang, T.; Yao, D.; Xu, J.; Luo, Q.; Liu, J. Interfacial Assembly of Signal Amplified Multienzymes and Biorecognized Antibody into Proteinosome for an Ultrasensitive Immunoassay. *Small* **2019**, *15* (15), 1900350.
<https://doi.org/10.1002/sml.201900350>.
- [57] Alhaji, M.; Zubair, M.; Farhana, A. Enzyme Linked Immunosorbent Assay. In *StatPearls*; StatPearls Publishing: Treasure Island (FL), 2023.
- [58] Luo, J.-X.; Yang, X.-C. Flow Injection Chemiluminescent Immunoassay with Para-Phenylphenol and Sodium Tetraphenylborate as Synergistic Enhancers. *Analytica Chimica Acta* **2003**, *485* (1), 57–62. [https://doi.org/10.1016/S0003-2670\(03\)00392-1](https://doi.org/10.1016/S0003-2670(03)00392-1).
- [59] Lin, J.; Yan, F.; Hu, X.; Ju, H. Chemiluminescent Immunosensor for CA19-9 Based on Antigen Immobilization on a Cross-Linked Chitosan Membrane. *Journal of Immunological Methods* **2004**, *291* (1), 165–174.
<https://doi.org/10.1016/j.jim.2004.06.001>.
- [60] Pei, X.; Zhang, B.; Tang, J.; Liu, B.; Lai, W.; Tang, D. Sandwich-Type Immunosensors and Immunoassays Exploiting Nanostructure Labels: A Review. *Analytica Chimica Acta* **2013**, *758*, 1–18. <https://doi.org/10.1016/j.aca.2012.10.060>.
- [61] Zhang, B.; Tang, D.; Liu, B.; Cui, Y.; Chen, H.; Chen, G. Nanogold-Functionalized Magnetic Beads with Redox Activity for Sensitive Electrochemical Immunoassay of Thyroid-Stimulating Hormone. *Analytica Chimica Acta* **2012**, *711*, 17–23.
<https://doi.org/10.1016/j.aca.2011.10.049>.
- [62] Segura-Gil, I.; Blázquez-Soro, A.; Galán-Malo, P.; Mata, L.; Tobajas, A. P.; Sánchez, L.; Pérez, M. D. Development of Sandwich and Competitive ELISA

- Formats to Determine β -Conglycinin: Evaluation of Their Performance to Detect Soy in Processed Food. *Food Control* **2019**, *103*, 78–85. <https://doi.org/10.1016/j.foodcont.2019.03.035>.
- [63] Jiang, X.; Li, D.; Xu, X.; Ying, Y.; Li, Y.; Ye, Z.; Wang, J. Immunosensors for Detection of Pesticide Residues. *Biosens Bioelectron* **2008**, *23* (11), 1577–1587. <https://doi.org/10.1016/j.bios.2008.01.035>.
- [64] Karunakaran, C.; Pandiaraj, M.; Santharaman, P. Immunosensors. In *Biosensors and Bioelectronics*; Elsevier, 2015; pp 205–245. <https://doi.org/10.1016/B978-0-12-803100-1.00004-9>.
- [65] Zhang, L.; Liu, Y.; Chen, T. A Mediatorless and Label-Free Amperometric Immunosensor for Detection of h-IgG. *International Journal of Biological Macromolecules* **2008**, *43* (2), 165–169. <https://doi.org/10.1016/j.ijbiomac.2008.04.010>.
- [66] Tang, H.; Chen, J.; Nie, L.; Kuang, Y.; Yao, S. A Label-Free Electrochemical Immunoassay for Carcinoembryonic Antigen (CEA) Based on Gold Nanoparticles (AuNPs) and Nonconductive Polymer Film. *Biosensors and Bioelectronics* **2007**, *22* (6), 1061–1067. <https://doi.org/10.1016/j.bios.2006.04.027>.
- [67] Loyprasert, S.; Thavarungkul, P.; Asawatreratanakul, P.; Wongkittisuksa, B.; Limsakul, C.; Kanatharana, P. Label-Free Capacitive Immunosensor for Microcystin-LR Using Self-Assembled Thiourea Monolayer Incorporated with Ag Nanoparticles on Gold Electrode. *Biosensors and Bioelectronics* **2008**, *24* (1), 78–86. <https://doi.org/10.1016/j.bios.2008.03.016>.
- [68] Wilson, R. The Use of Gold Nanoparticles in Diagnostics and Detection. *Chemical Society Reviews* **2008**, *37* (9), 2028–2045. <https://doi.org/10.1039/B712179M>.
- [69] Pollap, A.; Świt, P. Recent Advances in Sandwich SERS Immunosensors for Cancer Detection. *International Journal of Molecular Sciences* **2022**, *23* (9), 4740. <https://doi.org/10.3390/ijms23094740>.
- [70] Wang, L.; Hasanzadeh Kafshgari, M.; Meunier, M. Optical Properties and Applications of Plasmonic-Metal Nanoparticles. *Advanced Functional Materials* **2020**, *30* (51), 2005400. <https://doi.org/10.1002/adfm.202005400>.

- [71] Ngumbi, P. K.; Mugo, S. W.; Ngaruiya, J. M. Determination of Gold Nanoparticles Sizes via Surface Plasmon Resonance. *IOSR-JAC* **2018**, *11* (7), 25–29. <https://doi.org/10.9790/5736-1107012529>.
- [72] Hossain, S. M. Z.; Luckham, R. E.; Smith, A. M.; Lebert, J. M.; Davies, L. M.; Pelton, R. H.; Filipe, C. D. M.; Brennan, J. D. Development of a Bioactive Paper Sensor for Detection of Neurotoxins Using Piezoelectric Inkjet Printing of Sol–Gel-Derived Bioinks. *Anal. Chem.* **2009**, *81* (13), 5474–5483. <https://doi.org/10.1021/ac900660p>.
- [73] Martinez, A. W.; Phillips, S. T.; Whitesides, G. M.; Carrilho, E. Diagnostics for the Developing World: Microfluidic Paper-Based Analytical Devices. *Anal. Chem.* **2010**, *82* (1), 3–10. <https://doi.org/10.1021/ac9013989>.
- [74] Zhao, W.; Berg, A. van den. Lab on paper. *Lab on a chip* **2008**, *8* (12), 1988–1991. <https://doi.org/10.1039/b814043j>.
- [75] Qin, X.; Liu, J.; Zhang, Z.; Li, J.; Yuan, L.; Zhang, Z.; Chen, L. Microfluidic Paper-Based Chips in Rapid Detection: Current Status, Challenges, and Perspectives. *TrAC Trends in Analytical Chemistry* **2021**, *143*, 116371. <https://doi.org/10.1016/j.trac.2021.116371>.
- [76] M. Nargang, T.; Dierkes, R.; Bruchmann, J.; Keller, N.; Sachsenheimer, K.; Lee-Thedieck, C.; Kotz, F.; Helmer, D.; E. Rapp, B. Photolithographic Structuring of Soft, Extremely Foldable and Autoclavable Hydrophobic Barriers in Paper. *Analytical Methods* **2018**, *10* (33), 4028–4035. <https://doi.org/10.1039/C8AY01010B>.
- [77] Zhang, Y.; Ren, T.; He, J. Inkjet Printing Enabled Controllable Paper Superhydrophobization and Its Applications. *ACS Appl. Mater. Interfaces* **2018**, *10* (13), 11343–11349. <https://doi.org/10.1021/acsami.8b01133>.
- [78] Zhang, W.; Shen, W.; Weng, Y.; Lv, R.; Kang, F.; Huang, Z.-H. Steam Selective Etching: A Strategy to Effectively Enhance the Flexibility and Suppress the Volume Change of Carbonized Paper-Supported Electrodes. *ACS Nano* **2019**, *13* (5), 5731–5741. <https://doi.org/10.1021/acsnano.9b01173>.

- [79] Guo, R.; Chen, J.; Yang, B.; Liu, L.; Su, L.; Shen, B.; Yan, X. In-Plane Micro-Supercapacitors for an Integrated Device on One Piece of Paper. *Advanced Functional Materials* **2017**, *27* (43), 1702394. <https://doi.org/10.1002/adfm.201702394>.
- [80] Almeida, M. I. G. S.; Jayawardane, B. M.; Kolev, S. D.; McKelvie, I. D. Developments of Microfluidic Paper-Based Analytical Devices (μ PADs) for Water Analysis: A Review. *Talanta* **2018**, *177*, 176–190. <https://doi.org/10.1016/j.talanta.2017.08.072>.
- [81] Altundemir, S.; Uguz, A. K.; Ulgen, K. A Review on Wax Printed Microfluidic Paper-Based Devices for International Health. *Biomicrofluidics* **2017**, *11* (4), 041501. <https://doi.org/10.1063/1.4991504>.
- [82] Cinti, S.; Arduini, F. Graphene-Based Screen-Printed Electrochemical (Bio)Sensors and Their Applications: Efforts and Criticisms. *Biosensors and Bioelectronics* **2017**, *89*, 107–122. <https://doi.org/10.1016/j.bios.2016.07.005>.
- [83] Ghosh, R.; Gopalakrishnan, S.; Savitha, R.; Renganathan, T.; Pushpavanam, S. Fabrication of Laser Printed Microfluidic Paper-Based Analytical Devices (LP- μ PADs) for Point-of-Care Applications. *Sci Rep* **2019**, *9* (1), 7896. <https://doi.org/10.1038/s41598-019-44455-1>.
- [84] Yamada, K.; Shibata, H.; Suzuki, K.; Citterio, D. Toward Practical Application of Paper-Based Microfluidics for Medical Diagnostics: State-of-the-Art and Challenges. *Lab on a Chip* **2017**, *17* (7), 1206–1249. <https://doi.org/10.1039/C6LC01577H>.
- [85] Bahadır, E. B.; Sezgintürk, M. K. Lateral Flow Assays: Principles, Designs and Labels. *TrAC Trends in Analytical Chemistry* **2016**, *82*, 286–306. <https://doi.org/10.1016/j.trac.2016.06.006>.
- [86] O'Farrell, B. Lateral Flow Technology for Field-Based Applications - Basics and Advanced Developments. *Topics in Companion Animal Medicine* **2015**, *30* (4), 139–147.

- [87] Eltzov, E.; Guttel, S.; Low Yuen Kei, A.; Sinawang, P. D.; Ionescu, R. E.; Marks, R. S. Lateral Flow Immunoassays – from Paper Strip to Smartphone Technology. *Electroanalysis* **2015**, *27* (9), 2116–2130. <https://doi.org/10.1002/elan.201500237>.
- [88] Li, J.; Macdonald, J. Multiplexed Lateral Flow Biosensors: Technological Advances for Radically Improving Point-of-Care Diagnoses. *Biosensors and Bioelectronics* **2016**, *83*, 177–192. <https://doi.org/10.1016/j.bios.2016.04.021>.
- [89] Shafique, H.; de Vries, J.; Strauss, J.; Jahromi, A. K.; Moakhar, R. S.; Mahshid, S. Advances in the Translation of Electrochemical Hydrogel-Based Sensors. *Advanced Healthcare Materials* **2022**, *12* (1). <https://doi.org/10.1002/adhm.202201501>.
- [90] Herrmann, A.; Haag, R.; Schedler, U. Hydrogels and Their Role in Biosensing Applications. *Advanced Healthcare Materials* **2021**, *10* (11), 2100062. <https://doi.org/10.1002/adhm.202100062>.
- [91] Völlmecke, K.; Afroz, R.; Bierbach, S.; Brenker, L. J.; Frücht, S.; Glass, A.; Giebelhaus, R.; Hoppe, A.; Kanemaru, K.; Lazarek, M.; Rabbe, L.; Song, L.; Velasco Suarez, A.; Wu, S.; Serpe, M.; Kuckling, D. Hydrogel-Based Biosensors. *Gels* **2022**, *8* (12), 768. <https://doi.org/10.3390/gels8120768>.
- [92] Razavi, M. *Biomaterials for Tissue Engineering*; Bentham Science Publishers, 2017.
- [93] Zhang, H.; Cheng, J.; Ao, Q. Preparation of Alginate-Based Biomaterials and Their Applications in Biomedicine. *Marine Drugs* **2021**, *19* (5), 264. <https://doi.org/10.3390/md19050264>.
- [94] Lin, K.; Zhang, D.; Macedo, M. H.; Cui, W.; Sarmiento, B.; Shen, G. Advanced Collagen-Based Biomaterials for Regenerative Biomedicine. *Advanced Functional Materials* **2019**, *29* (3), 1804943. <https://doi.org/10.1002/adfm.201804943>.
- [95] Li, S.; Pei, M.; Wan, T.; Yang, H.; Gu, S.; Tao, Y.; Liu, X.; Zhou, Y.; Xu, W.; Xiao, P. Self-Healing Hyaluronic Acid Hydrogels Based on Dynamic Schiff Base Linkages as Biomaterials. *Carbohydrate Polymers* **2020**, *250*, 116922. <https://doi.org/10.1016/j.carbpol.2020.116922>.
- [96] Ho, T.-C.; Chang, C.-C.; Chan, H.-P.; Chung, T.-W.; Shu, C.-W.; Chuang, K.-P.; Duh, T.-H.; Yang, M.-H.; Tyan, Y.-C. Hydrogels: Properties and Applications in

- Biomedicine. *Molecules* **2022**, *27* (9), 2902.
<https://doi.org/10.3390/molecules27092902>.
- [97] Bashir, S.; Hina, M.; Iqbal, J.; Rajpar, A. H.; Mujtaba, M. A.; Alghamdi, N. A.; Wageh, S.; Ramesh, K.; Ramesh, S. Fundamental Concepts of Hydrogels: Synthesis, Properties, and Their Applications. *Polymers* **2020**, *12* (11), 2702.
<https://doi.org/10.3390/polym12112702>.
- [98] Zhang, C.; Losego, M. D.; Braun, P. V. Hydrogel-Based Glucose Sensors: Effects of Phenylboronic Acid Chemical Structure on Response. *Chem. Mater.* **2013**, *25* (15), 3239–3250. <https://doi.org/10.1021/cm401738p>.
- [99] Bhat, A.; Amanor-Boadu, J. M.; Guiseppi-Elie, A. Toward Impedimetric Measurement of Acidosis with a pH-Responsive Hydrogel Sensor. *ACS Sens.* **2020**, *5* (2), 500–509. <https://doi.org/10.1021/acssensors.9b02336>.
- [100] Peppas, N. A.; Van Blarcom, D. S. Hydrogel-Based Biosensors and Sensing Devices for Drug Delivery. *Journal of Controlled Release* **2016**, *240*, 142–150. <https://doi.org/10.1016/j.jconrel.2015.11.022>.
- [101] Abune, L.; Davis, B.; Wang, Y. Aptamer-functionalized Hydrogels: An Emerging Class of Biomaterials for Protein Delivery, Cell Capture, Regenerative Medicine, and Molecular Biosensing. *WIREs Nanomedicine and Nanobiotechnology* **2021**, *13* (6). <https://doi.org/10.1002/wnan.1731>.
- [102] Nagamine, K.; Mano, T.; Nomura, A.; Ichimura, Y.; Izawa, R.; Furusawa, H.; Matsui, H.; Kumaki, D.; Tokito, S. Noninvasive Sweat-Lactate Biosensor Employing a Hydrogel-Based Touch Pad. *Sci Rep* **2019**, *9* (1), 10102. <https://doi.org/10.1038/s41598-019-46611-z>.
- [103] Wang, L.; Xu, T.; Zhang, X. Multifunctional Conductive Hydrogel-Based Flexible Wearable Sensors. *TrAC Trends in Analytical Chemistry* **2021**, *134*, 116130. <https://doi.org/10.1016/j.trac.2020.116130>.
- [104] Chen, C.; Wang, J. Optical Biosensors: An Exhaustive and Comprehensive Review. *Analyst* **2020**, *145* (5), 1605–1628. <https://doi.org/10.1039/C9AN01998G>.

- [105] Martinkova, P.; Kostelnik, A.; Valek, T.; Pohanka, M. >Main Streams in the Construction of Biosensors and Their Applications. *International Journal of Electrochemical Science* **2017**, *12* (8), 7386–7403. <https://doi.org/10.20964/2017.08.02>.
- [106] Touhami, A. *Biosensors and Nanobiosensors: Design and Applications*; Nanomedicine, 2014.
- [107] Lazcka, O.; Campo, F. J. D.; Muñoz, F. X. Pathogen Detection: A Perspective of Traditional Methods and Biosensors. *Biosensors and Bioelectronics* **2007**, *22* (7), 1205–1217. <https://doi.org/10.1016/j.bios.2006.06.036>.
- [108] Vacher, M.; Fdez. Galván, I.; Ding, B.-W.; Schramm, S.; Berraud-Pache, R.; Naumov, P.; Ferré, N.; Liu, Y.-J.; Navizet, I.; Roca-Sanjuán, D.; Baader, W. J.; Lindh, R. Chemi- and Bioluminescence of Cyclic Peroxides. *Chem. Rev.* **2018**, *118* (15), 6927–6974. <https://doi.org/10.1021/acs.chemrev.7b00649>.
- [109] Hesari, M.; Ding, Z. Spooling Electrochemiluminescence Spectroscopy: Development, Applications and Beyond. *Nat Protoc* **2021**, *16* (4), 2109–2130. <https://doi.org/10.1038/s41596-020-00486-x>.
- [110] Moroni, G.; Calabria, D.; Quintavalla, A.; Lombardo, M.; Mirasoli, M.; Roda, A.; Gioiello, A. Thermochemiluminescence-Based Sensitive Probes: Synthesis and Photophysical Characterization of Acridine-Containing 1,2-Dioxetanes Focusing on Fluorophore Push-Pull Effects. *ChemPhotoChem* **2022**, *6* (1), e202100152. <https://doi.org/10.1002/cptc.202100152>.
- [111] Roda, A. *Chemiluminescence and Bioluminescence: Past, Present and Future*; Royal Society of Chemistry, 2011.
- [112] Créton, R.; Jaffe, L. F. Chemiluminescence Microscopy as a Tool in Biomedical Research. *BioTechniques* **2001**, *31* (5), 1098–1105. <https://doi.org/10.2144/01315rv01>.
- [113] Rizzo, F. Optical Immunoassays Methods in Protein Analysis: An Overview. *Chemosensors* **2022**, *10* (8), 326. <https://doi.org/10.3390/chemosensors10080326>.

- [114] Roda, A.; Pasini, P.; Guardigli, M.; Baraldini, M.; Musiani, M.; Mirasoli, M. Bio- and Chemiluminescence in Bioanalysis. *Fresenius J Anal Chem* **2000**, *366* (6), 752–759. <https://doi.org/10.1007/s002160051569>.
- [115] Dotsikas, Y.; Loukas, Y. L. Employment of 4-(1-Imidazolyl)Phenol as a Luminol Signal Enhancer in a Competitive-Type Chemiluminescence Immunoassay and Its Comparison with the Conventional Antigen–Horseradish Peroxidase Conjugate-Based Assay. *Analytica Chimica Acta* **2004**, *509* (1), 103–109. <https://doi.org/10.1016/j.aca.2003.12.007>.
- [116] Dotsikas, Y.; Loukas, Y. L. Effect of the Luminol Signal Enhancer Selection on the Curve Parameters of an Immunoassay and the Chemiluminescence Intensity and Kinetics. *Talanta* **2007**, *71* (2), 906–910. <https://doi.org/10.1016/j.talanta.2006.05.068>.
- [117] Marzocchi, E.; Grilli, S.; Della Ciana, L.; Prodi, L.; Mirasoli, M.; Roda, A. Chemiluminescent Detection Systems of Horseradish Peroxidase Employing Nucleophilic Acylation Catalysts. *Analytical Biochemistry* **2008**, *377* (2), 189–194. <https://doi.org/10.1016/j.ab.2008.03.020>.
- [118] Chouhan, R. S.; Vivek Babu, K.; Kumar, M. A.; Neeta, N. S.; Thakur, M. S.; Amitha Rani, B. E.; Pasha, A.; Karanth, N. G. K.; Karanth, N. G. Detection of Methyl Parathion Using Immuno-Chemiluminescence Based Image Analysis Using Charge Coupled Device. *Biosensors and Bioelectronics* **2006**, *21* (7), 1264–1271. <https://doi.org/10.1016/j.bios.2005.05.018>.
- [119] Wolter, A.; Niessner, R.; Seidel, M. Preparation and Characterization of Functional Poly(Ethylene Glycol) Surfaces for the Use of Antibody Microarrays. *Anal. Chem.* **2007**, *79* (12), 4529–4537. <https://doi.org/10.1021/ac070243a>.
- [120] Cheek, B. J.; Steel, A. B.; Torres, M. P.; Yu, Y.-Y.; Yang, H. Chemiluminescence Detection for Hybridization Assays on the Flow-Thru Chip, a Three-Dimensional Microchannel Biochip. *Anal. Chem.* **2001**, *73* (24), 5777–5783. <https://doi.org/10.1021/ac0108616>.

Proposal for the thesis

The theme of this thesis is the development of miniaturized analytical devices based on biospecific molecular recognition reactions, i.e. enzyme-based and immuno biosensors, which exploit chemiluminescence (CL) as detection technique. In Chapter 3, an investigation into paper-based immunosensors based on bioluminescent and chemiluminescent detection was conducted, to learn about the state of the art and the importance of this category of devices. The use of biospecific assays combined with chemiluminescent (CL) detection and paper-based technology offers an optimal approach to creating portable analytical tools for on-site applications. The distinctive features of these elements combine to create an exclusive synergy for meeting point of care (POC) needs. However, the translation of scientific advances into everyday use of such devices is lagging behind. This chapter attempts to highlight the remaining challenges responsible for this disparity and to identify the specific areas that require concentrated and focused research to enable the practical implementation of these methods in routine analysis. In Chapter 4, the development of a fully autonomous lab-on-chip platform for performing CL – based bioassays was investigated. A microfluidic paper-based analytical device (μ PAD) designed in an origami-like format was employed, which offers the advantage of preloading all reagents in a dried form onto the paper substrate, facilitating both device design and analytical procedures. The intention behind the device, which was incorporated into the AstroBio CubeSat (ABCS) nanosatellite, is

twofold: firstly, to validate the technology's performance in space, and secondly, to assess the functionality of the device and the durability of the (bio)molecules used in the assays when exposed to a radiation-rich environment. Chapter 5 reports the development of a novel origami paper-based device for the detection of ovalbumin (OVA) in food samples. This innovative biosensor uses a competitive immunoassay coupled with chemiluminescence detection. The use of magnetic microbeads plays a key role in the device preparation by facilitating the easy and efficient immobilization of OVA on paper. Immobilized OVA then competes with the naturally occurring OVA in the sample for a limited amount of enzyme (HRP)-labelled anti-OVA antibody. Using the origami design, a series of analytical steps can be performed using reagents preloaded on different paper layers, resulting in a convenient and ready-to-use immunosensing platform. In Chapter 6 a smartphone-based CL biosensor for the detection of H₂O₂ and glucose was developed. In particular, a binary guanosine hydrogel was prepared and loaded with a CL reagent (luminol) and a catalytic cofactor (hemin). Subsequently, the hydrogel was modified by incorporating glucose oxidase (GOD) enzyme to enable glucose biosensing. To enable point-of-care (POC) applications, the emitted photons were detected using a portable device equipped with a smartphone's CMOS (complementary metal oxide semiconductor) camera for CL emission detection.

Paper – Based Immunosensors with Bio – Chemiluminescence Detection

Reproduced from: “Paper – Based Immunosensors with Bio – Chemiluminescence Detection”

Maria Maddalena Calabretta, Martina Zangheri, Donato Calabria, Antonia Lopreside, Laura Montali, Elisa Marchegiani, Ilaria Trozzi, Massimo Guardigli, Mara Mirasoli

Sensors, 2021, 21(13), 4309

<https://doi.org/10.3390/s21134309>

Reproduced by the permission of MDPI (Open Access Article)

<https://creativecommons.org/licenses/by/4.0/>

3.1 Introduction

Immunoassays have been routinely used in laboratories equipped with bulky instrumentation and skilled personnel for the quantification of target analytes for various applications in healthcare, food safety and environmental monitoring. In recent years, research has mainly focused on making the immunoassay technique suitable for portable analytical formats, to perform low-cost tests directly on site [1]. Indeed, thanks to their selectivity and specificity, immunoassays allow the detection of analytes within complex matrices without the need for long-processing sample pretreatments. Among portable formats suitable for the development of point-of-care (POC) immunoassays, the paper-based approach has attracted strong interest thanks to its advantageous features, including low cost, straightforward procedures, flexibility of the paper-based support, short turnaround time and small consumption of samples and reagents. For these reasons, paper-based POC immunoassays are expected to become a feasible option for monitoring human healthcare, food safety or water quality in resource-limited settings and, thanks to the recent improvements in microfluidics and nanotechnologies, they have developed rapidly in recent years [1]. Among the different varieties of paper-based format biosensors, those combined most frequently with immunoassays are lateral-flow immunoassays (LFIA) and microfluidic paper-based devices (μ PADs) [2]. LFIA is an integrated platform in which pre-stored reagents are entrapped on a nitrocellulose strip. By adding the sample, these reagents are solubilized and, while they are flowing through the membrane, bioassays take place. On the surface of the nitrocellulose strip, different areas contain specific probes responsible for the recognition and detection of the target analyte. It is possible to exploit different bioassay formats, including sandwich, competitive or multiplex formats. As an alternative, μ PADs are characterized by the presence of hydrophilic and hydrophobic microchannels, which allow to develop different designs suitable for the desired application. The microfluidic pattern is generally obtained by exploiting chemical printing and/or cutting and it is possible to develop 2D or 3D configurations for moving fluids through vertical and horizontal pathways [2, 3]. The analytical performance of miniaturized analytical devices represents

the bottleneck when high sensitivity is required, such as for the detection of analytes present at trace levels in complex matrices [4, 5]. For this reason, one of the most important aspects in the development of these methods is the selection of the detection technique since it has to combine high sensitivity with reduced sensing equipment, providing the possibility of working with portable and low-cost devices and ease of operation even by non-specialized personnel [5]. Several attempts to avail popular detection methods, such as UV/Vis absorption spectroscopy [6, 7, 8, 9], have been reported in literature but the most promising techniques are those based on electrochemical and luminescence detection. In particular, chemical luminescence is based on the production of photons triggered by a chemical reaction, as for chemiluminescence (CL), and, when the reaction occurs within living organisms, the phenomenon is called bioluminescence (BL). Since BL and CL reactions start in the dark, photons can be measured with high efficiency ensuring the absence of nonspecific signals, thus avoiding the background commonly encountered with photoluminescence measurements. For this reason, CL-based analytical methods can achieve, in principle, high detectability and can represent an alternative or a complementary approach in the field of optical biosensors [10]. Together with their high sensitivity, CL and BL allow to work with a wide linear range, no radioactive reagents and simple equipment making them an ideal detection principle for POC analytical instrumentation [11]. *Figure 1* schematizes the advantages in combining paper-based immunosensors with CL and BL detection.

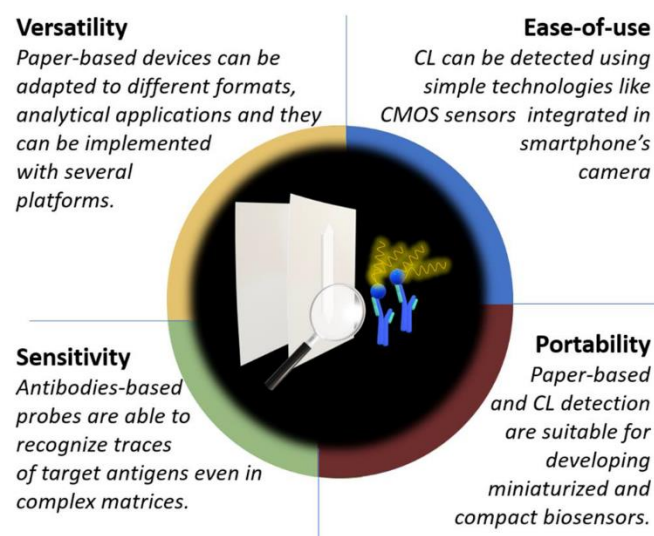
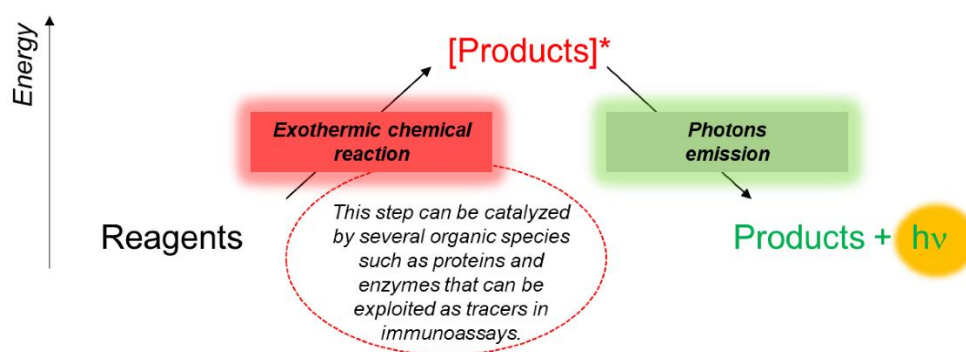


Figure 1. Scheme of the advantages obtained by combining paper-based immunosensor with CL detection.

The photons produced by CL reactions are due to the returns of a molecule to the ground state after the excitation to the singlet excited state reached through an exothermic chemical reaction (*Scheme 1*).



Scheme 1. Schematic representation of bio-chemiluminescent reactions.

The wavelengths typical of the CL emission are in the range of the visible and infrared spectrum [12, 13]. Since it occurs in living organisms, the BL phenomenon is generally based on the catalytic activity of enzymes (e.g., luciferases) or photoproteins [14]. BL and CL detection principles can be used in immunoassays by exploiting an enzymatic-label conjugate to an immunoreagent and a specific BL or CL substrate. Using either BL or CL, a significant amplification of the analytical signal (about 10⁴–10⁵ times) can be achieved thanks to the characteristic enzymatic turnover [15]. Horseradish peroxidase (HRP) is probably the most used CL label. HRP is able to catalyze the oxidation of luminol in the presence of a peroxide which leads to the formation of aminophthalate in a singlet excited state. The decay of this species to the ground state brings about the release of photons at a characteristic wavelength (428 nm) [16]. HRP shows good stability combined with a high enzymatic turnover number, making it an excellent candidate for CL-based biospecific assays. By adding to the CL cocktails suitable enhancers acting as electron transfer mediators (e.g., substituted phenols, substituted boronic acids, indophenols, N-alkyl phenothiazines [17] and 4-dialkylaminopyridine [18]), it is possible to increase the signal intensity and to stabilize the CL signal over time.

Firefly luciferase is the most exploited BL protein and it acts by catalyzing the formation of luciferyl-adenylate (LH2-AMP) from D-luciferin (D-LH2) and ATP. LH2-AMP is then involved in a multi-step oxidative process that leads to the formation of an excited product which drives the emission of photons at 550–570 nm. While firefly luciferase emission can be modulated by changing the environmental conditions (e.g., pH, temperature, light emissions of BL), reactions involving click beetles and rail-road worms do not depend on pH and temperature [19]. A significant advantage of using BL reactions is the high quantum yield of luciferase-catalyzed reactions (i.e., 44% for *Photinus pyralis* luciferase) that provide unbeatable sensitivities [20]. Exploiting genetic fusion of the luciferase to an antibody fragment and chemical conjugation of luciferases to monoclonal antibodies, several BL antibodies were used in bioanalytical assay and imaging techniques [21]. Add-and-read homogeneous immunoassays using the NanoLuc Binary Technology (NanoBiT), a protein complementation system based on NanoLuc luciferase, were successfully developed to monitor multiple signaling pathways' activation [22] and to detect the mycotoxin fumonisin B1 [23]. Currently, the coupling of these methods with new nanomaterials (e.g., gold nanoparticles, quantum dots and magnetic materials) promoted a great breakthrough in the effectiveness of these techniques [24, 25]. From the point of view of signal enhancement, several improvements made these techniques suitable for the ultrasensitive detection of target analytes, even in paper-based biosensor formats [4, 26]. Despite this, however, there are still open issues that need to be further investigated to promote a wider use and diffusion of CL/BL paper-based immunoassays for POC applications. One of the main issues is certainly due to the fact that such bioassays rely on bioreagents (e.g., enzymes and small-molecule substrates) that are not stable and require dedicated shipping and storage conditions such as dry ice and special packaging. These bioreagents can be affected by thermal denaturation and/or chemical modification, oxidation or hydrolysis processes [27 28]. The requirement of a strict cold chain hampers their use for on-site applications, especially in remote areas and developing countries [29]. For these applications, the implementation of BL is critical since luciferases and most of their substrates are very sensitive to environmental conditions and are often characterized by

a short shelf-life, thus requiring very precise storage temperatures. For this reason, the use of BL-immunoassay in the field of paper-based biosensors is quite limited. A promising approach has been recently reported by Hall et al. who developed a shelf-stable BL homogenous immunoassay reagent, in which all components were immobilized in a lyophilized cake, based on a Nanoluc complementation reporter system [30]. Another limitation to the use of CL and BL detections for paper immunoassays is connected to the requirement of substrate for triggering the luminescent reaction, making more complex the design of the analytical device and increasing its cost. The purpose of this review is to introduce the newest and most significant progress in the field of biosensors based on immunoassays coupled with paper format and CL-BL detection principle, evaluating the great improvements in sensitivity thanks to the use of innovative materials and enhancers and critically highlighting the main hurdles to real-life applicability in order to promote a targeted research for making these devices ready for their effective use.

3.2 Nanomaterials for Signal Enhancement of Chemiluminescence

The main limitations of CL-based detection are linked to the weakness of the light signals and short luminescence time [31]. Conventionally, for increasing the intensity of the signals and the stability of light emission over time, enhancers have been used to increase the sensitivity for CL-based immunoassays [32]. The aim is to achieve similar analytical performance of standard laboratory-based immunoassays which are able to detect target analytes even at the apto- zepto-molar levels with wide dynamic ranges (up to six orders of magnitude) [33]. In addition to the continuous progress made regarding enhancers development, different nanomaterials have recently been proposed as catalysts or chemicals carriers for enhancing CL signals [34, 35]. In *Table 1* the main strategies for enhancing the CL signal exploiting nanomaterials are reported. Metal nanoparticles (MNPs)-based enhanced CL have been extensively studied thanks to the

strong catalytic properties of MNPs, such as silver (Ag), gold (Au) and platinum (Pt), that allow to increase the surface area and surface electron density in CL reactions [36]. Furthermore, the MNPs are very frequently used for the development of paper-based devices as they are easy to immobilize by absorption and they are effectively re-solubilized with the flowing of a liquid phase. AuNPs have been widely employed since they combine the catalysis of the CL reaction and the easiness of conjugation with different kinds of chemicals and biomolecules (e.g., luminol, enzymes, antibodies, DNAszymes, etc.). Recently, Han et al. [37] developed a CL-LFIA biosensing platform incorporating AuNPs into a polymer-networked HRP with an antibody (Au-polyHRP-AB) as a new scheme for enhanced enzyme conjugation. This approach involved a mass-producible and time-programmable amplification process based on a water-swellable polymer that allows to automate sequential reactions (immunoassay and signal amplification). The authors developed a specific part of the analytical device (amplification part) using the water-swellable polymer as a fluid switch and integrated it into the platform for triggering automated sequential reactions. The amplification part was produced using fabrication methods (lamination, cutting and assembly) that are widespread and well known in the LFIA industry. The test strip and amplification part were then integrated into a single device through a comprehensive housing assembly. The developed platform was used to quantitatively evaluate cardiac troponin I (cTnI) in serum samples, within 20 min obtaining a detection range of six orders of magnitude and a detection limit of 0.84 pg mL^{-1} when compared to the standard laboratory equipment, making it suitable for clinical use. Hua Cui's group proposed the simultaneous determination of three acute myocardial infarction (AMI) biomarkers by a three-dimensional (3D) μ PAD exploiting a time-resolved CL emission approach [38]. They immobilized on the test zone a primary antibody functionalized with AuNPs (Ab1-AuNPs), and a secondary antibody labeled with both Co(II) catalyst luminol and AuNPs (Co(II)-Ab2-luminol-AuNPs). The CL activity of Co(II)-Ab2-luminol-GNPs was due to the simultaneous catalytic effect of Co(II) and GNPs. Indeed, Co(II) catalyzed the decomposition of H_2O_2 , generating the hydroxyl radical $\cdot\text{OH}$ and a luminol radical which further reacted with O_2 to produce an O_2^- radical. The catalytic effect of Co(II)

was enhanced by the coordination of Co(II) to the surface of luminol-GNPs. The reaction between the luminol radical and O_2^- radical was responsible for the strong CL emission. Another effect promoting a further amplification was the presence of COO-groups in Ab2 and BSA that could also react with the O_2^- radical, forming reactive $-CO_4^{2-}$ radicals. Moreover, GNPs could also bind a large number of luminol molecules and Co(II) catalyst, resulting in further enhanced CL signal. CL immunoreactions were performed at three detection zones by assembling Ab1-AuNPs, antigen and Co(II)-Ab2-luminol-AuNPs. Thanks to the flow of H_2O_2 to different detection zones at different times, CL signals were temporally resolved allowing a multiplexing analysis format. Another example of MNPs-enhanced CL was reported by Zong et al. [39] who developed an immunoassay for the detection of C-reactive protein (CRP) exploiting two AgNP probes, i.e., probe A, composed of DNA-hemin/DNA-A/biotin-DNA modified with AgNPs, and probe B, consisting in DNA-hemin/DNA-B modified with AgNPs. By DNA-A and DNA-B hybridization, a CL signal was generated. Thanks to the high content of hemin molecules, the AgNP hybrid probes showed excellent CL signal amplification, allowing a detection limit for CRP down to $0.05 \text{ ng}\cdot\text{mL}^{-1}$ (Figure 2a).

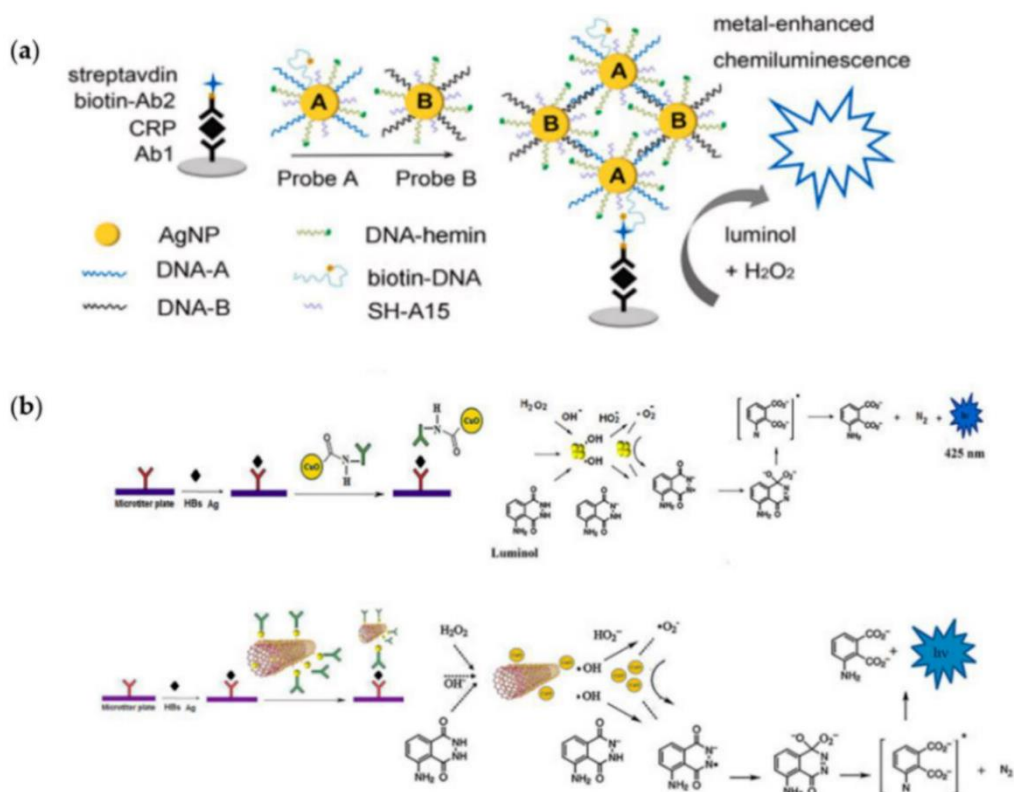


Figure 2. Nanomaterials for CL signal enhancement: **(a)** a novel silver nanoparticle hybrid probe designed for ultrasensitive metal-enhanced CL immunoassay of the marker of cerebrovascular disease. Reprinted with permission from ref. [39]. Copyright 2019 Elsevier.; **(b)** a sandwich-type CL immunoassay using the as-prepared CuONPs–Ab conjugate and a sandwich-type CL immunoassay using the as-prepared Ab-MWCNT/CuONPs conjugate. Reprinted with permission from ref. [49]. Copyright 2017 Elsevier.

In addition to MNPs, quantum dots (QDs), have gained great attraction as catalysts of CL reactions [40]. In particular, they act in two different steps: firstly, they take part in the decomposition of H_2O_2 to generate free radicals, and secondly, they promote CL by energy transfer and electron transfer annihilation effects. Since QDs enhance the CL signal by serving as the direct CL emitters/catalyzer of redox CL reactions, they are usually employed for the development of electrochemiluminescent (ECL)-based biosensors. In this case, the light is produced as a result of a chemical reaction triggered by either direct oxidation of CL reagents or indirect enhancing/inhibitory effects of certain luminescent compounds [41]. For this reason, several QD-ECL-based biosensors have been reported in literature for the detection of proteins [42, 43], small molecules [44] and cells [45]. As an alternative to conventional QDs, carbon nanomaterials (CNMs) have emerged to improve CL systems, thanks to their low toxicity, environmental friendliness, low cost and simple synthetic routes [46]. In particular, carbon nanoparticles (CNPs), graphene, graphene oxide (GO) and carbon nanotubes (CNTs), possess unique optical, catalytic and biocompatible properties. A paper-based CL immunodevice was described for sensitive determination of the carcinoembryonic antigen by Chen et al. [47]. Capture antibody was immobilized on the paper-based chip following a plasma treatment of the paper surface. A detection antibody was obtained by its labeling with carbon nanospheres functionalized with HRP (multi-HRP-HCS-Ab2). The authors exploited highly carbonized nanospheres (HCS), which showed abundant carboxyl groups on their surface, functioning as an ideal carrier for signal molecule loading. Multiple enzymes can be immobilized on HCS through carboxyl groups leading to signal enhancement. In this case, the detection antibody, multi-HRP-HCS-Ab2, was not pre-stored on the paper-surface but it was added by the operator after the sample

incubation during the detection step. TiO₂ nanoparticles coated multiwalled carbon nanotubes (TiO₂/MWCNTs) were synthesized as an amplification catalyst label by Li et al. [48]. A capture antibody was immobilized on modified-chitosan paper membrane and, after the recognition reaction, the TiO₂/MWCNTs were used as catalysts for the luminol-p-iodophenol-H₂O₂ CL system, producing an enhanced CL emission. They applied the developed bioassay to detect prostate-specific antigen demonstrating a good linear response range from 0.001 to 20 ng/mL with a detection limit of 0.8 pg/mL. Another study reported the comparison of CuO nanoparticles and CuO/MWCNT nanocomposites as enhancers for CL immunoassays for detection of the hepatitis B surface antigen [49]. CuO nanoparticles and CuO/MWCNT nanocomposites significantly enhanced the luminol CL intensity, and the detection limits (1.8 and 0.85 ng·mL⁻¹, respectively) were comparable with those obtained with a clinical routine CL immunoassay (*Figure 2b*). Currently, the combination of nanomaterials-based enhanced CL-immunoassays with paper platform is still at the proof-of-concept stage, but the interesting results reported in literature show that it is a promising strategy for developing a great variety of sensitive analytical methods and further in-depth studies will be required to identify the best approaches.

Nanomaterial	Enhancement Mechanism Exploiting Luminol/H ₂ O ₂ CL System	Features	Ref.
Metal nanoparticles (AgNPs, AuNPs, PtNPs, etc.)	MNPs catalyze the decomposition of H ₂ O ₂ leading to the formation of a hydroxyl radical, which reacts with a luminol anion and HO ₂ ⁻ . These species are involved in the production of a luminol radical and a superoxide anion leading to light emission. The radical generation and electron transfer processes take place on the surface of the MNPs, which are therefore responsible for the facilitation of these processes.	<ul style="list-style-type: none"> • chemical reactivity • catalytic properties • surface properties • biocompatibility • ease of self-assembly 	[50]
Quantum dots	Quantum dots act first by decomposing H ₂ O ₂ to generate free radicals and then promoting CL by energy transfer and electron transfer annihilation effects.	<ul style="list-style-type: none"> • catalytic properties for redox reactions • size-dependent catalytic action 	[41]

Nanomaterial	Enhancement Mechanism Exploiting Luminol/H ₂ O ₂ CL System	Features	Ref.
		<ul style="list-style-type: none"> • controllable charge-electron-transfer events, • biocompatibility 	
Carbon nanomaterials(carbon nanoparticles (CNPs), graphene, graphene oxide (GO) and carbon nanotubes (CNTs))	<p>A possible mechanism involves the reaction between carbon materials with π-rich electronic structures and luminol allowing the formation of the activated transition complex. This complex may accelerate electron-transfer processes during the luminol-dissolved oxygen CL reaction.</p>	<ul style="list-style-type: none"> • low toxicity, environmental friendliness • low cost • simple synthetic routes • tunable catalytic activities depending on surface functionalization 	[51]

Table 1. Nanomaterials and related mechanism proposed for CL enhancement.

3.3 Fluid Control and Fluid Handling

Microfluidic paper-based (μ PADs) analytical devices provide an alternative platform for liquid transport via capillary forces without the need for external pumps [52] and they can be easily implemented for multiplexed analysis by simply adding channels [3]. Moreover, hydrophobic patterning can be employed to spatially confine the flow of hydrophilic solvent including biofluids [53]. Fabrication techniques include photolithography, wax printing, screen printing, inkjet printing and plasma oxidation [54]. The use of wax as the blocking material to construct microfluidic platforms (*Figure 3a*) has become a major trend; indeed it guarantees simplicity, rapidity, low-cost, suitability for producing prototypal μ PADs on a large scale [55]. Among the different methods for wax patterning (including use of wax pens, screen printing and direct printing by wax printers), painting with a wax pen is the simplest method since hydrophobic barriers (*Figure 3b*) are easily obtained and characterized by high flexibility [56].

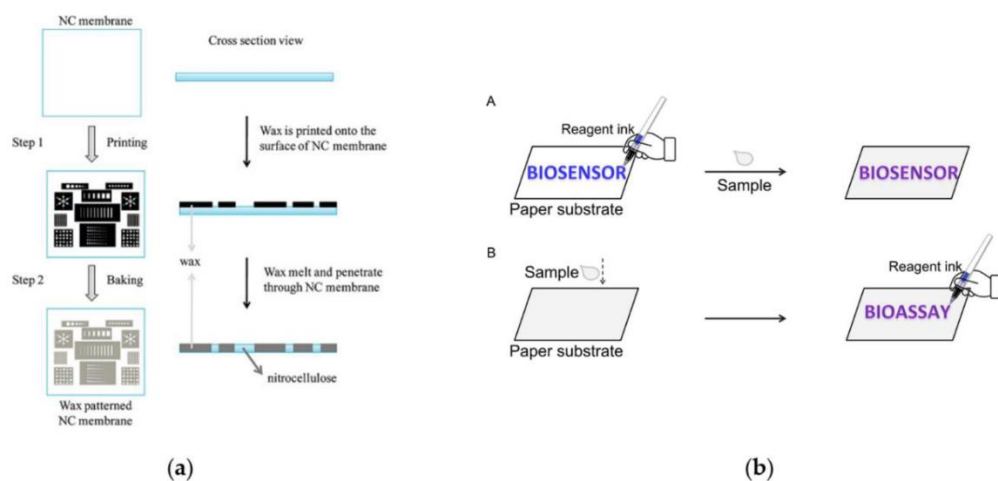


Figure 3. Fluid control and fluid handling: **(a)** schematic illustration of processes to fabricate paper-based microfluidics in an NC membrane by wax printing. It includes mainly two steps: step 1 is to print the wax pattern onto the surface of the NC membrane with a wax printer; step 2 is to bake the wax-printed NC membrane in an oven at 125 °C for 5 min to let the wax melt and penetrate through the membrane fully. Reprinted with permission from [55]. Copyright (2010) American Chemical Society. **(b)** Design of "pen-writing" technique. (A) When writing biosensors on paper, the sensing elements are directly written to form patterned paper biosensors and would be expected to function at the initial location after introduction of samples leading to the fact that the colored product may not stick in the area where these biomolecules are written. (B) The proposed approach is not dependent on hydrophobic barriers to define the patterning of paper substrates, providing an alternative for sensor fabrication. Paper substrates are directly employed for the collection and transportation of samples, and then the reagent ink pen is used for sample analysis Reprinted with permission from [56]. Copyright 2019 Elsevier.

Yang et al. used a crayon and a pencil to construct a hand-drawn and written pen-on-paper electrochemiluminescence immunodevice for POCT [57]. Using wax printing technology, Wang et al., developed a portable analytical device based on CL immunoassay integrated into a low-cost μ -PAD by covalently immobilizing capture antibody on a chitosan membrane [58]. Exploiting tumor markers as target analytes and paper microzone plate as platform, the application of the proposed system was successfully optimized achieving a linear range of 0.1–35.0 ng mL⁻¹ for α -fetoprotein, 0.5–80.0 U mL⁻¹ for cancer antigen 125 and 0.1–70.0 ng mL⁻¹ for carcinoembryonic antigen. The combination of chitosan modification and wax-screen-printing methodology for μ PADs can be applied to other signal reporting approaches and other receptors for detecting different target analytes (such as DNA, proteins and small

molecules) fitting the POCT purposes. Another covalent fabrication strategy focused on the activation of μ PADs by periodate oxidation, which can form covalent bonds between polysaccharides and proteins, was exploited by the same group [59]. This strategy was used to covalently immobilize antibodies on paper while the wax-printing technology was employed for defining the reactive area of the μ PAD. Another protein immobilization method was proposed by Zhao et al. [60] based on plasma treatment of paper for the development of a low-cost immunosensor. The antibody was immobilized on the paper surface after 4 min oxygen plasma treatment. Plasma treatment allowed to produce an aldehyde group which was necessary for the direct immobilization of the antibody without any additional pretreatment. A sandwich CL immunoassay method was developed for carcinoembryonic antigen (CEA) detection in human serum obtaining a linear range of 0.1–80.0 ng/mL and a detection limit of 0.03 ng/mL. Liu et al. proposed a CL immunoassay-based device developed by a craft-cutter to define flow channels, followed by lamination [61]. This approach for fabricating μ PAD by cutting/lamination shares great similarities with the procedures employed for making an identification card. The procedure is very simple and offers a valid alternative to conventional methods employed for patterning paper using wax. They also proposed a protocol based on localized incision and paper-folding to separate the detection zone from flow channels. This trick eliminated possible reagent diffusion and flow during antibody immobilization steps and the requirement for washing steps. By incorporating luminol-based CL for detecting HRP-conjugated cotinine, they detected cotinine in mouse serum using competitive immunoassay. Thanks to the peculiarities of the proposed device, a 2D or 3D structure was obtained enabling both vertical and horizontal liquid flow. This feature allows tuning according to diagnostic requirements and simplifies multiplexed analyses [2]. Ge et al. [62] exploited the origami-based approach in order to combine on the same platform a system for blood plasma separation from whole blood, the automation of rinse steps and multiplexed CL detections. A 3D origami-based device was developed composed of a test pad surrounded by four folding tabs that could be patterned and fabricated by wax-printing on paper. In the proposed work, a sandwich-type CL immunoassay was developed, allowing to separate the operational procedures into

several steps triggered by folding the pad and the addition of reagents/buffer. The developed 3D origami-based CL immunodevice was combined with a luminol-H₂O₂ CL system catalyzed by Ag nanoparticles and it was demonstrated that the excellent analytical performances allowed the simultaneous detection of four tumor markers. The same origami-based approach exploiting wax printing technology was recently proposed for the development of a multienzyme CL foldable paper-based biosensor for on-site detection of acetylcholinesterase (AChE) inhibitors [63]. To summarize, considerable progress has been achieved in the adaptation of existing batch and flow analysis methods to μ PAD format in the field of CL-based assays. It is possible to imagine that this trend will continue unabated and soon a wide variety of μ PADs will be developed for the detection of different biomarkers. As it concerns fabrication methods, they should be as simple and cheap as possible and suitable for scaling up device production. In this context, the most employed methods for developing μ PADs are based on wax printing and paper cutting which are low-cost and easily applicable on a large scale. The widespread adoption of these devices requires some advances in some crucial issues such as a proper validation and adequate long-term storage stability. The use of mobile phones and tablets for signal detection and real-time processing of data could significantly strengthen the portability and user-friendliness of μ PADs, making them accessible to both chemists and non-chemists.

3.4 Progress in Reagents Storage and Self-Contained Devices for POC Application

Conventional microfluidic devices rely on multiple-steps procedures for completing an analysis, posing a limit in their use for untrained personnel. The possibility to pre-store all the necessary reagents in “self-contained” POC devices is an emerging subject of study since it should bypass current limitations of BL and CL sensors [64]. The reagents related to POC testing comprise different chemical and biochemical species, including antibodies, enzymes, substrates and buffer solutions [65]. Different reagents require

different storage and manipulation conditions. An ideal self-contained POC device can store all the reagents stably and release them easily and controllably. Paper can provide a low-cost platform for diagnostics, but the instability of biological molecules, such as proteins and enzymes immobilized on this support, can severely limit its commercial development. Indeed, the low stability of such biomolecules impedes the obtainment of biosensors that are stable during storage and shipping, as required by the market. CL-based immunoassays are based on the use of labile enzymes and substrates that need special care, challenging their routine employment for POC or field applications. For such assays, maintaining the long-term stability of enzymes and signal-generating small molecules remains a significant challenge, since reagents should work in extreme conditions far away from the well-controlled lab environments [66]. Antibodies play a crucial role in current bioactive paper-based diagnostics [58, 67, 68]. In particular they are widely employed in LFIA where they are immobilized in specific areas of the nitrocellulose membrane called test and control lines. The interaction between proteins and the nitrocellulose membrane is initially based on electrostatic interactions. Then, a combination of hydrophobic and hydrogen bonds allows the establishment of long-term bonding. There are several factors that can affect the binding process, such as reagent choices (the presence of non-specific proteins, materials that interfere with hydrogen bonds, materials that interfere with hydrophobic interactions, etc.), environment (e.g., humidity, temperature), processing methods (e.g., dispensing methods, drying methods) [69]. There is an extensive literature on methods for improving the stability of antibodies immobilized on different paper-based materials, including covalent binding [70], addition of preservatives for stabilizing the protein [71], plasma treatment of paper [60], leading to increased shelf life of the immunoreagents with unaltered immunological activity. Despite recent advances in immobilizing proteinaceous biomolecules on paper through different strategies, the implementation of a CL-immunoassay, comprising antibodies, enzyme-labeled reagents and CL substrate into a unique paper platform, is still little explored. Deng et al. developed a self-contained and easily processable CL-LFIA comprised of three parts: the LFIA strip, the substrate pad and a polycarbonate (PC) holder [72]. In this case, the label employed for the immunoassay was composed of

AuNPs immobilized on the conjugate pad labeled with antibody and HRP, simultaneously (*Figure 4a*). In this work, H₂O₂ was replaced by sodium perborate as oxidant of CL reaction and the CL substrate was lyophilized on the glass fiber for the assembly of the CL-LFIA. After performing the test, substrate was dissolved with deionized water and the substrate pad covered the LFIA for a short time to transfer the substrate to the NC membrane. The substrate mixture reacted under the catalysis of HRP and generated a CL signal for quantitative detection. In this case, the user must add to the biosensor only the sample and, during the detection step, water to dissolve the lyophilized CL substrate.

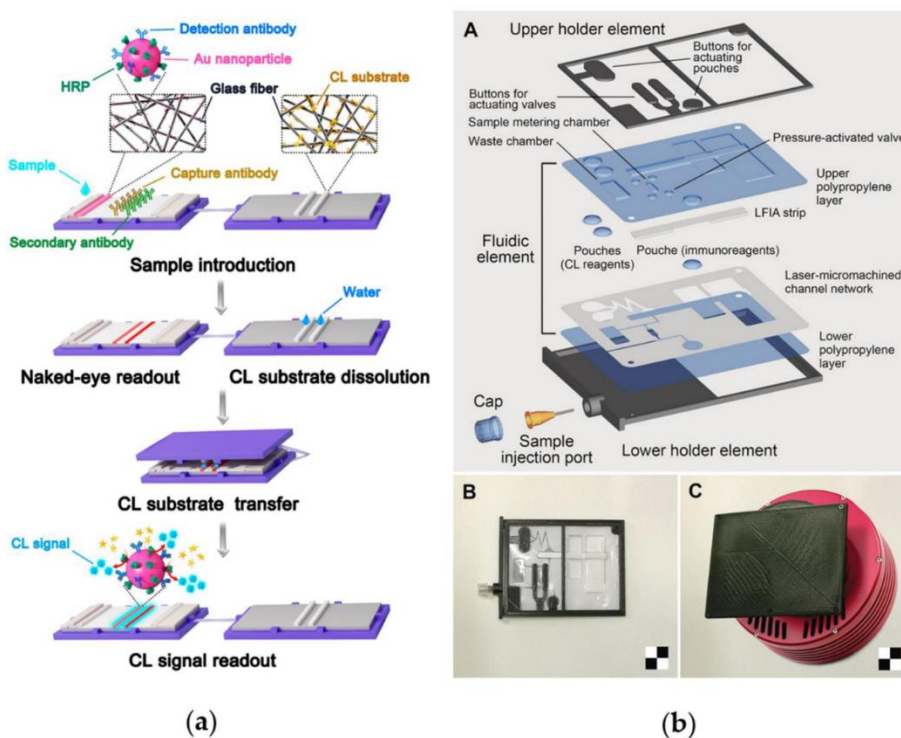


Figure 4. Self-contained devices for POC application: **(a)** a self-contained and easily processable CL lateral flow assay for POC testing. Reprinted with permission from ref. [64]. Copyright 2019 WILEY-VCH Verlag GmbH & Co. KGaA, Weinheim; **(b)** CL lateral flow immunoassay portable device to simultaneously detect two proteins (collagen and ovalbumin) for diagnostic campaigns on paintings: (A) Layout and (B) image of the disposable analytical cartridge; (C) CCD camera with 3D-printed mini dark box. Scale checkerboard is 2 × 2 cm. Reprinted with permission from ref. [76]. Copyright 2018 Wiley-VCH Verlag GmbH & Co. KGaA, Weinheim.

Alternatively, it is possible to build “self-contained” devices which integrate all the reagents necessary for performing the test in a microfluidic chip. On-chip reagents storage replaces manual reagents introduction, simplifying the detection process and reducing potential contamination risks. Recently, we [73] reported self-contained CL-LFIA for salivary cortisol quantification composed of a disposable 3D-printed plastic cartridge (which contains a fluidic element with the LFIA strip, reagents reservoirs and valves manually activated), and a CL reader based on an ultrasensitive cooled CCD camera employed in a “contact imaging” configuration [74, 75]. The analysis protocol was based on a simple manual procedure, started by operating valves and buttons to activate flow of sample and reagents which is then sustained by capillary forces. This biosensor was successfully used by the Italian astronaut Paolo Nespoli during the VITA mission (July–December 2017), thus demonstrating the possibility of performing sensitive CL-LFIA analyses directly onboard the International Space Station even in microgravity conditions [73]. CL-LFIA portable devices were also developed to simultaneously detect two proteins (collagen and ovalbumin) for diagnostic campaigns on paintings [76]. Since the immunological method required a multistep analytical protocol with sequential additions of sample and reagents, a disposable analytical cartridge was developed to streamline the procedure. In particular, the developed cartridge was ad hoc designed to contain the LFIA strip and all necessary reagents; thus, the analysis only required sample addition (*Figure 4b*).

3.5 Light Detection Technologies Integrated with CL Paper-Based Immunoassay Devices

Together with the enhanced CL system based on the use of innovative nanomaterials, the technologies related to the ultra-sensitive detection of photons have also improved considerably in the last decade. Indeed, the main requisite of CL measurements is the ability to collect as much light as possible to achieve the highest detectability and there are no limitations posed by specific optics geometry [14]. Several portable and easy-to-

use detectors were proposed for the integration with paper-based compact analytical devices [77, 78]. The main technologies for CL detectors implemented into portable immunosensors paper-based are reported in *Table 2*.

Detector for CL Paper-Based Immunosensor	Detection Principle	Pros	Cons
Photomultiplier tube (PMT)	Each PMT can detect just one wavelength. It captures emitted photons and its photocathode layer, then converts these photons to electricity. Dynodes are then used to multiply this charge multi-fold, making it readable for the instrument.	<ul style="list-style-type: none"> • Excellent signal amplification • Short response times • High sensitivity • Low noise 	<ul style="list-style-type: none"> • Expensive • Large size • Each wavelength needs a specific element • High energy consumption • Low design flexibility
Charged coupled device (CCD)	In a CCD image sensor, pixels represent the basic building blocks, and they are composed of p-doped metal-oxide-semiconductor (MOS) capacitors. Pixels allow the conversion of incoming photons into electron charges at the semiconductor-oxide interface; the CCD is then used to read out these charges.	<ul style="list-style-type: none"> • Good sensitivity • Small dark current • Wide range of wavelength • Compact • High image quality 	<ul style="list-style-type: none"> • High power consumption • Difficult system integration • More expensive than CMOS
Complementary metal-oxide semiconductor (CMOS) sensor	CMOS has emerged as alternative to CCD. Differently from CCD, each pixel sensor unit has a photodetector.	<ul style="list-style-type: none"> • Low-cost • Wide range of wavelength • Easy implementation into portable device (e.g., smartphone's camera) • Low power consumption • High speed 	<ul style="list-style-type: none"> • Lower sensitivity respect CCD • Large dark current
Thin-film photosensors	There is a wide variety of photosensors based on different materials but they are typically based on a p-n junction that converts light photons into current. The	<ul style="list-style-type: none"> • Low-cost • Easy implementation into portable device • Low power consumption • Possibility 	<ul style="list-style-type: none"> • Large dark current • Low thermal stability • Low sensitivity

Detector for CL Paper-Based Immunosensor	Detection Principle	Pros	Cons
	absorbed photons make electron-hole pairs in the depletion region.	to develop disposable platforms based on thin-film photosensors <ul style="list-style-type: none"> • Custom geometries can be developed 	

Table 2. Technologies for CL detectors implemented into paper-based portable immunosensors.

A conventional detector for CL measurements is the photomultiplier tube (PMT), which provides the highest sensitivity and, due to its size and cost, is typically used as benchtop laboratory equipment. However, recent technological advances allowed the use of portable and compact PMT-based detectors, as reported by Alahmad et al. [79]. They developed a miniaturized detection system for CL reaction, generated on μ PAD using optical fibers. Wax printing technology was employed for developing the μ PAD which comprised six separate parallel channels. Each channel was composed of three different zones (injection, reaction and waste, respectively). The CL signal was acquired by placing the μ PAD on a plastic holder equipped with six optical fibers connected to a small PMT module (*Figure 5a*).

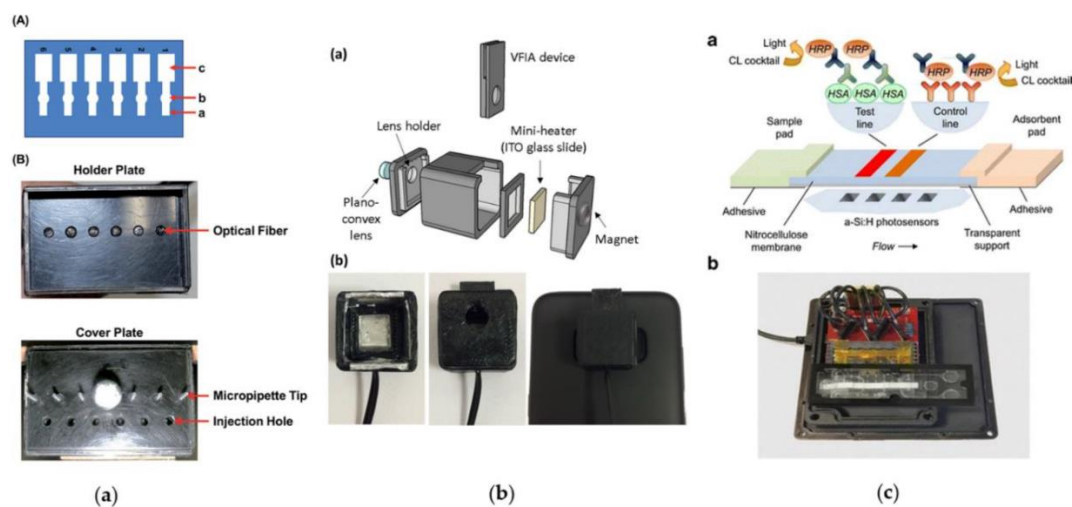


Figure 2. Light detection technologies integrated with CL paper-based immunoassay devices: **(a)** a miniaturized chemiluminescence detection system for a microfluidic paper-based analytical device and its application to the determination of chromium (III) (A): (a) injection zone, (b) reaction zone, and (c) waste zone. (B) holder: upper, holder of the μ PAD. The optical fibers are located at the positions of the reaction zone. Lower, the cover of the holder. The CL reagents were introduced from the injection holes located at the μ PAD injection zones. Reproduced from Ref. [79] with permission from The Royal Society of Chemistry. **(b)** Scheme of the integrated thermochemiluminescent vertical flow immunoassay device: (a) Scheme of the integrated TCL-VFIA device; (b) inside view of the mini-dark box (left), mini-dark box with VFIA device inserted (center), configuration for TCL signal acquisition (right). Reproduced with permission from Ref [84]. Copyright 2018 Elsevier; **(c)** scheme of the CL-LFIA strip showing the assay principle, the position of the photosensors below the strip, and a picture of the complete device, comprising the PDMS microfluidic cartridge with integrated a-Si:H photosensors and the custom readout electronics: (a) Scheme of the CL-LFIA strip showing the assay principle (top) and the position of the photosensors below the strip (bottom). (b) Picture of the complete device, comprising the PDMS microfluidic cartridge with integrated a-Si:H photosensors and the custom readout electronics. Reproduced with permission from Ref [95]. Copyright 2016, Springer-Verlag Berlin Heidelberg.

Recently, several detectors combining adequate sensitivity with portability have been proposed in order to overcome the main limitation of the relatively weak CL signal and to allow the development of ultrasensitive POCT assays [33]. For example, CL-based biosensors were implemented with a new generation of (thermally cooled) back-illuminated (BI) CCD integrated with LFIA technologies [73, 75, 76, 80]. In these examples, the CL measures were conducted in the “contact imaging” approach which consists in placing the LFIA strip directly in contact with CCD sensors through a fiber optic faceplate in order to maximize the photon collection efficiency [81]. As a low cost, easy-to-use and compact alternative, the smartphone complementary metal-oxide semiconductor (CMOS) camera has been reported as a CL detector for different POC applications. Indeed, smartphone-based biosensors have great potential since their connectivity and data processing capabilities can be exploited to perform on site and POC analyses [78, 82]. Several examples have been reported in literature coupling CL-LFIA with this innovative sensing platforms (*Figure 5b*) [83, 84]. All the mentioned biosensors showed performances that are comparable to those obtained with reference methods. A digital camera was used by Xue et al. [85] for the development of a portable and low-cost diagnostic biosensor based on BL detection. In particular, the authors

proposed a method that can be adapted to different applications for transforming antibodies into ratiometric, bioluminescent sensor proteins for the quantitative detection of target analytes. The approach is based on the genetic fusion of antibody fragments to NanoLuc luciferase and SNAP-tag. SNAP-tag was labeled with a synthetic fluorescent competitor of the antigen. According to the competitive immunoassay method, when the antigen binds to the antibody, the displacement of the tethered fluorescent competitor occurs. This phenomenon brings about the disruption of the bioluminescent resonance energy transfer (BRET) between the luciferase and fluorophore. The semisynthetic sensor offers the possibility to tune the response range (submicromolar to submillimolar) and to obtain a large dynamic range. Moreover, it allows to quantify analytes simply by spotting the samples on a paper support and exploiting a digital camera for signal acquisition. Generally, a robust BRET sensor is characterized by the ability to control ligand-induced switching between a high BRET-state and a low BRET-state, in which luciferase and the FL acceptor are in close proximity or are well separated, respectively. Ni et al. introduced a new class of ratiometric BL sensor proteins based on the competitive intramolecular complementation of split NanoLuc luciferase as an alternative to the classical BRET sensor design. As proof of concept the authors developed a blue-red light emitting sensor protein for the detection of anti-HIV-p17 antibodies. In particular, the sensor format (NB-LUMABS) is designed with a single copy of the large fragment (LB) fused to two copies of the small fragment (SB) yielding a protein switch that can exist in two conformations, where either the N- or the C-terminal SB binds to the LB and reconstitutes luciferase activity. The red-emitting fluorophore, coupled to one of the SBs, allows an efficient BRET with a consequently emission of red light in only one of the two conformations, while the intramolecular interaction of the fluorescently labeled SB is disrupted by the bivalent binding of the antibody. This allows for the reconstitution of NanoLuc by the nonfluorescently labeled SB, resulting in a color transition from red to blue [86]. As an alternative, the integration of relatively inexpensive thin-film photosensors in the analytical device was also investigated since this approach could reduce costs, electrical power consumption and memory storage space. Among the different reported technologies, amorphous silicon

thin-film photodiodes [87, 88], organic photodiodes [89, 90], carbon nanotubes coated with photovoltaic polymers [91] and metal–semiconductor–metal photodetectors [92] have gained great interest. By optimizing chip design, sensor architecture and readout electronics, photon collection efficiency can be increased to achieve analytical performances comparable with CCDs [93, 94]. Recently we developed a disposable cartridge for CL-LFIA with integrated amorphous silicon (a-Si:H) photosensors array for detecting human serum albumin (HSA) in urine samples [95]. The proposed approach is based on an indirect competitive immunoassay in which HRP acts as a tracer that is detected upon the addition of the luminol/enhancer/hydrogen peroxide CL cocktail. A PDMS cartridge that housed the LFIA strip and the reagents necessary for the CL immunoassay was optically coupled to the array of a-Si:H photosensors which were deposited on a glass substrate. This configuration ensures to obtain an integrated analytical device controlled by a portable read-out electronics. The analytical performances of this biosensor demonstrate that implementing the CL-LFIA technique with the a-Si:H photosensors array allows to obtain a compact, sensitive and low-cost system for CL-based bioassays with a wide range of applications for in-field and point-of-care bioanalyses. Furthermore, multiplexed bioassays can be easily developed by exploiting arrayed photosensors with custom geometries (*Figure 5c*).

3.6 Conclusions

The combination of immunoassays with CL detection and paper-based technology represents an ideal solution for the realization of last generation analytical devices for POC applications. Indeed, it is possible to obtain high selectivity and specificity even in complex and untreated matrices typical of the biospecific molecular recognition methods, together with the simplicity of the instrumentation necessary to measure the light signal. Furthermore, paper-based devices add great versatility, ease of use and compactness of the entire system. Even though significant progresses are continuously appearing in literature, some limitations are still hindering their spread in the market. Due to the limited stability over time of the bioreagents and the need to add reagents

manually while performing the analytical protocol, the number of commercial paper-based CL-immunoassays remains low, having difficulties meeting the end-users' needs. This issue is even more relevant for BL immunosensors, explaining why very few examples have been reported in the literature. The approach of Hall et al., who developed a stable lyophilized cake integrating all reagents and substrates required for the BL reaction, surely represents one of the most promising strategies that could solve the issues related to scarce shelf-life of BL sensors and boost their implementation in the market [30]. Researchers are now focusing their efforts on improving these systems for fulfilling the ideal POC biosensors requirement for the transition of this technology from laboratory to the market. Innovative materials and solutions are proposed in order to make these devices manageable by end-users, enabling the development of several analytical devices for a wide variety of applications. The expected diffusion of these bioanalytic tools in commerce and everyday life will pave the way for a great change in the field of analytical chemistry, making POC devices more accessible to everyone, significantly reducing time and costs for analysis, thus allowing the widespread availability of these kind of tools.

Funding

This work was supported in part by the Italian Ministry for University and Research in the framework of “Bando PRIN 2017”, projects number 2017YER72K and 2017Y2PAB8 and by PRIMA program, project Fedkito. The PRIMA program is supported by the European Union.

References

- [1] Li, F.; You, M.; Li, S.; Hu, J.; Liu, C.; Gong, Y.; Yang, H.; Xu, F. Paper-Based Point-of-Care Immunoassays: Recent Advances and Emerging Trends. *Biotechnology Advances* **2020**, *39*, 107442. <https://doi.org/10.1016/j.biotechadv.2019.107442>.
- [2] Zhu, G.; Yin, X.; Jin, D.; Zhang, B.; Gu, Y.; An, Y. Paper-Based Immunosensors: Current Trends in the Types and Applied Detection Techniques. *TrAC Trends in Analytical Chemistry* **2019**, *111*, 100–117. <https://doi.org/10.1016/j.trac.2018.09.027>.
- [3] Ozer, T.; McMahan, C.; Henry, C. S. Advances in Paper-Based Analytical Devices. *Annual Review of Analytical Chemistry* **2020**, *13* (1), 85–109. <https://doi.org/10.1146/annurev-anchem-061318-114845>.
- [4] Al Mughairy, B.; Al-Lawati, H. A. J. Recent Analytical Advancements in Microfluidics Using Chemiluminescence Detection Systems for Food Analysis. *TrAC Trends in Analytical Chemistry* **2020**, *124*, 115802. <https://doi.org/10.1016/j.trac.2019.115802>.
- [5] Akyazi, T.; Basabe-Desmonts, L.; Benito-Lopez, F. Review on Microfluidic Paper-Based Analytical Devices towards Commercialisation. *Analytica Chimica Acta* **2018**, *1001*, 1–17. <https://doi.org/10.1016/j.aca.2017.11.010>.
- [6] Gai, H.; Li, Y.; Yeung, E. S. Optical Detection Systems on Microfluidic Chips. In *Microfluidics: Technologies and Applications*; Lin, B., Ed.; Topics in Current Chemistry; Springer: Berlin, Heidelberg, 2011; pp 171–201. https://doi.org/10.1007/128_2011_144.
- [7] Kuswandi, B.; Nuriman; Huskens, J.; Verboom, W. Optical Sensing Systems for Microfluidic Devices: A Review. *Analytica Chimica Acta* **2007**, *601* (2), 141–155. <https://doi.org/10.1016/j.aca.2007.08.046>.
- [8] Baker, C. A.; Duong, C. T.; Grimley, A.; Roper, M. G. Recent Advances in Microfluidic Detection Systems. *Bioanalysis* **2009**, *1* (5), 967–975. <https://doi.org/10.4155/bio.09.86>.

- [9] Krishnan, M.; Namasivayam, V.; Lin, R.; Pal, R.; Burns, M. A. Microfabricated Reaction and Separation Systems. *Current Opinion in Biotechnology* **2001**, *12* (1), 92–98. [https://doi.org/10.1016/S0958-1669\(00\)00166-X](https://doi.org/10.1016/S0958-1669(00)00166-X).
- [10] Roda, A.; Guardigli, M. Analytical Chemiluminescence and Bioluminescence: Latest Achievements and New Horizons. *Anal Bioanal Chem* **2012**, *402* (1), 69–76. <https://doi.org/10.1007/s00216-011-5455-8>.
- [11] Xiao, Q.; Lin, J.-M. Advances and Applications of Chemiluminescence Immunoassay in Clinical Diagnosis and Foods Safety. *Chinese Journal of Analytical Chemistry* **2015**, *43* (6), 929–938. [https://doi.org/10.1016/S1872-2040\(15\)60831-3](https://doi.org/10.1016/S1872-2040(15)60831-3).
- [12] Gámiz-Gracia, L.; García-Campaña, A. M.; Huertas-Pérez, J. F.; Lara, F. J. Chemiluminescence Detection in Liquid Chromatography: Applications to Clinical, Pharmaceutical, Environmental and Food Analysis—A Review. *Analytica Chimica Acta* **2009**, *640* (1), 7–28. <https://doi.org/10.1016/j.aca.2009.03.017>.
- [13] Fereja, T. H.; Hymete, A.; Gunasekaran, T. A Recent Review on Chemiluminescence Reaction, Principle and Application on Pharmaceutical Analysis. *ISRN Spectroscopy* **2013**, *2013*, 1–12. <https://doi.org/10.1155/2013/230858>.
- [14] Roda, A.; Mirasoli, M.; Michelini, E.; Di Fusco, M.; Zangheri, M.; Cevenini, L.; Roda, B.; Simoni, P. Progress in Chemical Luminescence-Based Biosensors: A Critical Review. *Biosensors and Bioelectronics* **2016**, *76*, 164–179. <https://doi.org/10.1016/j.bios.2015.06.017>.
- [15] Roda, A.; Guardigli, M.; Pasini, P.; Mirasoli, M.; Michelini, E.; Musiani, M. Bio- and Chemiluminescence Imaging in Analytical Chemistry. *Analytica Chimica Acta* **2005**, *541* (1), 25–35. <https://doi.org/10.1016/j.aca.2004.11.083>.
- [16] Créton, R.; Jaffe, L. F. Chemiluminescence Microscopy as a Tool in Biomedical Research. *BioTechniques* **2001**, *31* (5), 1098–1105. <https://doi.org/10.2144/01315rv01>.
- [17] Reschiglian, P.; Zomer, G. *The Nature of Chemiluminescent Reactions*; Roda, A., Ed.; The Royal Society of Chemistry, 2010. <https://doi.org/10.1039/9781849732024-00051>.

- [18] Marzocchi, E.; Grilli, S.; Della Ciana, L.; Prodi, L.; Mirasoli, M.; Roda, A. Chemiluminescent Detection Systems of Horseradish Peroxidase Employing Nucleophilic Acylation Catalysts. *Analytical Biochemistry* **2008**, *377* (2), 189–194. <https://doi.org/10.1016/j.ab.2008.03.020>.
- [19] White, E. H.; Rapaport, E.; Seliger, H. H.; Hopkins, T. A. The Chemi- and Bioluminescence of Firefly Luciferin: An Efficient Chemical Production of Electronically Excited States. *Bioorganic Chemistry* **1971**, *1* (1), 92–122. [https://doi.org/10.1016/0045-2068\(71\)90009-5](https://doi.org/10.1016/0045-2068(71)90009-5).
- [20] Niwa, K.; Ichino, Y.; Kumata, S.; Nakajima, Y.; Hiraishi, Y.; Kato, D.; Viviani, V. R.; Ohmiya, Y. Quantum Yields and Kinetics of the Firefly Bioluminescence Reaction of Beetle Luciferases. *Photochemistry and Photobiology* **2010**, *86* (5), 1046–1049. <https://doi.org/10.1111/j.1751-1097.2010.00777.x>.
- [21] Wouters, S. F. A.; Vugs, W. J. P.; Arts, R.; de Leeuw, N. M.; Teeuwen, R. W. H.; Merckx, M. Bioluminescent Antibodies through Photoconjugation of Protein G–Luciferase Fusion Proteins. *Bioconjugate Chem.* **2020**, *31* (3), 656–662. <https://doi.org/10.1021/acs.bioconjchem.9b00804>.
- [22] Hwang, B. (Brian); Engel, L.; Goueli, S. A.; Zegzouti, H. A Homogeneous Bioluminescent Immunoassay to Probe Cellular Signaling Pathway Regulation. *Commun Biol* **2020**, *3* (1), 1–12. <https://doi.org/10.1038/s42003-019-0723-9>.
- [23] Alsulami, T.; Nath, N.; Flemming, R.; Wang, H.; Zhou, W.; Yu, J.-H. Development of a Novel Homogeneous Immunoassay Using the Engineered Luminescent Enzyme NanoLuc for the Quantification of the Mycotoxin Fumonisin B1. *Biosensors and Bioelectronics* **2021**, *177*, 112939. <https://doi.org/10.1016/j.bios.2020.112939>.
- [24] Azim, M.; Hasan, M.; Ansari, I.; Nasreen, F. Chemiluminescence Immunoassay: Basic Mechanism and Applications. *Bangladesh Journal of Nuclear Medicine* **2018**, *18*, 171. <https://doi.org/10.3329/bjnm.v18i2.35240>.
- [25] Hasanzadeh, M.; Shadjou, N. Advanced Nanomaterials for Use in Electrochemical and Optical Immunoassays of Carcinoembryonic Antigen. A Review. *Microchim Acta* **2017**, *184* (2), 389–414. <https://doi.org/10.1007/s00604-016-2066-2>.

- [26] Fu, L.-M.; Wang, Y.-N. Detection Methods and Applications of Microfluidic Paper-Based Analytical Devices. *TrAC Trends in Analytical Chemistry* **2018**, *107*, 196–211. <https://doi.org/10.1016/j.trac.2018.08.018>.
- [27] Arakawa, T.; Prestrelski, S. J.; Kenney, W. C.; Carpenter, J. F. Factors Affecting Short-Term and Long-Term Stabilities of Proteins. *Advanced Drug Delivery Reviews* **2001**, *46* (1), 307–326. [https://doi.org/10.1016/S0169-409X\(00\)00144-7](https://doi.org/10.1016/S0169-409X(00)00144-7).
- [28] Miller, K. D.; Barnette, R.; Light, R. W. Stability of Adenosine Deaminase During Transportation. *Chest* **2004**, *126* (6), 1933–1937. <https://doi.org/10.1378/chest.126.6.1933>.
- [29] Jahanshahi-Anbuhi, S.; Pennings, K.; Leung, V.; Liu, M.; Carrasquilla, C.; Kannan, B.; Li, Y.; Pelton, R.; Brennan, J. D.; Filipe, C. D. M. Pullulan Encapsulation of Labile Biomolecules to Give Stable Bioassay Tablets. *Angewandte Chemie International Edition* **2014**, *53* (24), 6155–6158. <https://doi.org/10.1002/anie.201403222>.
- [30] Hall, M. P.; Kincaid, V. A.; Jost, E. A.; Smith, T. P.; Hurst, R.; Forsyth, S. K.; Fitzgerald, C.; Ressler, V. T.; Zimmermann, K.; Lazar, D.; Wood, M. G.; Wood, K. V.; Kirkland, T. A.; Encell, L. P.; Machleidt, T.; Dart, M. L. Toward a Point-of-Need Bioluminescence-Based Immunoassay Utilizing a Complete Shelf-Stable Reagent. *Anal. Chem.* **2021**, *93* (12), 5177–5184. <https://doi.org/10.1021/acs.analchem.0c05074>.
- [31] Xiao, Q.; Xu, C. Research Progress on Chemiluminescence Immunoassay Combined with Novel Technologies. *TrAC Trends in Analytical Chemistry* **2020**, *124*, 115780. <https://doi.org/10.1016/j.trac.2019.115780>.
- [32] Cinquanta, L.; Fontana, D. E.; Bizzaro, N. Chemiluminescent Immunoassay Technology: What Does It Change in Autoantibody Detection? *Autoimmun Highlights* **2017**, *8* (1), 9. <https://doi.org/10.1007/s13317-017-0097-2>.
- [33] Roda, A.; Arduini, F.; Mirasoli, M.; Zangheri, M.; Fabiani, L.; Colozza, N.; Marchegiani, E.; Simoni, P.; Moscone, D. A Challenge in Biosensors: Is It Better to Measure a Photon or an Electron for Ultrasensitive Detection? *Biosensors and Bioelectronics* **2020**, *155*, 112093. <https://doi.org/10.1016/j.bios.2020.112093>.

- [34] Su, Y.; Xie, Y.; Hou, X.; Lv, Y. Recent Advances in Analytical Applications of Nanomaterials in Liquid-Phase Chemiluminescence. *Applied Spectroscopy Reviews* **2014**, *49* (3), 201–232. <https://doi.org/10.1080/05704928.2013.819514>.
- [35] Han, S.; Zhang, Z.; Li, S.; Qi, L.; Xu, G. Chemiluminescence and Electrochemiluminescence Applications of Metal Nanoclusters. *Sci. China Chem.* **2016**, *59* (7), 794–801. <https://doi.org/10.1007/s11426-016-0043-3>.
- [36] Li, N.; Liu, D.; Cui, H. Metal-Nanoparticle-Involved Chemiluminescence and Its Applications in Bioassays. *Anal Bioanal Chem* **2014**, *406* (23), 5561–5571. <https://doi.org/10.1007/s00216-014-7901-x>.
- [37] Han, G.-R.; Ki, H.; Kim, M.-G. Automated, Universal, and Mass-Produced Paper-Based Lateral Flow Biosensing Platform for High-Performance Point-of-Care Testing. *ACS Appl. Mater. Interfaces* **2020**, *12* (1), 1885–1894. <https://doi.org/10.1021/acsami.9b17888>.
- [38] Li, F.; Guo, L.; Hu, Y.; Li, Z.; Liu, J.; He, J.; Cui, H. Multiplexed Chemiluminescence Determination of Three Acute Myocardial Infarction Biomarkers Based on Microfluidic Paper-Based Immunodevice Dual Amplified by Multifunctionalized Gold Nanoparticles. *Talanta* **2020**, *207*, 120346. <https://doi.org/10.1016/j.talanta.2019.120346>.
- [39] Zong, C.; Zhang, D.; Jiang, F.; Yang, H.; Liu, S.; Li, P. Metal-Enhanced Chemiluminescence Detection of C-Reaction Protein Based on Silver Nanoparticle Hybrid Probes. *Talanta* **2019**, *199*, 164–169. <https://doi.org/10.1016/j.talanta.2019.02.060>.
- [40] Khataee, A.; Hasanzadeh, A.; Iranifam, M.; Joo, S. W. A Novel Flow-Injection Chemiluminescence Method for Determination of Baclofen Using l-Cysteine Capped CdS Quantum Dots. *Sensors and Actuators B: Chemical* **2015**, *215*, 272–282. <https://doi.org/10.1016/j.snb.2015.03.066>.
- [41] Chen, H.; Lin, L.; Li, H.; Lin, J.-M. Quantum Dots-Enhanced Chemiluminescence: Mechanism and Application. *Coordination Chemistry Reviews* **2014**, *263–264*, 86–100. <https://doi.org/10.1016/j.ccr.2013.07.013>.

- [42] Deng, S.; Lei, J.; Huang, Y.; Cheng, Y.; Ju, H. Electrochemiluminescent Quenching of Quantum Dots for Ultrasensitive Immunoassay through Oxygen Reduction Catalyzed by Nitrogen-Doped Graphene-Supported Hemin. *Anal. Chem.* **2013**, *85* (11), 5390–5396. <https://doi.org/10.1021/ac3036537>.
- [43] Zhao, P.; Zhou, L.; Nie, Z.; Xu, X.; Li, W.; Huang, Y.; He, K.; Yao, S. Versatile Electrochemiluminescent Biosensor for Protein–Nucleic Acid Interaction Based on the Unique Quenching Effect of Deoxyguanosine-5'-Phosphate on Electrochemiluminescence of CdTe/ZnS Quantum Dots. *Anal. Chem.* **2013**, *85* (13), 6279–6286. <https://doi.org/10.1021/ac4004437>.
- [44] Liu, S.; Zhang, X.; Yu, Y.; Zou, G. A Monochromatic Electrochemiluminescence Sensing Strategy for Dopamine with Dual-Stabilizers-Capped CdSe Quantum Dots as Emitters. *Anal. Chem.* **2014**, *86* (5), 2784–2788. <https://doi.org/10.1021/ac500046s>.
- [45] Jie, G.; Zhao, Y.; Niu, S. Amplified Electrochemiluminescence Detection of Cancer Cells Using a New Bifunctional Quantum Dot as Signal Probe. *Biosensors and Bioelectronics* **2013**, *50*, 368–372. <https://doi.org/10.1016/j.bios.2013.06.048>.
- [46] Ying Lim, S.; Shen, W.; Gao, Z. Carbon Quantum Dots and Their Applications. *Chemical Society Reviews* **2015**, *44* (1), 362–381. <https://doi.org/10.1039/C4CS00269E>.
- [47] Chen, Y.; Chu, W.; Liu, W.; Guo, X.; Jin, Y.; Li, B. Paper-Based Chemiluminescence Immunodevice for the Carcinoembryonic Antigen by Employing Multi-Enzyme Carbon Nanosphere Signal Enhancement. *Microchim Acta* **2018**, *185* (3), 187. <https://doi.org/10.1007/s00604-018-2726-5>.
- [48] Li, W.; Ge, S.; Wang, S.; Yan, M.; Ge, L.; Yu, J. Highly Sensitive Chemiluminescence Immunoassay on Chitosan Membrane Modified Paper Platform Using TiO₂ Nanoparticles/Multiwalled Carbon Nanotubes as Label. *Luminescence* **2013**, *28* (4), 496–502. <https://doi.org/10.1002/bio.2482>.
- [49] Ehsani, M.; Chaichi, M. J.; Nezammeddin Hosseini, S. Comparison of CuO Nanoparticle and CuO/MWCNT Nanocomposite for Amplification of Chemiluminescence Immunoassay for Detection of the Hepatitis B Surface

- Antigen in Biological Samples. *Sensors and Actuators B: Chemical* **2017**, *247*, 319–328. <https://doi.org/10.1016/j.snb.2017.02.019>.
- [50] Zhang, Z.-F.; Cui, H.; Lai, C.-Z.; Liu, L.-J. Gold Nanoparticle-Catalyzed Luminol Chemiluminescence and Its Analytical Applications. *Anal. Chem.* **2005**, *77* (10), 3324–3329. <https://doi.org/10.1021/ac050036f>.
- [51] Guo, Y.; Li, B. Carbon Dots-Initiated Luminol Chemiluminescence in the Absence of Added Oxidant. *Carbon* **2015**, *82*, 459–469. <https://doi.org/10.1016/j.carbon.2014.10.089>.
- [52] Sun, L.; Jiang, Y.; Pan, R.; Li, M.; Wang, R.; Chen, S.; Fu, S.; Man, C. A Novel, Simple and Low-Cost Paper-Based Analytical Device for Colorimetric Detection of *Cronobacter* Spp. *Analytica Chimica Acta* **2018**, *1036*, 80–88. <https://doi.org/10.1016/j.aca.2018.05.061>.
- [53] Park, M.; Kang, B.-H.; Jeong, K.-H. Paper-Based Biochip Assays and Recent Developments: A Review. *BioChip J* **2018**, *12* (1), 1–10. <https://doi.org/10.1007/s13206-017-2101-3>.
- [54] Arduini, F.; Cinti, S.; Scognamiglio, V.; Moscone, D. Paper-Based Electrochemical Devices in Biomedical Field: Recent Advances and Perspectives. In *Past, Present, and Future Challenges of Biosensors and Bioanalytical Tools in Analytical Chemistry: A Tribute to Professor Marco Mascini*; Elsevier, 2017; Vol. 77, pp 385–413. <https://doi.org/10.1016/bs.coac.2017.06.005>.
- [55] Lu, Y.; Shi, W.; Qin, J.; Lin, B. Fabrication and Characterization of Paper-Based Microfluidics Prepared in Nitrocellulose Membrane By Wax Printing. *Anal. Chem.* **2010**, *82* (1), 329–335. <https://doi.org/10.1021/ac9020193>.
- [56] Liu, S.; Cao, R.; Wu, J.; Guan, L.; Li, M.; Liu, J.; Tian, J. Directly Writing Barrier-Free Patterned Biosensors and Bioassays on Paper for Low-Cost Diagnostics. *Sensors and Actuators B: Chemical* **2019**, *285*, 529–535. <https://doi.org/10.1016/j.snb.2019.01.091>.
- [57] Yang, H.; Kong, Q.; Wang, S.; Xu, J.; Bian, Z.; Zheng, X.; Ma, C.; Ge, S.; Yu, J. Hand-Drawn&written Pen-on-Paper Electrochemiluminescence Immunodevice

- Powered by Rechargeable Battery for Low-Cost Point-of-Care Testing. *Biosensors and Bioelectronics* **2014**, *61*, 21–27. <https://doi.org/10.1016/j.bios.2014.04.051>.
- [58] Wang, S.; Ge, L.; Song, X.; Yu, J.; Ge, S.; Huang, J.; Zeng, F. Paper-Based Chemiluminescence ELISA: Lab-on-Paper Based on Chitosan Modified Paper Device and Wax-Screen-Printing. *Biosensors and Bioelectronics* **2012**, *31* (1), 212–218. <https://doi.org/10.1016/j.bios.2011.10.019>.
- [59] Wang, S.; Ge, L.; Song, X.; Yan, M.; Ge, S.; Yu, J.; Zeng, F. Simple and Covalent Fabrication of a Paper Device and Its Application in Sensitive Chemiluminescence Immunoassay. *Analyst* **2012**, *137* (16), 3821–3827. <https://doi.org/10.1039/C2AN35266D>.
- [60] Zhao, M.; Li, H.; Liu, W.; Guo, Y.; Chu, W. Plasma Treatment of Paper for Protein Immobilization on Paper-Based Chemiluminescence Immunodevice. *Biosensors and Bioelectronics* **2016**, *79*, 581–588. <https://doi.org/10.1016/j.bios.2015.12.099>.
- [61] Liu, W.; Cassano, C. L.; Xu, X.; Fan, Z. H. Laminated Paper-Based Analytical Devices (LPAD) with Origami-Enabled Chemiluminescence Immunoassay for Cotinine Detection in Mouse Serum. *Anal. Chem.* **2013**, *85* (21), 10270–10276. <https://doi.org/10.1021/ac402055n>.
- [62] Ge, L.; Wang, S.; Song, X.; Ge, S.; Yu, J. 3D Origami-Based Multifunction-Integrated Immunodevice: Low-Cost and Multiplexed Sandwich Chemiluminescence Immunoassay on Microfluidic Paper-Based Analytical Device. *Lab on a Chip* **2012**, *12* (17), 3150–3158. <https://doi.org/10.1039/C2LC40325K>.
- [63] Montali, L.; Calabretta, M. M.; Lopreside, A.; D’Elia, M.; Guardigli, M.; Micheli, E. Multienzyme Chemiluminescent Foldable Biosensor for On-Site Detection of Acetylcholinesterase Inhibitors. *Biosensors and Bioelectronics* **2020**, *162*, 112232. <https://doi.org/10.1016/j.bios.2020.112232>.
- [64] Deng, J.; Jiang, X. Advances in Reagents Storage and Release in Self-Contained Point-of-Care Devices. *Advanced Materials Technologies* **2019**, *4* (6), 1800625. <https://doi.org/10.1002/admt.201800625>.

- [65] Hitzbleck, M.; Delamarche, E. Reagents in Microfluidics: An ‘in’ and ‘out’ Challenge. *Chemical Society Reviews* **2013**, *42* (21), 8494–8516. <https://doi.org/10.1039/C3CS60118H>.
- [66] Jahanshahi-Anbuhi, S.; Kannan, B.; Leung, V.; Pennings, K.; Liu, M.; Carrasquilla, C.; White, D.; Li, Y.; H. Pelton, R.; D. Brennan, J.; M. Filipe, C. D. Simple and Ultrastable All-Inclusive Pullulan Tablets for Challenging Bioassays. *Chemical Science* **2016**, *7* (3), 2342–2346. <https://doi.org/10.1039/C5SC04184H>.
- [67] Martinez, A. W. Microfluidic Paper-Based Analytical Devices: From POCKET to Paper-Based ELISA. *Bioanalysis* **2011**, *3* (23), 2589–2592. <https://doi.org/10.4155/bio.11.258>.
- [68] Wang, J.; Yiu, B.; Obermeyer, J.; Filipe, C. D. M.; Brennan, J. D.; Pelton, R. Effects of Temperature and Relative Humidity on the Stability of Paper-Immobilized Antibodies. *Biomacromolecules* **2012**, *13* (2), 559–564. <https://doi.org/10.1021/bm2017405>.
- [69] Kim, D.; Herr, A. E. Protein Immobilization Techniques for Microfluidic Assays. *Biomicrofluidics* **2013**, *7* (4), 041501. <https://doi.org/10.1063/1.4816934>.
- [70] Holstein, C. A.; Chevalier, A.; Bennett, S.; Anderson, C. E.; Keniston, K.; Olsen, C.; Li, B.; Bales, B.; Moore, D. R.; Fu, E.; Baker, D.; Yager, P. Immobilizing Affinity Proteins to Nitrocellulose: A Toolbox for Paper-Based Assay Developers. *Anal Bioanal Chem* **2016**, *408* (5), 1335–1346. <https://doi.org/10.1007/s00216-015-9052-0>.
- [71] Cao, R.; Tian, W.; Shen, W. Polysaccharides as Protectants for Paper-Based Analytical Devices with Antibody. *Talanta* **2017**, *165*, 357–363. <https://doi.org/10.1016/j.talanta.2016.12.079>.
- [72] Deng, J.; Yang, M.; Wu, J.; Zhang, W.; Jiang, X. A Self-Contained Chemiluminescent Lateral Flow Assay for Point-of-Care Testing. *Anal. Chem.* **2018**, *90* (15), 9132–9137. <https://doi.org/10.1021/acs.analchem.8b01543>.
- [73] Zangheri, M.; Mirasoli, M.; Guardigli, M.; Di Nardo, F.; Anfossi, L.; Baggiani, C.; Simoni, P.; Benassai, M.; Roda, A. Chemiluminescence-Based Biosensor for Monitoring Astronauts’ Health Status during Space Missions: Results from the

- International Space Station. *Biosensors and Bioelectronics* **2019**, *129*, 260–268. <https://doi.org/10.1016/j.bios.2018.09.059>.
- [74] Mirasoli, M.; Bonvicini, F.; Dolci, L. S.; Zangheri, M.; Gallinella, G.; Roda, A. Portable Chemiluminescence Multiplex Biosensor for Quantitative Detection of Three B19 DNA Genotypes. *Anal Bioanal Chem* **2013**, *405* (2), 1139–1143. <https://doi.org/10.1007/s00216-012-6573-7>.
- [75] Mirasoli, M.; Buragina, A.; Dolci, L. S.; Simoni, P.; Anfossi, L.; Giraudi, G.; Roda, A. Chemiluminescence-Based Biosensor for Fumonisin Quantitative Detection in Maize Samples. *Biosensors and Bioelectronics* **2012**, *32* (1), 283–287. <https://doi.org/10.1016/j.bios.2011.11.039>.
- [76] Sciutto, G.; Zangheri, M.; Anfossi, L.; Guardigli, M.; Prati, S.; Mirasoli, M.; Di Nardo, F.; Baggiani, C.; Mazzeo, R.; Roda, A. Miniaturized Biosensors to Preserve and Monitor Cultural Heritage: From Medical to Conservation Diagnosis. *Angewandte Chemie* **2018**, *130* (25), 7507–7511. <https://doi.org/10.1002/ange.201713298>.
- [77] Maddalena Calabretta, M.; Zangheri, M.; Lopreside, A.; Marchegiani, E.; Montali, L.; Simoni, P.; Roda, A. Precision Medicine, Bioanalytics and Nanomaterials: Toward a New Generation of Personalized Portable Diagnostics. *Analyst* **2020**, *145* (8), 2841–2853. <https://doi.org/10.1039/C9AN02041A>.
- [78] Calabretta, M. M.; Montali, L.; Lopreside, A.; Fragapane, F.; Iacoangeli, F.; Roda, A.; Bocci, V.; D’Elia, M.; Michelini, E. Ultrasensitive On-Field Luminescence Detection Using a Low-Cost Silicon Photomultiplier Device. *Anal. Chem.* **2021**, *93* (20), 7388–7393. <https://doi.org/10.1021/acs.analchem.1c00899>.
- [79] Alahmad, W.; Uraisin, K.; Nacapricha, D.; Kaneta, T. A Miniaturized Chemiluminescence Detection System for a Microfluidic Paper-Based Analytical Device and Its Application to the Determination of Chromium(III). *Analytical Methods* **2016**, *8* (27), 5414–5420. <https://doi.org/10.1039/C6AY00954A>.
- [80] Zangheri, M.; Nardo, F. D.; Anfossi, L.; Giovannoli, C.; Baggiani, C.; Roda, A.; Mirasoli, M. A Multiplex Chemiluminescent Biosensor for Type B-Fumonisin and

- Aflatoxin B1 Quantitative Detection in Maize Flour. *Analyst* **2015**, *140* (1), 358–365. <https://doi.org/10.1039/C4AN01613K>.
- [81] Roda, A.; Mirasoli, M.; Dolci, L. S.; Buragina, A.; Bonvicini, F.; Simoni, P.; Guardigli, M. Portable Device Based on Chemiluminescence Lensless Imaging for Personalized Diagnostics through Multiplex Bioanalysis. *Anal. Chem.* **2011**, *83* (8), 3178–3185. <https://doi.org/10.1021/ac200360k>.
- [82] Calabretta, M. M.; Álvarez-Diduk, R.; Michelini, E.; Roda, A.; Merkoçi, A. Nano-Lantern on Paper for Smartphone-Based ATP Detection. *Biosensors and Bioelectronics* **2020**, *150*, 111902. <https://doi.org/10.1016/j.bios.2019.111902>.
- [83] Roda, A.; Calabretta, M. M.; Calabria, D.; Caliceti, C.; Cevenini, L.; Lopreside, A.; Zangheri, M. Smartphone-Based Biosensors. In *Past, Present and Future Challenges of Biosensors and Bioanalytical Tools in Analytical Chemistry: A Tribute to Professor Marco Mascini*; Elsevier, 2017; Vol. 77, p 237.
- [84] Roda, A.; Zangheri, M.; Calabria, D.; Mirasoli, M.; Caliceti, C.; Quintavalla, A.; Lombardo, M.; Trombini, C.; Simoni, P. A Simple Smartphone-Based Thermochemiluminescent Immunosensor for Valproic Acid Detection Using 1,2-Dioxetane Analogue-Doped Nanoparticles as a Label. *Sensors and Actuators B: Chemical* **2019**, *279*, 327–333. <https://doi.org/10.1016/j.snb.2018.10.012>.
- [85] Xue, L.; Yu, Q.; Griss, R.; Schena, A.; Johnsson, K. Bioluminescent Antibodies for Point-of-Care Diagnostics. *Angewandte Chemie* **2017**, *129* (25), 7218–7222. <https://doi.org/10.1002/ange.201702403>.
- [86] Ni, Y.; Arts, R.; Merckx, M. Ratiometric Bioluminescent Sensor Proteins Based on Intramolecular Split Luciferase Complementation. *ACS Sens.* **2019**, *4* (1), 20–25. <https://doi.org/10.1021/acssensors.8b01381>.
- [87] Caputo, D.; de Cesare, G.; Dolci, L. S.; Mirasoli, M.; Nascetti, A.; Roda, A.; Scipinotti, R. Microfluidic Chip With Integrated A-Si:H Photodiodes for Chemiluminescence-Based Bioassays. *IEEE Sensors Journal* **2013**, *13* (7), 2595–2602. <https://doi.org/10.1109/JSEN.2013.2256889>.
- [88] Pereira, A. T.; Pimentel, A. C.; Chu, V.; Prazeres, D. M. F.; Conde, J. P. Chemiluminescent Detection of Horseradish Peroxidase Using an Integrated

- Amorphous Silicon Thin-Film Photosensor. *IEEE Sensors Journal* **2009**, *9* (10), 1282–1290. <https://doi.org/10.1109/JSEN.2009.2027414>.
- [89] Wang, X.; Amatatongchai, M.; Nacapricha, D.; Hofmann, O.; de Mello, J. C.; Bradley, D. D. C.; de Mello, A. J. Thin-Film Organic Photodiodes for Integrated on-Chip Chemiluminescence Detection – Application to Antioxidant Capacity Screening. *Sensors and Actuators B: Chemical* **2009**, *140* (2), 643–648. <https://doi.org/10.1016/j.snb.2009.04.068>.
- [90] Wojciechowski, J. R.; Shriver-Lake, L. C.; Yamaguchi, M. Y.; Füreder, E.; Pieler, R.; Schamesberger, M.; Winder, C.; Prall, H. J.; Sonnleitner, M.; Ligler, F. S. Organic Photodiodes for Biosensor Miniaturization. *Anal. Chem.* **2009**, *81* (9), 3455–3461. <https://doi.org/10.1021/ac8027323>.
- [91] Shim, J. S.; Ahn, C. H. Optical Immunosensor Using Carbon Nanotubes Coated with a Photovoltaic Polymer. *Biosensors and Bioelectronics* **2012**, *34* (1), 208–214. <https://doi.org/10.1016/j.bios.2012.02.004>.
- [92] Lin, C.-C.; Ko, F.-H.; Chen, C.-C.; Yang, Y.-S.; Chang, F.-C.; Wu, C.-S. Miniaturized Metal Semiconductor Metal Photocurrent System for Biomolecular Sensing via Chemiluminescence. *ELECTROPHORESIS* **2009**, *30* (18), 3189–3197. <https://doi.org/10.1002/elps.200900120>.
- [93] Mirasoli, M.; Nascetti, A.; Caputo, D.; Zangheri, M.; Scipinotti, R.; Cevenini, L.; de Cesare, G.; Roda, A. Multiwell Cartridge with Integrated Array of Amorphous Silicon Photosensors for Chemiluminescence Detection: Development, Characterization and Comparison with Cooled-CCD Luminograph. *Anal Bioanal Chem* **2014**, *406* (23), 5645–5656. <https://doi.org/10.1007/s00216-014-7971-9>.
- [94] Nascetti, A.; Mirasoli, M.; Marchegiani, E.; Zangheri, M.; Costantini, F.; Porchetta, A.; Iannascoli, L.; Lovecchio, N.; Caputo, D.; de Cesare, G.; Pirrotta, S.; Roda, A. Integrated Chemiluminescence-Based Lab-on-Chip for Detection of Life Markers in Extraterrestrial Environments. *Biosensors and Bioelectronics* **2019**, *123*, 195–203. <https://doi.org/10.1016/j.bios.2018.08.056>.
- [95] Zangheri, M.; Di Nardo, F.; Mirasoli, M.; Anfossi, L.; Nascetti, A.; Caputo, D.; De Cesare, G.; Guardigli, M.; Baggiani, C.; Roda, A. Chemiluminescence Lateral Flow

Immunoassay Cartridge with Integrated Amorphous Silicon Photosensors Array for Human Serum Albumin Detection in Urine Samples. *Anal Bioanal Chem* **2016**, *408* (30), 8869–8879. <https://doi.org/10.1007/s00216-016-9991-0>.

AstroBio – CubeSat: A lab – In – Space For Chemiluminescence – Based Astrobiology Experiments

Reproduced from: “AstroBio-CubeSat: A lab-in-space for chemiluminescence-based astrobiology experiments”
Donato Calabria, Ilaria Trozzi, Elisa Lazzarini, Andrea Pace, Martina Zangheri, Lorenzo Iannascoli, Nithin
Maipan Davis, Sagar Sarvad Gosikere Matadha, Thiago Baratto De Albuquerque, Simone Pirrotta, Marta Del
Bianco, Gabriele Impresario, Lijana Popova, Nicola Lovecchio, Giampiero de Cesare, Domenico Caputo, John Brucato,
Augusto Nascetti, Massimo Guardigli, Mara Mirasoli

Biosensors and Bioelectronics, 2023, 226, 115110

<https://doi.org/10.1016/j.bios.2023.115110>

Reproduced by permission of Elsevier (Open Access Article)

<http://creativecommons.org/licenses/by/4.0/>

<https://s100.copyright.com/AppDispatchServlet?publisherName=ELS&contentID=S0956566323000520&orderBeanReset=true>

<https://beta.elsevier.com/about/policies-and-standards/copyright>

4.1 Introduction

Human space exploration is facing a new era. The planned missions to the orbit and the surface of the Moon and of Mars, as indicated in the Global Exploration Roadmap [1], and the entry in the space economy of private companies offering commercial spaceflights to non-professional travelers will lead to an exponential growth in number and duration of manned missions. This scenario will prompt the development and in-flight validation of technologies suitable for sustaining life and protecting the health of humans in space. Manned missions, especially beyond Low Earth Orbit (LEO), will expose astronauts to the spaceflight environment (altered gravity, high levels of ionising radiation, isolation, altered diet and circadian rhythms, etc.) for long periods of time, with possible negative outcomes on their health and performance. Biosensors can play an important role in monitoring astronauts' health [2, 3]. Portable and wearable biosensors could be used for quantitative detection of biomarkers of clinical interest in biological fluids. Biosensing devices would represent valuable tools for environmental and food safety monitoring, both whilst on board the spacecraft and during human permanence on the Moon or Mars [4]. Biosensors could also be employed to assess the impact of deep space conditions on biological systems (e.g., microbial, fungal, and plant communities) that would be used to sustain the life of the crew in artificial habitats on the Moon and Mars and for In-Situ Resource Utilisation (ISRU), i.e., for obtaining/producing onsite materials that would otherwise be brought from Earth [5]. Finally, biosensors would help in investigating the traces of past or present life in extra-terrestrial environments, thus evaluating their potential habitability. It is widely accepted that unambiguous life detection in planetary exploration requires a suite of techniques providing complementary information [6] and various wet chemistry analytical suites were proposed for the search of extant or extinct life markers [6, 7, 8]. As of today, bioanalytical and biomonitoring capabilities in space are limited [1], thus significant technological advancements in this field are required in a relatively short time frame. Analytical devices suitable for spaceflight must be small and lightweight, use little resources (e.g., power, reagents and other consumables, data bandwidth) and operate in

harsh conditions (e.g., reduced or null gravity, high radiation levels) with the highest possible autonomy [1, 2, 3]. Such requirements could be addressed by exploiting Lab-on-Chip (LoC) technologies, which enable the miniaturisation of analytical devices while still maintaining good analytical performance. This would also improve the efficiency of the analytical process in terms of sample size, reagents consumption, response time, analytical productivity, integration, and automation [6, 9, 10, 11, 8, 3]. Microfluidic analytical devices relying on capillary flow are particularly promising for space applications, as they are remarkably simple and their operation is unaffected by altered gravity [9, 10, 12, 13]. We recently developed PLEIADES, a chemiluminescence (CL) - based integrated analytical platform for the detection of biomarkers suitable for astrobiological applications [8]. Such analytical platform employed a capillary force-driven microfluidic network and an array of photosensors to perform CL bioassays for the highly sensitive detection of life biomarkers in a simple and compact LoC configuration. Since space conditions cannot be completely reproduced on ground, validation of analytical devices in space is pivotal to their successful application [14]. Altered gravity conditions influence many physical phenomena, including fluid dynamics, which can jeopardize the correct operation of fluidic devices and negatively affect their performance [3, 12]. Additionally, space radiations can damage both hardware components and chemical and biochemical reagents [15]. This aspect is particularly relevant for missions beyond LEO, where payloads would be exposed to constant low-flux, and high-energy ionising radiations, such as those from galactic cosmic rays and solar particle events [2]. The International Space Station (ISS) is a unique opportunity for testing analytical devices in real space conditions and their usability by astronauts. However, the crew time available for scientific experiments onboard the ISS is limited and, since its orbit lies within the Earth's magnetosphere, the ISS is still shielded from radiations. At present, technologies can be validated in the deep space radiation environment only in unmanned missions. Besides conventional, large-sized satellites, small satellites such as CubeSats are nowadays increasingly used as fast and low-cost platforms for conducting experiments in space. CubeSats were first developed in 1999 by Stanford and California Polytechnic State Universities for

educational purposes. They have a modular configuration, in which the base unit (U) is a 10 cm – cube with a mass up to 1.33 kg. Larger spacecrafts have a form factor corresponding to the given number of 1U CubeSats that were combined. Thanks to the standardised format, engineering and production costs of CubeSats are consistently reduced. Launch and deployment of CubeSats are also cheaper, since CubeSats are often launched as secondary payloads of other missions, employing a common deployment system that is independent of the CubeSat manufacturer [16]. However, the development of payloads for CubeSats is constrained by the limited size, mass, and power. Moreover, the experiments must be performed automatically without any human supervision, and no sample-return is possible [17]. Despite these constraints, CubeSats are broadly used, and the scientific community has been advancing the development of miniaturized instruments able to operate on CubeSats [18]. In this paper, we report the development of a fully autonomous LoC platform for conducting chemiluminescence (CL)-based bioassays in space, built as heritage of the PLEIADES project [8]. CL detection is particularly advantageous for implementation in miniaturized, integrated analytical devices [19, 20] and its performance in real space conditions has already been shown [13]. We employed the origami-like microfluidic paper-based analytical device (μ PAD) format [21, 22], which allowed preloading of all the reagents in the dried form on the paper substrate. This simplified analytical protocols, as the assays were initiated by injecting a buffer solution in the μ PAD, and facilitated autonomous assay execution. The device to be hosted in the AstroBio CubeSat (ABCS) nanosatellite has the aim of validating the technology in space, as well as to test the device operation and the stability of (bio)molecules employed in the assays in a radiation environment. This project constitutes the first step to develop a mature technology to conduct research in space, e.g., evaluating the effect of deep space conditions on living organisms or searching molecular evidence of life, at lower cost and with greater frequency than previously possible.

4.2 Materials and methods

4.2.1 Chemicals

Peroxidase from horseradish (HRP, EC 1.11.1.7, Type VI, specific activity ≥ 250 U mg^{-1} solid), microbial xanthine oxidase (XO, EC 1.17.3.2, specific activity ≥ 7 U mg^{-1} solid), glucose oxidase (GOD, EC 1.1.3.4, from *Aspergillus niger*, specific activity ≥ 250 U mg^{-1} solid), luminol sodium salt, glucose, xanthine, bovine hemin, potassium hexacyanoferrate (III), sodium perborate, pullulan from *Aureobasidium pullulans*, and poly (allylamine) hydrochloride (average Mw = 50,000 Da) were purchased from Sigma Aldrich (St Louis, MO). Whatman CHR 1 chromatographic paper (20×20 cm² sheets) was also bought from Sigma-Aldrich. Buffer loading pads were cut from cellulose fibre pads purchased from Millipore (Billerica, MA). All the other chemicals were of the highest analytical grade.

4.2.2 Fabrication of the origami device

To produce the origami μ PAD device the pattern of the hydrophobic areas drawn in PowerPoint (*Fig. 1a*) was printed on chromatographic paper using a commercial solid ink Phaser 8560DN printer (Xerox Co., Norwalk, CT). The μ PAD was cut from the paper sheet (*Fig. 1c, left*) and heated at 110 °C for 10 min in an oven to melt the wax-based ink and generate the hydrophobic areas. Then, the reagents were loaded into the μ PAD by dispensing their solutions into the hydrophilic channels in layer B, and the hydrophilic areas in layers A and C (the reagents deposited in the μ PAD for the different experiments are reported in *Table 1*). Finally, after air drying at room temperature in the dark for 1 h, the μ PAD was folded as shown in *Fig. 1b* to its final configuration (*Fig. 1c, right*). The separation lines between the sections corresponding to the layers of the device aided folding since after heat treatment they remained more flexible than the wax-printed areas. During the installation of the origami μ PAD six 3×9 mm² buffer loading pads were applied over the hydrophilic areas of layer A to avoid the spreading of the buffer. Pads were kept in place by the assembly holder, which also applied pressure to the μ PAD to guarantee a tight contact between the layers.

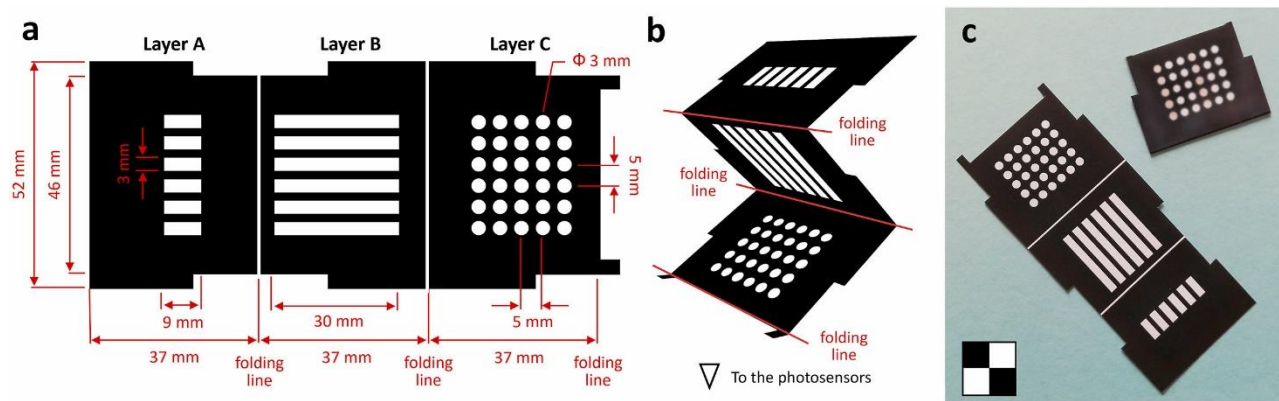


Figure 1. The ABCS μ PAD. **(a)** Layout of the μ PAD with hydrophobic areas printed in black. **(b)** Folding of the μ PAD for insertion in the assembly holder. **(c)** Photo of the μ PAD, before (left) and after (right) heating, preloading of reagents and folding (the yellow colour of some “wells” in layer C is due to the potassium hexacyanoferrate (III) CL catalyst).

Table 1. Reagents employed for the experiments developed for the origami μ PAD.

Experiment	Reagent reservoir ^a	Origami μ PAD ^b		
		Layer A	Layer B	Layer C (for each “well”)
#1	ca. 200 μ L PB ^c	0.6 μ mol NaBO ₃ in 20 μ L PB	2.0 μ mol luminol in 40 μ L PB	0.8 μ mol K ₃ Fe(CN) ₆ in 4.0 μ L PB
#2	ca. 200 μ L PB	0.6 μ mol NaBO ₃ in 20 μ L PB	2.0 μ mol luminol in 40 μ L PB	0.2 μ mol hemin in 4.0 μ L PB
#3	ca. 200 μ L PB	0.6 μ mol NaBO ₃ in 20 μ L PB	2.0 μ mol luminol in 40 μ L PB	0.1 U HRP in 4.0 μ L PB with 1 mg mL ⁻¹ pullulan
#4	ca. 200 μ L PB	0.2 μ mol glucose in 20 μ L PB	12 U GOD and 2.0 μ mol luminol in 40 μ L PB with 1 mg mL ⁻¹ pullulan	0.5 U HRP in 4.0 μ L PB with 1 mg mL ⁻¹ pullulan
#5	ca. 200 μ L PB	0.1 μ mol xanthine in 20 μ L PB	8 U XO and 2.0 μ mol luminol in 40 μ L PB with 1 mg mL ⁻¹ pullulan	0.5 U HRP in 4.0 μ L PB with 1 mg mL ⁻¹ pullulan
#6 (blank)	ca. 200 μ L PB	0.6 μ mol NaBO ₃ in 20 μ L PB	2.0 μ mol luminol in 40 μ L PB	4.0 μ L PB

a) This reagent (in excess to the amount used in the experiments) was loaded in the reagent reservoirs.

b) The reagents in the origami μ PAD were dispensed in the hydrophilic areas of the layers, then air-dried.

c) PB: 0.1 M phosphate buffer, pH 7.5.

4.2.3 Optimization of the experimental conditions

The optimization of the experimental conditions was carried out using a ground model of the ABCS CL measurement subsystem. The system was equipped with a removable origami μ PAD assembly holder to allow for the rapid replacements of the μ PAD. The CL measurement subsystem was shielded from the ambient light and connected via an USB cable to a laptop that powered the photocurrent readout board and recorded the CL signals measured by the photosensors. To perform an experiment, the PB buffer was injected in the μ PAD using a fluid transfer line connected to a miniature peristaltic pump (modified as those installed in ABCS) and inserted in the desired fluid inlet of the assembly holder. The kinetic profile of the CL emission of each “well” was recorded by plotting the photocurrent (in pA) measured by the corresponding photodiode against time. The analytical CL signal was obtained by integrating the area under the curve (AUC). CL imaging experiments were performed to assess the spatial distribution of the CL emission, employing an ATIK 11000 Charge-Coupled Device (CCD) camera (ATIK Cameras, New Road, Norwich). The camera was equipped with a large format, high resolution Kodak KAI 11002 monochrome sensor cooled by a two – stage Peltier element to reduce thermal noise.

4.2.4 Mission scenario and protocol of experiments

The AstroBio CubeSat (*Fig. 2a*) is a 3U ($100 \times 100 \times 340 \text{ mm}^3$) nanosatellite that has been launched with the Vega – C qualification maiden flight on July 13th, 2022, as a “piggy – back” of the Italian Space Agency (ASI) LARES – 2 main satellite. It was deployed in a circular orbit at about 5850 km of altitude and 70° of inclination, thus spending a significant amount of its orbital period within the internal Van Allen belt, very close to its radiation peak zone. The ABCS ground operations were mainly performed by the School of Aerospace Engineering of the Sapienza - University of Rome (SIA Ground Station). A network of radio amateurs and third part ground stations was also involved for collection of telemetry and science data packages.

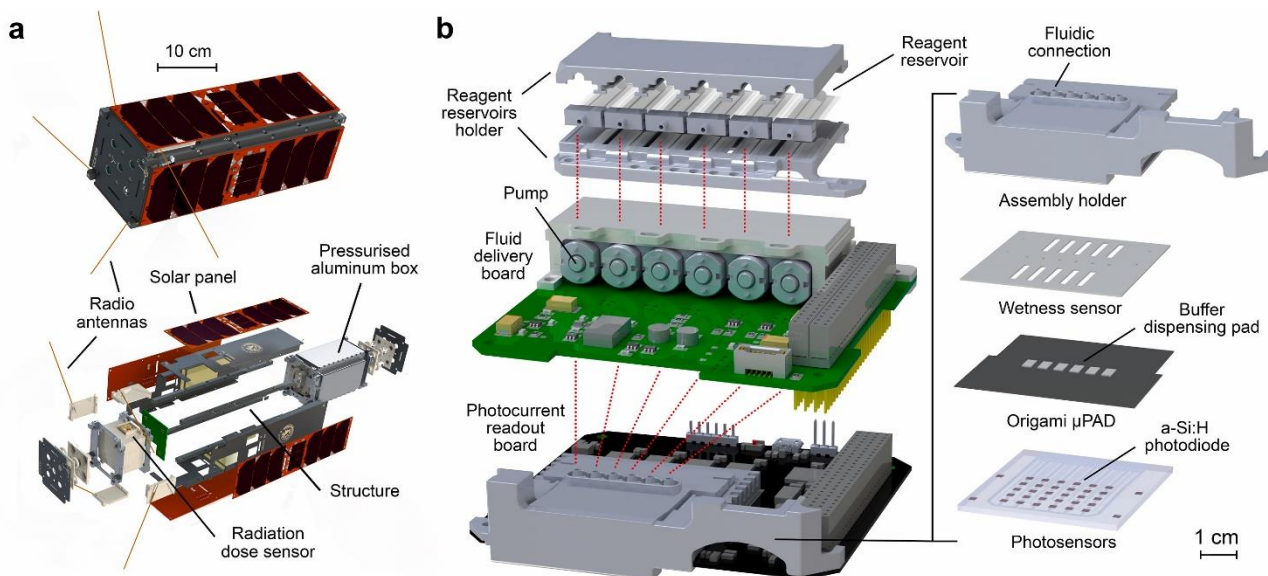


Figure 2. The ABCS and its subsystems for bioanalytical experiments. **(a)** Scheme of the ABCS nanosatellite. **(b)** Scheme of the ABCS subsystems used for bioanalytical experiments. The red dotted lines represent the buffer transfer lines.

For the in-flight experiment, three CL-based reactions were chosen, namely those reported as experiments #1, #3, and #4 in *Table 1*. Since each channel of the μ PAD can be independently activated, each experiment will be carried out in duplicate. The general experimental procedure can be summarised as follows.

- a) Injection of buffer solution ($40 \mu\text{L}$) from the reservoir to the fluid inlet of the assembly holder and μ PAD. The wetness sensor is used to confirm the delivery of the buffer solution and to control the volume dispensed (after detection of the arrival of the buffer to the fluid inlet the pump, providing a $120 \mu\text{L min}^{-1}$ flow, is maintained active for further 20 s).
- b) Dissolution of reagents and transport to the reaction sites of the μ PAD by capillary action.
- c) Activation of the CL reactions.
- d) Detection of photons emission and acquisition of CL signal readout.

The recorded photon emission data is transmitted to ground and then analysed to investigate both the intensity of the CL emission and the kinetics of the CL reactions, as

compared with parallel experiments performed on ground. To consider the effect of temperature on the stability of reagents and, more importantly, on the kinetics of the reactions, thus on the intensity of the CL emission, reference ground experiments will be conducted reproducing the temperature profile of the payload monitored during in – flight operation.

4.3 Results and discussion

4.3.1 Rationale of experiment design

The main aim of ABCS is the in-flight test of an integrated multi-parametric analytical platform for the implementation of CL – based bioassays. Both the proper functioning of the device (e.g., delivery of buffer, transportation and mixing of reactants, detection of CL emission, electronics, data storage and transmission) and the stability in space conditions of the chemicals and the biomolecules required to perform the bioassays will be evaluated. The ability to autonomously handle various adverse events (low power, low temperature, system resets) will be also assessed. A significant challenge for the proper function of ABCS is represented by the high radiation environment (i.e., within the internal Van Allen belt) in which it will operate. It has been estimated that ABCS will be exposed to a radiation dose of more than 16 Gy for 24 h [23]. For reference, the typical daily dose inside the ISS ranges from 0.0002 to 0.0005 Gy [24]. Additional transient, non-predictable off-nominal sources of charged particle radiation would be solar particle events, where particles are ejected from the sun in prompt and short-lived bursts of energy. As in ABCS all reagents are deposited in dried form onto a paper substrate, the main events causing their degradation would be the primary ionisation occurring directly in the hit molecules. As concerns proteins, it has been reported that every molecule that suffered a direct ionisation is destroyed [25]. Furthermore, there is a limited possibility for controlling the payload temperature during the phase of integration of ABCS into the launcher as well as during the time between integration and experiment execution in orbit, which can be days to months long. This can pose a

serious threat to biological experiments' success, thus requiring careful optimization of reagents' stability [26]. We studied for implementation in ABCS a range of CL reactions in which light emission is derived from the oxidation of luminol by reactive oxygen species (ROS). The luminol/H₂O₂ reaction catalysed by HRP was chosen as a model, being a well-established and widely studied CL system, easily implemented in miniaturized analytical devices. In addition, it provides intense and long-lasting CL signals, which facilitates signal measurement in extreme environments. Furthermore, employment of coupled enzyme reactions could represent a promising approach for the detection of those life markers of astrobiological interest which are not easily recognized by antibodies, such as sugars or enzyme cofactors. The selected reactions (*Table 2*) follow an “evolutionary” approach, aimed at reproducing a model for the development of catalytic activity in iron-containing catabolic enzymes, which can be extended in principle to other metal-porphyrin prosthetic groups. It was indeed reported that the catalytic ability of ferric iron progressively increases when combined with protoporphyrin, and when the iron-porphyrin group is further combined with a protein moiety [27]. It is also worth noting that it is commonly recognized that life on Earth evolved in the presence of hydrogen peroxide, and other peroxides also emerged before and with the rise of aerobic metabolism [27].

Table 2. CL reactions implemented in the ABCS origami μ PAD.

Experiment	Oxidant-producing reaction	Oxidant	Catalyst	CL reactant
#1		NaBO ₃ ^a	K ₃ Fe(CN) ₆ (inorganic)	Luminol
#2		NaBO ₃	Hemin (organic)	Luminol
#3		NaBO ₃	HRP (enzyme)	Luminol
#4	Oxidation of glucose by GOD	(H ₂ O ₂) ^b	HRP (enzyme)	Luminol
#5	Oxidation of xanthine by XO	(H ₂ O ₂)	HRP (enzyme)	Luminol

a) NaBO₃ releases hydrogen peroxide by reacting with water.

b) The oxidant H₂O₂ is produced by the enzyme reactions catalysed by GOD and XO.

It should be also noted that experiments #4 and #5 simulated analytical devices for detecting model astrobiological markers: glucose, used as a representative example of biomolecules such as carbohydrates (but also a routine physiological marker in view of possible diagnostic applications of the technology), and xanthine, an intermediate in nucleobases metabolism [28].

4.3.2 The AstroBio CubeSat and the subsystems for bioanalytical experiments

4.3.2.1 Bioanalytical payload requirements and implementation solutions

To meet the requirements arising from the mission scenario, several innovative solutions, ranging from peculiar system-level arrangements to optimized experimental protocol, have been implemented. In this process, the design choices have been driven by system requirements and by the binding constraints of CubeSat missions. The subsystems for performing the bioanalytical were contained in an aluminium payload box ($106 \times 160 \times 71 \text{ mm}^3$) together with all the satellite-bus electronics (i.e., electrical power system, batteries, on-board computer, and radio). The box was hermetically sealed with an indium wire gasket and pressurized with air (1 bar) at room temperature to ensure an ambient pressure environment suitable for bioassays once in orbit. Apart from avoiding evaporation of fluids, the sealed box design provided additional advantages. The most obvious advantage of the aluminum box is its partial radiation shielding effect thanks to the 3 – 6 mm thick aluminum walls [29]. In addition, the pressurized environment facilitates the thermal control of the payload since it improves temperature uniformity inside the box and provides for heat exchange by air conduction (no natural convection can take place in the weightlessness environment). Indeed, in accordance with the mission scenario, in absence of any control the expected satellite internal temperature range would have been between $-40 \text{ }^\circ\text{C}$ and $-20 \text{ }^\circ\text{C}$. To maintain the payload temperature within an acceptable range (the target temperature is from 12

°C to 16 °C, while the maximum acceptable temperature excursion is between +4 °C and +28 °C) the power dissipation of the satellite-bus electronics and communication system has been exploited in an active thermal control approach. Since the radio represents the main contribution of the dissipated power, the beacon repetition time is dynamically modulated according to the box internal temperature: the lower the temperature the shorter the beacon interval. To make this temperature control strategy more effective, the payload box is thermally decoupled from the CubeSat structure through Teflon elements. To comply with the need to preserve the chemicals from degradation, the board stack-up has been designed to allow the late integration of the μ PAD and the liquid reagents just right before the box sealing procedure. In addition, the whole satellite structure features a modular design that enables the assembly of the sealed box in a later stage and stowage of the sealed box in a controlled temperature environment (i.e., in the range 4 – 9 °C), until the satellite is due for final integration.

4.3.2.2 ABCS subsystems for bioanalytical experiments

The AstroBio CubeSat has been developed using commercial off-the-shelf (COTS) as well as in-house designed parts to deliver a highly integrated analytical platform for autonomous execution of bioanalytical experiments in space. Special attention has been given to the on-board software design to ensure a high level of fault tolerance. The firmware of the on-board computer includes a scheduler that starts each experiment at a defined time, and a finite state machine that controls all the steps required for the execution of an experiment, considering system feedbacks, such as the reading of the wetness sensor. Data is automatically transmitted to the ground and can also be downloaded via telecommand from the ground. Reliable software design techniques have been used to ensure correct experiment execution, even in the event of system reboots or power cycles, low battery voltage, or anomalous temperature situations. In the case of anomalies, the recovery action taken depends on the current step of the experiment (for example, if the fluid has already been delivered to the origami μ PAD, data acquisition will proceed also in case of low battery by saving power from other

subsystems). The technology subsystems of ABCS designed to perform the experiments (Fig. 2b) include the following components.

- a) **μ PAD.** The μ PAD (Fig. 1) has been designed exploiting the origami approach and contains all the reagents and CL catalysts in a dried form to reduce their possible degradation due to exposure to a high radiation environment. The μ PAD is composed of three layers: A (buffer injection/reagent storage), B (fluid transport/reagent storage), and C (CL catalyst storage/CL signal production). During the experiment, the buffer is dispensed on the buffer dispensing pads applied to layer A, then, the buffer migrates by capillarity into the μ PAD and dissolves the reagents, transporting them to the hydrophilic “wells” of layer C, in which the CL reactions take place. For each channel of the μ PAD there are five hydrophilic “wells” in layer C, thus in the μ PAD there are a total of 30 hydrophilic “wells”, each of them coupled with a photosensor for measuring its CL emission.
- b) **Wetness sensor.** This element is a printed circuit board containing two sensors, each of them consisting of two interdigitated, gold-finished conductive traces in contact with the buffer dispensing pads. The sensors confirm the correct delivery of the phosphate buffer to the μ PAD through monitoring the increase of the electrical conductivity of the buffer dispensing pads: each sensor measures the overall conductivity of three dispensing pads, and the geometry of the interdigitated traces has been optimized to have a constant relative drop of the measured electrical resistance every time a new pad has been wetted.
- c) **Assembly holder.** This 3D – printed element holds the μ PAD, the buffer dispensing pads and the wetness sensor. This element attaches to the photocurrent readout board and guarantees the close contact between the buffer dispensing pads, the μ PAD and the glass chip with the photosensors (since the CL detection system does not use optics, a tight contact between the μ PAD and the glass chip with the photosensors is critical to improve light detection efficiency and minimise the cross-talks between adjacent photosensors). The

assembly holder also accepts the fluid transfer lines for injection of the phosphate buffer in the μ PAD.

- d) **Photosensors and photocurrent readout board.** The CL emission is detected by a 6×5 array of 2×2 mm² high sensitivity and low dark current noise a-Si:H photosensors deposited on a 50×50 mm² borosilicate glass chip inserted in the photocurrent readout board [30, 31, 32, 8, 33]. The readout board (MARIE, Multichannel Array Readout Integrated Environment) is an extended and improved version of a previously developed one and employs a custom low noise electronics for the biasing of the photodiodes and the measurement of the photocurrents generated by the incident light [34].
- e) **Fluid delivery board.** The fluid delivery board contains six miniature peristaltic pumps (RP-Q1, Aquatec International Inc., Irvine, CA), each of them connected to a reagent reservoir. When activated, the pumps deliver the phosphate buffer to the buffer dispensing pads of the μ PAD. The pumps have been modified by installing a 3D – printed pump head to accommodate a 0.5 mm i. d. silicone tubing. This decreased the flow rate from the nominal value of $450 \mu\text{L min}^{-1}$ to $120 \mu\text{L min}^{-1}$, thus allowing an easier control of the volume of buffer transferred to the μ PAD.
- f) **Reagent reservoirs.** Six 200 μL – volume reagent reservoirs enclosed in a 3D – printed dedicated holder contain the phosphate buffer. Each reservoir is a small polyethylene bag (length 35 mm, width 12 mm) obtained by a polyethylene foil by thermal sealing and it is mounted on a 3D – printed support for easy connection to the fluid transfer line.

The fluid transfer lines of ABCS are made of flexible silicone rubber tubing (0.5 mm i. d., 1.0 mm o. d.). A commercial bicomponent epoxy glue has been used to seal all fluidic connections.

4.3.3 Optimization of origami μ PAD and experimental protocols

As stated before, one of the aims of the ABCS mission is to evaluate the stability in space conditions of the reagents used to perform the CL – based assays. We focused our investigation on the stability of CL catalysts (potassium hexacyanoferrate (III), hemin, and HRP) and of the enzymes (GOD and XO) employed in the coupled enzyme systems. Therefore, a large excess of CL reactant (luminol), oxidant (NaBO_3), and enzyme substrates (glucose and xanthine) was used, while the amounts of CL catalysts and enzymes were selected within the dynamic range of the assays to observe a decrease of the CL signal due to the possible degradation of such species. The amount of oxidant (NaBO_3) was optimized considering experiment #3 as a model, in which HRP is employed as the CL catalyst (this experiment gave the highest CL signals, thus the highest consumption rate of oxidant). *Fig. 3a* shows the CL signals measured for different amounts of NaBO_3 loaded in the hydrophilic areas of layer A of the μ PAD. According to the experimental results, 0.6 μmol has been selected as the amount of NaBO_3 for the preparation of the μ PAD. In the case of luminol, which has a relatively low solubility (about 0.2 M) in phosphate buffer at pH 7.5, we used a saturated solution further diluted 1:4 (v/v) with PB to guarantee its dissolution during the experiments. It must be noted that luminol solubility increases with pH, but pH 7.5 was selected as a common value for all assays. Indeed, the overall performance of the CL system depend on both the influence of pH on the enzyme activity and the effect of pH on the generated CL signal. While the luminol CL reaction is more favoured under alkaline conditions, the optimal pH values for the used enzymes are lower, i.e., between pH 6.0 and 6.5 for HRP [35] and between pH 6.0 and 6.5 for GOD from *A. niger* [36]. The working pH was therefore chosen as a compromised optimum due to the combination of elements with different pH optimal values.

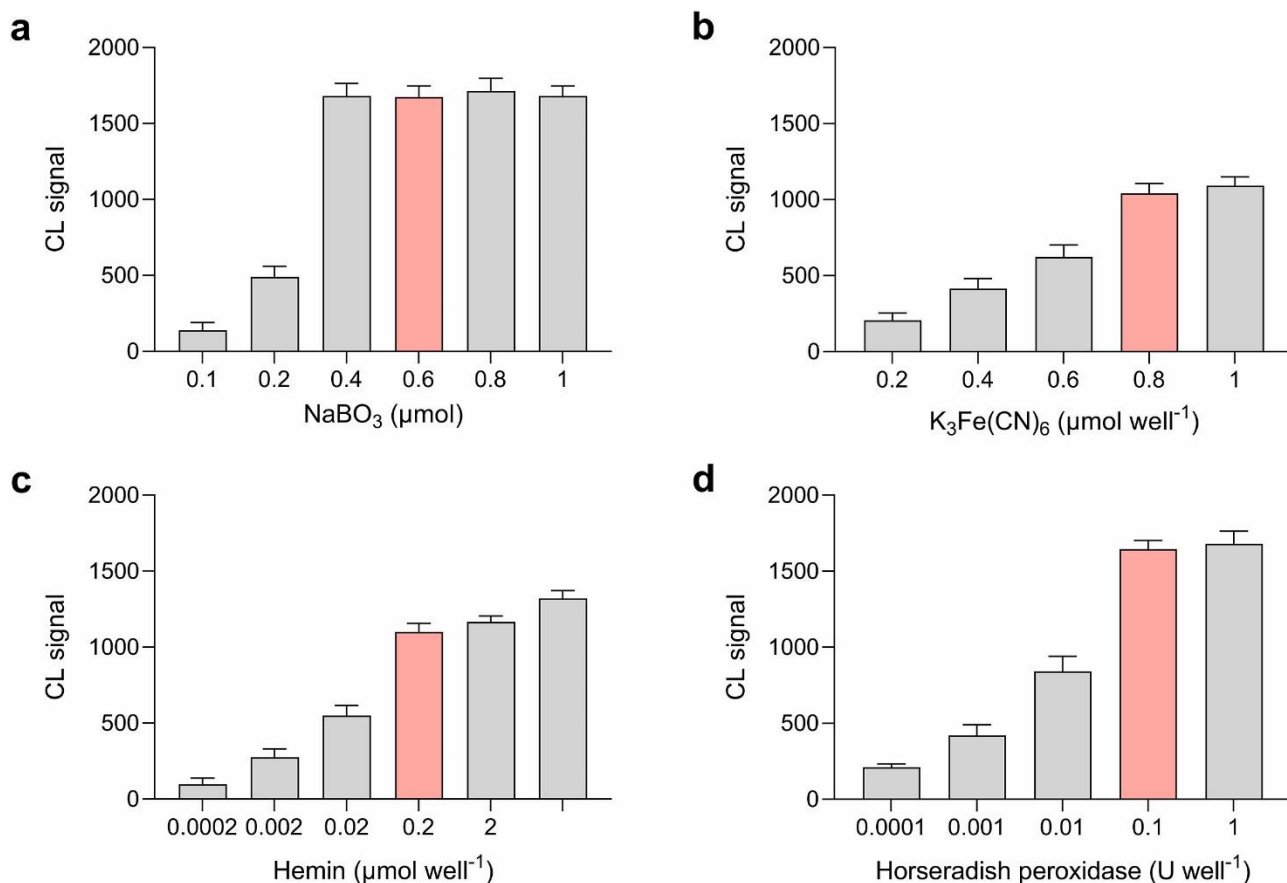


Figure 3. Optimization of amount of NaBO₃ oxidant and of experimental conditions of the experiments involving K₃Fe(CN)₆, hemin and HRP as CL catalysts. (a) CL signals obtained for experiment #3 performed in μPADs prepared with different amounts of NaBO₃ and for (b) experiment #1, (c) experiment #2, and (d) experiment #3 performed in μPADs prepared with different amounts of CL catalyst (potassium hexacyanoferrate (III), hemin, and HRP, respectively). All the other reagents were used at their optimal amounts. Each data is the mean ± SD of CL signals measured in the “wells” of three μPAD channels. The amounts of reactants selected for the preparation of the μPAD are highlighted in red.

For experiments #1, #2, and #3 the highest amounts of CL catalysts comprised in the dynamic range of the assays were selected, in order to obtain a high CL signal still maintaining, as stated before, the ability to detect a possible degradation of the catalyst. Fig. 3 shows the CL signals measured for different amounts of CL catalysts, i.e., potassium hexacyanoferrate (III) (Fig. 3b), hemin (Fig. 3c), and HRP (Fig. 3d), loaded in the “wells” of layer C of the μPAD. According to the results, the optimal amounts selected for the preparation of the μPAD were 0.8, μmol well⁻¹, 0.2 μmol well⁻¹, and 0.1 U well⁻¹ for potassium hexacyanoferrate (III), hemin, and HRP, respectively. A similar

approach was used to optimize the amounts of the enzymes GOD and XO involved in the coupled enzyme reactions exploited in experiments #4 and #5 (these reactions also involved HRP, which was used in excess with respect to the amount individuated for experiment #3). Fig. 4 showed the CL signals measured for different amounts of GOD (Fig. 4a) and XO (Fig. 4b) loaded in the layer B of the μ PAD. According to the results, the amounts selected for the preparation of the μ PAD were 12 U and 8 U for GOD and XO, respectively.

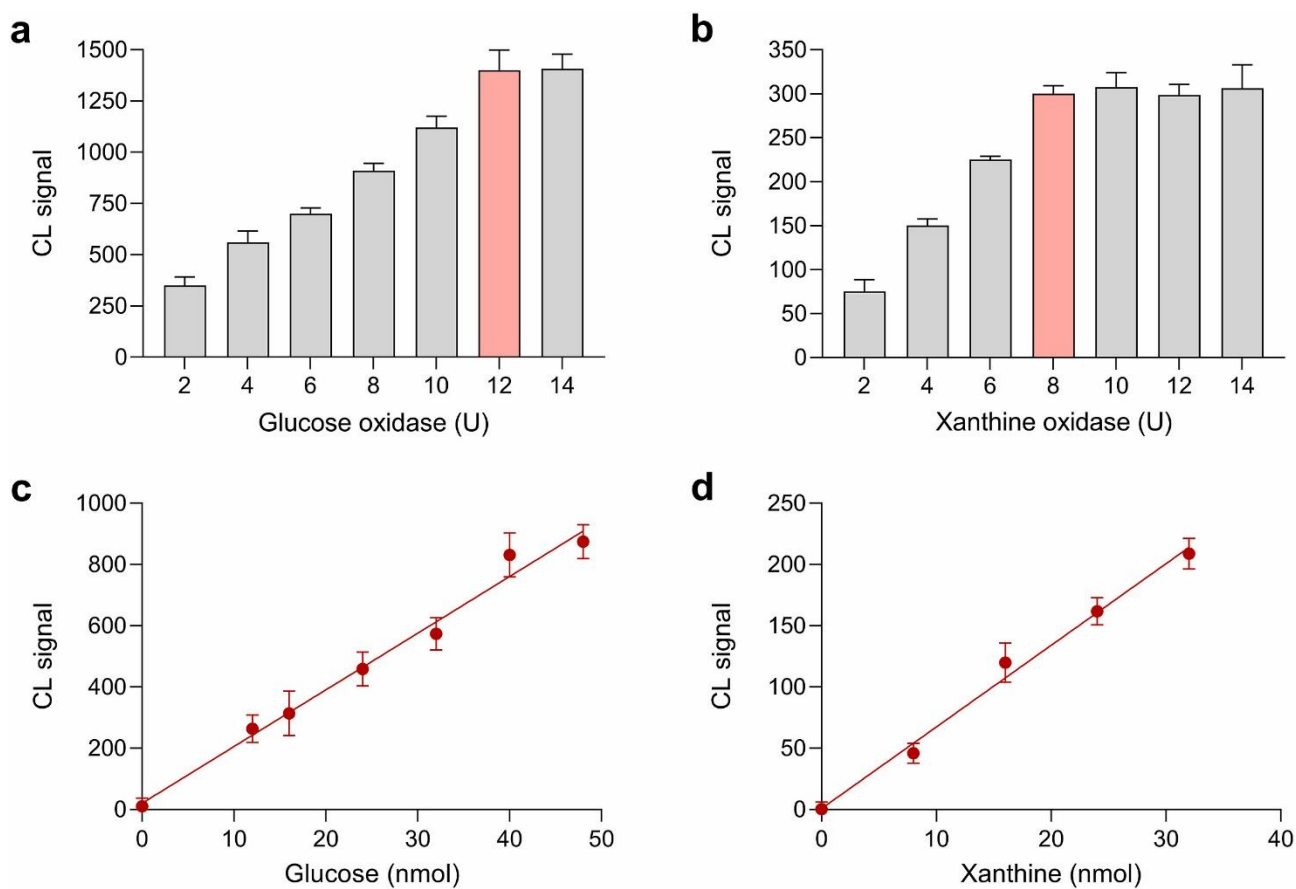


Figure 4. Optimization of experimental conditions of the experiment involving the GOD/HRP system. Panels (a) and (b) show the CL signals obtained for experiment #4 and experiment #5, respectively, performed in μ PADs prepared with different amounts of GOD and XO. The amounts of enzymes selected for the preparation of the μ PAD are highlighted in red. Panels (c) and (d) show the calibration curves generated for experiment #4 and experiment #5, respectively, by analysing μ PADs prepared with different amounts of enzyme substrates. All the other reagents were used at their optimal amounts. The equations of the linear calibration curves were $Y = (18.5 \pm 2.5)X + (20.2 \pm 70.2)$ ($R^2 = 0.989$) and $Y = (6.66 \pm 1.14)X + (0.67 \pm 22.52)$

($R^2 = 0.991$) for glucose and xanthine, respectively. Each data is the mean \pm SD of CL signals measured in the “wells” of three μ PAD channels.

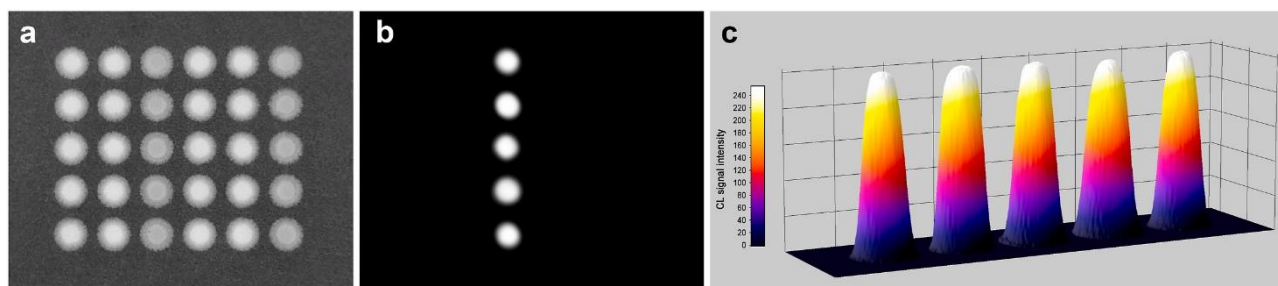


Figure 5. Study of the spatial distribution of the CL signal. **(a)** Images of the μ PAD and **(b)** of the CL emission obtained when PB was injected in one of the channels containing potassium hexacyanoferrate (III) as the CL catalyst (i.e., the third channel from the left). To allow localization of the CL emission, both images were acquired using the same CCD camera. **(c)** 3D profiles of the distribution of the CL signal along the active channel of the μ PAD.

We also investigated in detail the correlation between the CL signal and the amount of enzyme substrates (glucose and xanthine) used in experiments #4 and #5. Indeed, besides the selection of the amount of glucose and xanthine for the preparation of the ABCS μ PAD, we were also interested in the possibility to quantify these substrates in view of possible applications of this technology for the search of astrobiological markers or in diagnostics. *Fig. 4* also shows the calibration curves generated by analysing μ PADs prepared with different amounts of glucose (*Fig. 4c*) and xanthine (*Fig. 4d*) loaded in the hydrophilic areas of layer A. For both substrates linear calibration curves were obtained extending up to 50 nmol for glucose and 30 nmol for xanthine, indicating the possibility to quantify these substances. The limits of detection (LODs), calculated as the amount of substrate giving a signal corresponding to the mean of blank plus 3 standard deviations, were about 4 nmol and 2 nmol for glucose and xanthine, respectively. For the preparation of the μ PAD for ABCS, amounts of glucose and xanthine well above the upper limits of the calibration curves (i.e., 200 nmol for glucose and 100 nmol for xanthine) were used. Besides the intensity of the CL signals, we also evaluated their distribution on the μ PAD. Indeed, the photosensors measure the intensity of the CL signal but do not give any information about their actual spatial distribution in each

“well” nor on the presence of CL emissions in other areas of the μ PAD, e.g., due to fluid leaks towards the hydrophobic areas. To investigate these aspects, we performed CL imaging measurements of the μ PAD by using a high sensitivity CCD camera. *Fig. 5* shows the results of a CL imaging experiment performed by injecting the buffer in the channel of the μ PAD containing potassium hexacyanoferrate (III) as the CL catalyst. Comparison of the images of the μ PAD (*Fig. 5a*) and of the CL emission (*Fig. 5b*) clearly indicated that CL is generated only in the hydrophilic “wells” of the active μ PAD channel. Furthermore, a detailed investigation of the spatial distribution of the CL signal (*Fig. 5c*) showed a homogeneous distribution of the CL signal in each “well” and a good reproducibility (the variation of the CL signals of the different “wells” is less than 5%).

4.3.4 Stability requirements and testing

To prevent science loss, it was agreed with ESA that the payload would be conserved at 4°C before integration, allowing a maximum 2 – week period at ambient temperature during integration and pre-launch activities (nevertheless, it was not possible to exclude a longer integration-to-launch waiting time). We thus used protective agents to reduce the thermal degradation of the enzymes (HRP, GOD, and XO) deposited in the μ PAD. We tested either poly (allylamine) hydrochloride, a polyelectrolyte polymer used in layer – by – layer (LBL) enzyme immobilisation and as coating agent to preserve enzymes deposited on solid supports [37], and pullulan, a natural polysaccharide that has already proved capable to increase the stability of enzymes in the dried state (e.g., in tablets) [38] or immobilised on paper [39]. To assess the effect of protective agents we compared the CL signals of μ PADs prepared with and without the protective agents and stored for various times at temperatures ranging between 4 °C and 37 °C. *Fig. 6* reports the CL signals obtained for experiment #3, in which HRP was used as the CL catalyst. The results clearly show that pullulan significantly increased the stability of the enzyme, since it reduced the decrease in enzyme activity to approximately 10% even after 4 weeks of storage at 37 °C. A similar improvement in enzyme stability has been obtained also for

experiments #4 and #5 employing the enzyme coupled systems GOD/HRP and XO/HRP, respectively (data not shown).

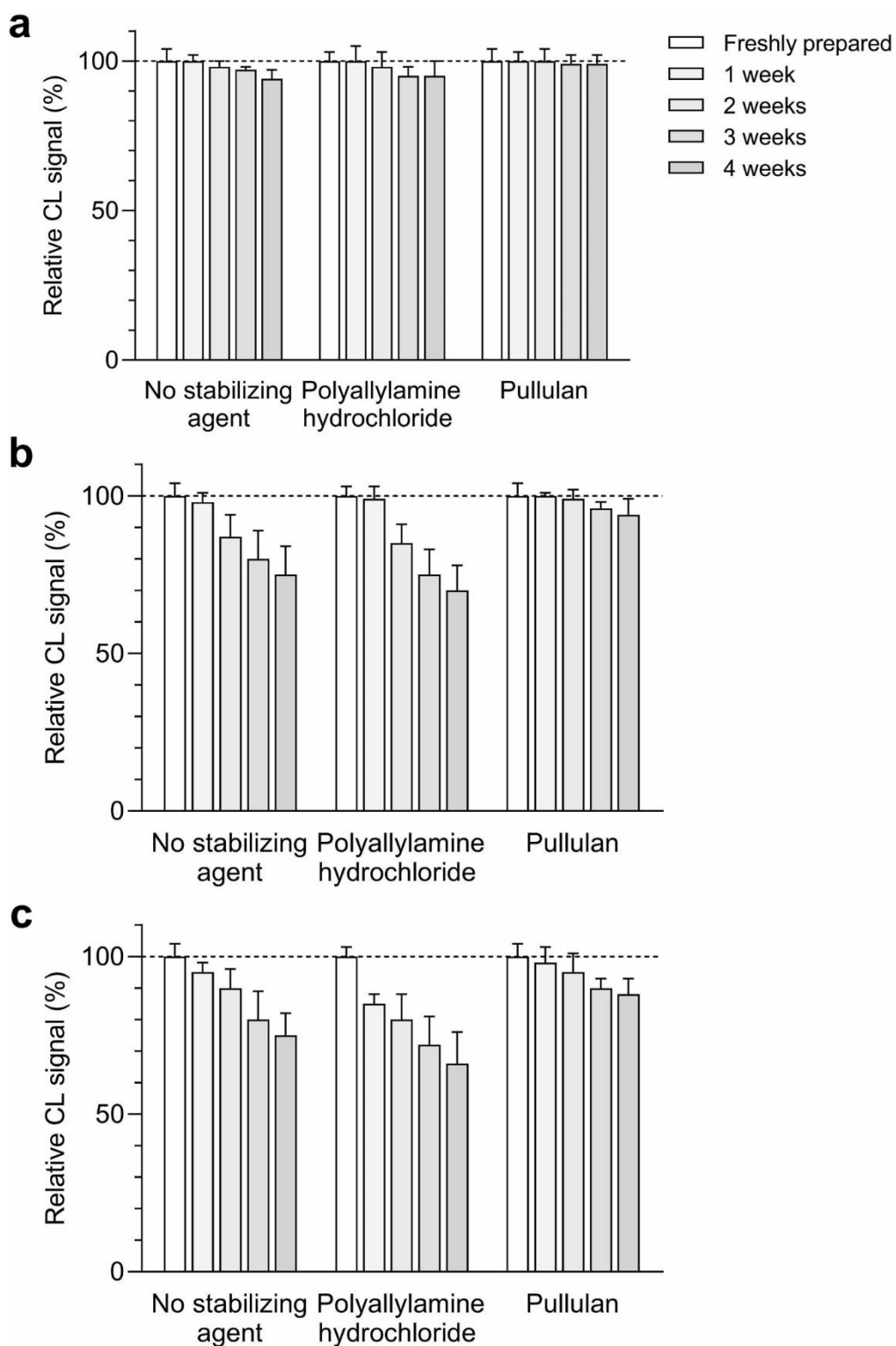


Figure 6. Study of stability of the μ PAD upon storage. The CL signals obtained for experiment #3 performed in μ PADs prepared with and without protective agents (the concentration of both protective agents in the

enzyme solutions deposited in the μ PAD was 1.0 mg mL^{-1}) and stored for various times at **(a)** $4 \text{ }^\circ\text{C}$, **(b)** $25 \text{ }^\circ\text{C}$, and **(c)** $37 \text{ }^\circ\text{C}$ are reported. Each data is the mean \pm SD of the values obtained in the “wells” of three μ PAD channels (in all graphs the signal intensity was normalised to that measured immediately after preparation of the μ PAD).

4.3.5 Test experiments performed on the ground model of ABCS

As a final test, the experiments selected for ABCS were performed in the ground model of the nanosatellite according to the experimental protocol outlined in Section 2.4. Representative CL kinetic profiles obtained for such experiments are shown in *Fig. 7*. The blank experiment (experiment #6 in *Table 1*) displayed no significant CL emission (data not shown). All the experiments were correctly executed, and it was possible to follow the time course of the CL emission, therefore possible changes in emission intensity and/or kinetics during in – flight experiments could be observed. Since each experiment was independently optimized, the comparison of CL emission intensities is not so straightforward. Nevertheless, the nature of the CL system remarkably affected the emission kinetics. It can be observed that the CL emissions of the systems employing either potassium hexacyanoferrate (III) or HRP as catalysts suddenly reached the peak intensity, while the onset of the CL emission for the experiment based on the GOD/HRP system was slower. This can be easily explained considering that the peroxide oxidant required for CL emission was immediately available for the first two systems, while it was gradually produced by the GOD – catalysed reaction in the GOD/HRP system. In addition, the decay of the CL signal was faster for the reaction catalysed by potassium hexacyanoferrate (III) with respect to that catalysed by HRP. This can be ascribed to a more rapid substrate consumption, as indicated by the higher CL emission intensity reached by the first CL system (this is not in contrast with the highest catalytic activity expected for HRP with respect to potassium hexacyanoferrate (III), since the molar amount of the inorganic catalyst deposited on the μ PAD was much higher than that of HRP).

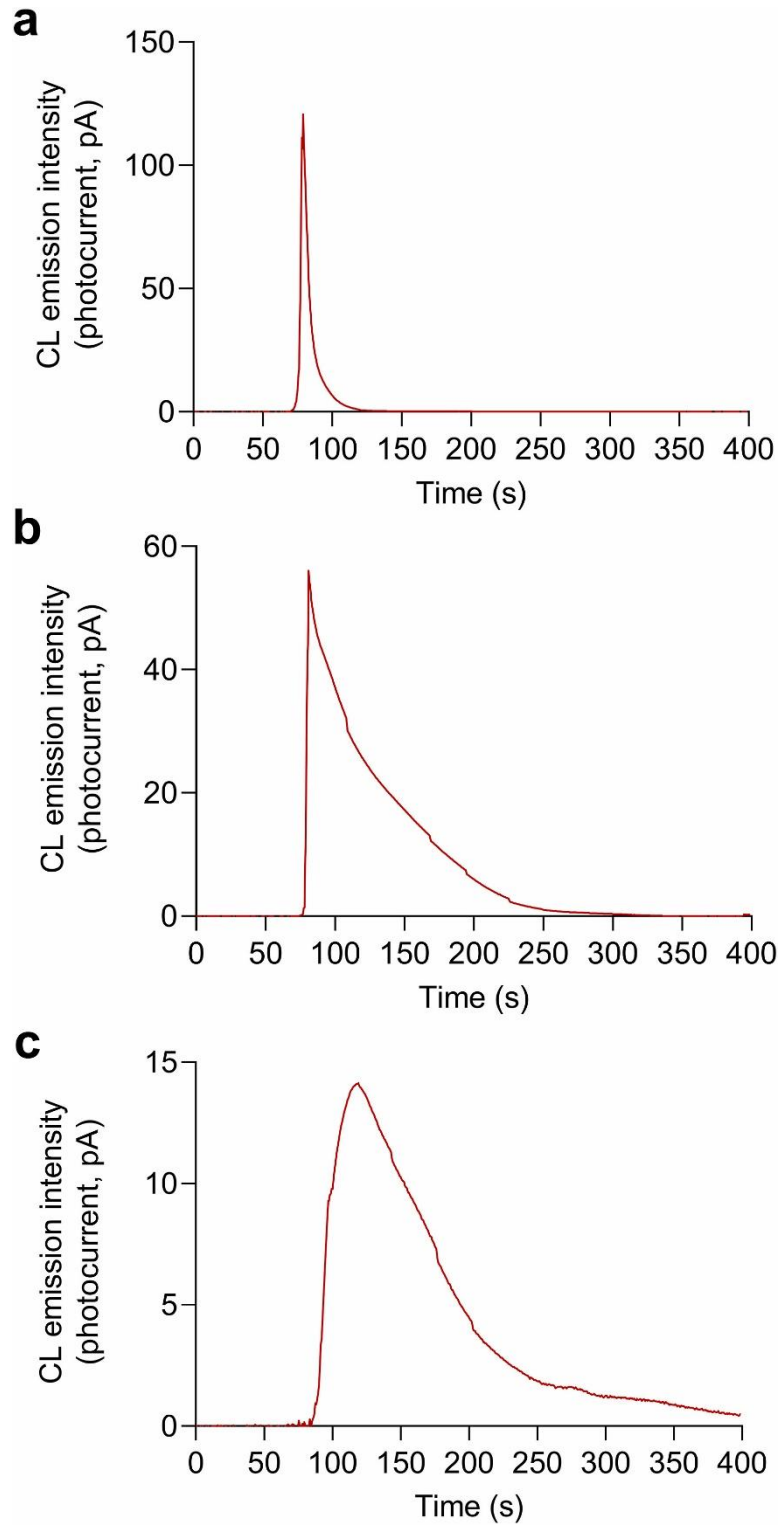


Figure 7. Measurements performed using the ground model of ABCS. The figure shows representative CL kinetic profiles obtained for **(a)** experiment #1, **(b)** experiment #3, and **(c)** experiment #4. The CL signal acquisition started 10 s before the activation of the pump, while buffer delivering was continued for 20 s after the wetness sensor indicated the arrival of the buffer to the μ PAD.

4.4 Conclusions

In conclusion, the ABCS payload demonstrated able to autonomously perform different CL-based bioassays involving systems with increasing chemical complexity, from a single inorganic catalyst to coupled enzymes. The selected CL systems provided intense, easily detectable CL emissions, whose intensities depended on the amounts of reagents and catalysts loaded into the μ PAD. This will allow the monitoring of the CL reactions in in-flight experiments as well as (thanks to the comparison with parallel ground experiments) the assessment of a possible degradation of reagents due to the space radiation environment. Assessment of enzymes' stability will be of particular interest, as coupling of enzyme reactions would be a promising approach for the biodetection of astrobiological life markers that are not easily recognized by antibodies. Finally, the paper-based origami-like analytical format allowed to simplify the architecture of the analytical platform, since all the reagents were preloaded on the paper substrate and triggering of the CL reactions only required injection of phosphate buffer with a miniaturized peristaltic pump. Upon in – flight validation, this approach should constitute the first step to implement a mature technology with the aim to conduct life science research in space more easily and at lower cost than previously possible.

Acknowledgements

We are grateful to Antonio Bardi, Michele Balsamo, and Alessandro Donati (Kayser Italia s.r.l.), Andrea Meneghin (INAF-Astrophysical Observatory of Arcetri), Claudia Pacelli (Italian Space Agency) for fruitful discussion.

References

- [1] GER, 2018. The Global Exploration Roadmap January 2018. https://www.globalspaceexploration.org/wordpress/wp-content/isec/g/GER_2018_small_mobile.pdf.
- [2] Kanapskyte, A.; Hawkins, E. M.; Liddell, L. C.; Bhardwaj, S. R.; Gentry, D.; Santa Maria, S. R. Space Biology Research and Biosensor Technologies: Past, Present, and Future. *Biosensors* **2021**, *11* (2), 38. <https://doi.org/10.3390/bios11020038>.
- [3] Roda, A.; Mirasoli, M.; Guardigli, M.; Zangheri, M.; Caliceti, C.; Calabria, D.; Simoni, P. Advanced Biosensors for Monitoring Astronauts' Health during Long-Duration Space Missions. *Biosensors and Bioelectronics* **2018**, *111*, 18–26. <https://doi.org/10.1016/j.bios.2018.03.062>.
- [4] Amalfitano, S.; Levantesi, C.; Copetti, D.; Stefani, F.; Locantore, I.; Guarnieri, V.; Lobascio, C.; Bersani, F.; Giacosa, D.; Detsis, E.; Rossetti, S. Water and Microbial Monitoring Technologies towards the near Future Space Exploration. *Water Research* **2020**, *177*, 115787. <https://doi.org/10.1016/j.watres.2020.115787>.
- [5] Cousins, C. R.; Cockell, C. S. An ESA Roadmap for Geobiology in Space Exploration. *Acta Astronautica* **2016**, *118*, 286–295. <https://doi.org/10.1016/j.actaastro.2015.10.022>.
- [6] Blanco, Y.; Gallardo-Carreño, I.; Ruiz-Bermejo, M.; Puente-Sánchez, F.; Cavalcante-Silva, E.; Quesada, A.; Prieto-Ballesteros, O.; Parro, V. Critical Assessment of Analytical Techniques in the Search for Biomarkers on Mars: A Mummified Microbial Mat from Antarctica as a Best-Case Scenario. *Astrobiology* **2017**, *17* (10), 984–996. <https://doi.org/10.1089/ast.2016.1467>.
- [7] Moreno-Paz, M.; Gómez-Cifuentes, A.; Ruiz-Bermejo, M.; Hofstetter, O.; Maquieira, Á.; Manchado, J. M.; Morais, S.; Sephton, M. A.; Niessner, R.; Knopp, D.; Parro, V. Detecting Nonvolatile Life- and Nonlife-Derived Organics in a Carbonaceous Chondrite Analogue with a New Multiplex Immunoassay and Its Relevance for Planetary Exploration. *Astrobiology* **2018**, *18* (8), 1041–1056. <https://doi.org/10.1089/ast.2017.1747>.

- [8] Nascetti, A.; Mirasoli, M.; Marchegiani, E.; Zangheri, M.; Costantini, F.; Porchetta, A.; Iannascoli, L.; Lovecchio, N.; Caputo, D.; de Cesare, G.; Pirrotta, S.; Roda, A. Integrated Chemiluminescence-Based Lab-on-Chip for Detection of Life Markers in Extraterrestrial Environments. *Biosensors and Bioelectronics* **2019**, *123*, 195–203. <https://doi.org/10.1016/j.bios.2018.08.056>.
- [9] ESA, 2020. *Space cholesterol: A new testing technology*. https://www.esa.int/Enabling_Support/Space_Engineering_Technology/Shaping_the_Future/Space_cholesterol_A_new_testing_technology.
- [10] ISS National Laboratory, 2020. *Leveraging Microgravity to Improve Medical Diagnostics – One Drop at a Time*. <https://www.issnationallab.org/1drop-diagnostics-leverage-microgravity-improve-medical-diagnostics/>.
- [11] Mora, M. F.; Kehl, F.; Tavares da Costa, E.; Bramall, N.; Willis, P. A. Fully Automated Microchip Electrophoresis Analyzer for Potential Life Detection Missions. *Anal. Chem.* **2020**, *92* (19), 12959–12966. <https://doi.org/10.1021/acs.analchem.0c01628>.
- [12] Xu, T.; Shi, W.; Huang, J.; Song, Y.; Zhang, F.; Xu, L.-P.; Zhang, X.; Wang, S. Superwetable Microchips as a Platform toward Microgravity Biosensing. *ACS Nano* **2017**, *11* (1), 621–626. <https://doi.org/10.1021/acsnano.6b06896>.
- [13] Zangheri, M.; Mirasoli, M.; Guardigli, M.; Di Nardo, F.; Anfossi, L.; Baggiani, C.; Simoni, P.; Benassai, M.; Roda, A. Chemiluminescence-Based Biosensor for Monitoring Astronauts' Health Status during Space Missions: Results from the International Space Station. *Biosensors and Bioelectronics* **2019**, *129*, 260–268. <https://doi.org/10.1016/j.bios.2018.09.059>.
- [14] Ferranti, F.; Del Bianco, M.; Pacelli, C. Advantages and Limitations of Current Microgravity Platforms for Space Biology Research. *Applied Sciences* **2021**, *11* (1), 68. <https://doi.org/10.3390/app11010068>.
- [15] Freissinet, C.; Millan, M.; Glavin, D. P.; Li, X.; Grubisic, A.; Eigenbrode, J. E.; Stern, J. C.; Dworkin, J. P.; Buch, A.; Szopa, C.; Guzman, M. A.; Carts, M. A.; Getty, S. A.; Brinckerhoff, W. B. Investigating the Effects of Gamma Radiation on Selected Chemicals for Use in Biosignature Detection Instruments on the Surface

- of Jupiter's Moon Europa. *Planetary and Space Science* **2019**, *175*, 1–12. <https://doi.org/10.1016/j.pss.2019.05.009>.
- [16] Poghosyan, A.; Golkar, A. CubeSat Evolution: Analyzing CubeSat Capabilities for Conducting Science Missions. *Progress in Aerospace Sciences* **2017**, *88*, 59–83. <https://doi.org/10.1016/j.paerosci.2016.11.002>.
- [17] Padgen, M. R.; Liddell, L. C.; Bhardwaj, S. R.; Gentry, D.; Marina, D.; Parra, M.; Boone, T.; Tan, M.; Ellingson, L.; Rademacher, A.; Benton, J.; Schooley, A.; Mousavi, A.; Friedericks, C.; Hanel, R. P.; Ricco, A. J.; Bhattacharya, S.; Santa Maria, S. R. BioSentinel: A Biofluidic Nanosatellite Monitoring Microbial Growth and Activity in Deep Space. *Astrobiology* **2023**, *23* (6), 637–647. <https://doi.org/10.1089/ast.2020.2305>.
- [18] National Academies of Sciences, Engineering, and Medicine. *Achieving Science with CubeSats: Thinking Inside the Box*; National Academies Press: Washington, D.C., 2016. <https://doi.org/10.17226/23503>.
- [19] Al Mughairy, B.; Al-Lawati, H. A. J. Recent Analytical Advancements in Microfluidics Using Chemiluminescence Detection Systems for Food Analysis. *TrAC Trends in Analytical Chemistry* **2020**, *124*, 115802. <https://doi.org/10.1016/j.trac.2019.115802>.
- [20] Roda, A.; Arduini, F.; Mirasoli, M.; Zangheri, M.; Fabiani, L.; Colozza, N.; Marchegiani, E.; Simoni, P.; Moscone, D. A Challenge in Biosensors: Is It Better to Measure a Photon or an Electron for Ultrasensitive Detection? *Biosensors and Bioelectronics* **2020**, *155*, 112093. <https://doi.org/10.1016/j.bios.2020.112093>.
- [21] Calabretta, M. M.; Zangheri, M.; Calabria, D.; Lopreside, A.; Montali, L.; Marchegiani, E.; Trozzi, I.; Guardigli, M.; Mirasoli, M.; Michelini, E. Paper-Based Immunosensors with Bio-Chemiluminescence Detection. *Sensors* **2021**, *21* (13), 4309. <https://doi.org/10.3390/s21134309>.
- [22] Tong, X.; Ga, L.; Zhao, R.; Ai, J. Research Progress on the Applications of Paper Chips. *RSC Advances* **2021**, *11* (15), 8793–8820. <https://doi.org/10.1039/D0RA10470A>.

- [23] Brucato, J. R.; Nascetti, A.; Iannascoli, L.; Meneghin, A.; Paglialunga, D.; Poggiali, G.; Pirrotta, S.; Pacelli, C.; Impresario, G.; Carletta, S.; Schirone, L.; Anfossi, L.; Mirasoli, M.; Calabria, D.; Popova, L.; Donati, A.; Bardi, A.; Balsamo, M. Astrobio-Cubesat: A Highly Integrated Laboratory to Test in Space Immunoassay Techniques to Detect Biomolecules. **2021**, 2494.
- [24] Kodaira, S.; Naito, M.; Uchihori, Y.; Hashimoto, H.; Yano, H.; Yamagishi, A. Space Radiation Dosimetry at the Exposure Facility of the International Space Station for the Tanpopo Mission. *Astrobiology* **2021**, *21* (12), 1473–1478. <https://doi.org/10.1089/ast.2020.2427>.
- [25] Kempner, E. S. Effects of High-Energy Electrons and Gamma Rays Directly on Protein Molecules. *Journal of Pharmaceutical Sciences* **2001**, *90* (10), 1637–1646. <https://doi.org/10.1002/jps.1114>.
- [26] Robson, D. J.; Cappelletti, C. Biomedical Payloads: A Maturing Application for CubeSats. *Acta Astronautica* **2022**, *191*, 394–403. <https://doi.org/10.1016/j.actaastro.2021.11.017>.
- [27] Ball, R.; Brindley, J. The Power Without the Glory: Multiple Roles of Hydrogen Peroxide in Mediating the Origin of Life. *Astrobiology* **2019**, *19* (5), 675–684. <https://doi.org/10.1089/ast.2018.1886>.
- [28] He, Y.; Buch, A.; Morisson, M.; Szopa, C.; Freissinet, C.; Williams, A.; Millan, M.; Guzman, M.; Navarro-Gonzalez, R.; Bonnet, J. Y.; Coscia, D.; Eigenbrode, J. L.; Malespin, C. A.; Mahaffy, P.; Glavin, D. P.; Dworkin, J. P.; Lu, P.; Johnson, S. S. Application of TMAH Thermochemolysis to the Detection of Nucleobases: Application to the MOMA and SAM Space Experiment. *Talanta* **2019**, *204*, 802–811. <https://doi.org/10.1016/j.talanta.2019.06.076>.
- [29] Burgio, N.; Cretara, L.; Corcione, M.; Frullini, M.; Iannascoli, L.; Nascetti, A.; Santagata, A.; Palmerini, G.; Quintino, A.; Brucato, J. R.; Meneghin, A.; Paglialunga, D. Modelling the Interaction of the Astro Bio Cube Sat with the Van Allen’s Belt Radiative Field Using Monte Carlo Transport Codes. *Radiat Detect Technol Methods* **2022**, *6* (2), 262–279. <https://doi.org/10.1007/s41605-022-00321-9>.

- [30] Lovecchio, N.; Costantini, F.; Parisi, E.; Nardecchia, M.; Tucci, M.; Nascetti, A.; de Cesare, G.; Caputo, D. Integrated Optoelectronic Device for Detection of Fluorescent Molecules. *IEEE Transactions on Biomedical Circuits and Systems* **2018**, *12* (6), 1337–1344. <https://doi.org/10.1109/TBCAS.2018.2880922>.
- [31] Mirasoli, M.; Nascetti, A.; Caputo, D.; Zangheri, M.; Scipinotti, R.; Cevenini, L.; de Cesare, G.; Roda, A. Multiwell Cartridge with Integrated Array of Amorphous Silicon Photosensors for Chemiluminescence Detection: Development, Characterization and Comparison with Cooled-CCD Luminograph. *Anal Bioanal Chem* **2014**, *406* (23), 5645–5656. <https://doi.org/10.1007/s00216-014-7971-9>.
- [32] Mirasoli, M.; Bonvicini, F.; Lovecchio, N.; Petrucci, G.; Zangheri, M.; Calabria, D.; Costantini, F.; Roda, A.; Gallinella, G.; Caputo, D.; de Cesare, G.; Nascetti, A. On-Chip LAMP-BART Reaction for Viral DNA Real-Time Bioluminescence Detection. *Sensors and Actuators B: Chemical* **2018**, *262*, 1024–1033. <https://doi.org/10.1016/j.snb.2018.02.086>.
- [33] Zangheri, M.; Di Nardo, F.; Mirasoli, M.; Anfossi, L.; Nascetti, A.; Caputo, D.; De Cesare, G.; Guardigli, M.; Baggiani, C.; Roda, A. Chemiluminescence Lateral Flow Immunoassay Cartridge with Integrated Amorphous Silicon Photosensors Array for Human Serum Albumin Detection in Urine Samples. *Anal Bioanal Chem* **2016**, *408* (30), 8869–8879. <https://doi.org/10.1007/s00216-016-9991-0>.
- [34] Nascetti, A.; Colonia, G.; Caputo, D.; De Cesare, G. Sophie: A General Purpose Sub-Picoamps Current Readout Electronics. In *Sensors*; Compagnone, D., Baldini, F., Di Natale, C., Betta, G., Siciliano, P., Eds.; Lecture Notes in Electrical Engineering; Springer International Publishing: Cham, 2015; pp 285–289. https://doi.org/10.1007/978-3-319-09617-9_50.
- [35] Oosthuizen, M. M. J.; Englbrecht, M. E.; Lambrechts, H.; Greyling, D.; Levy, R. D. The Effect of pH on Chemiluminescence of Different Probes Exposed to Superoxide and Singlet Oxygen Generators. *Journal of Bioluminescence and Chemiluminescence* **1997**, *12* (6), 277–284. [https://doi.org/10.1002/\(SICI\)1099-1271\(199711/12\)12:6<277::AID-BIO455>3.0.CO;2-B](https://doi.org/10.1002/(SICI)1099-1271(199711/12)12:6<277::AID-BIO455>3.0.CO;2-B).

- [36] Bankar, S. B.; Bule, M. V.; Singhal, R. S.; Ananthanarayan, L. Glucose Oxidase — An Overview. *Biotechnology Advances* **2009**, *27* (4), 489–501. <https://doi.org/10.1016/j.biotechadv.2009.04.003>.
- [37] Cejudo-Sanches, J.; Orrego, A. H.; Jaime-Mendoza, A.; Ghobadi, R.; Moreno-Perez, S.; Fernandez-Lorente, G.; Rocha-Martin, J.; Guisan, J. M. High Stabilization of Immobilized *Rhizomucor Miehei* Lipase by Additional Coating with Hydrophilic Crosslinked Polymers: Poly-Allylamine/Aldehyde–Dextran. *Process Biochemistry* **2020**, *92*, 156–163. <https://doi.org/10.1016/j.procbio.2020.02.026>.
- [38] Jahanshahi-Anbuhi, S.; Kannan, B.; Leung, V.; Pennings, K.; Liu, M.; Carrasquilla, C.; White, D.; Li, Y.; H. Pelton, R.; D. Brennan, J.; M. Filipe, C. D. Simple and Ultrastable All-Inclusive Pullulan Tablets for Challenging Bioassays. *Chemical Science* **2016**, *7* (3), 2342–2346. <https://doi.org/10.1039/C5SC04184H>.
- [39] Kannan, B.; Jahanshahi-Anbuhi, S.; Pelton, R. H.; Li, Y.; Filipe, C. D. M.; Brennan, J. D. Printed Paper Sensors for Serum Lactate Dehydrogenase Using Pullulan-Based Inks to Immobilize Reagents. *Anal. Chem.* **2015**, *87* (18), 9288–9293. <https://doi.org/10.1021/acs.analchem.5b01923>.

An Origami Paper-Based Biosensor for Allergen Detection by Chemiluminescence Immunoassay on Magnetic Microbeads

Reproduced from: “An Origami Paper-Based Biosensor for Allergen Detection by Chemiluminescence Immunoassay on Magnetic Microbeads”

Elisa Lazarini, Andrea Pace, Ilaria Trozzi, Martina Zangheri, Massimo Guardigli, Donato Calabria, Mara Mirasoli

Biosensors, 2022, 12(10), 825

<https://doi.org/10.3390/bios12100825>

Reproduced by permission of MDPI (Open Access Article)

<https://creativecommons.org/licenses/by/4.0/>

5.1 Introduction

Adverse reactions to food can be classified as food allergies and intolerances. According to the Expert Panel Report sponsored by the National Institute of Allergy and Infectious Diseases (NIAID), food allergy is defined as “an adverse health effect arising from a specific immune response that occurs reproducibly on exposure to a given food”, while food intolerance consists of “nonimmune reactions that include metabolic, toxic, pharmacologic, and undefined mechanisms”. In contrast to food intolerance, allergy is dose independent; thus, even the presence of traces of allergens can cause serious consequences [1]. As an effective treatment for food allergies is not yet available, allergen-suspicious food avoidance by sensitive consumers is the only possible strategy to avoid negative outcomes. Presently, no regulatory threshold exists for allergenic contents in food samples; therefore, highly sensitive analytical methods are required [2]. Egg allergy is one of the most common allergies, especially among infants and children, and can cause symptoms involving the respiratory system, or even potentially fatal anaphylaxis [3]. The egg white proteins ovalbumin, lysozyme, ovomucoid and ovotransferrin are the major egg allergens. Ovalbumin (OVA) is the most abundant, making up approximately 54% of the total albumen proteins [4], and is, therefore, considered as the best detection target for the search of egg allergens [5]. OVA is a phospho-glycoprotein of about 45 kDa, composed of 385 amino acids. OVA is not only present in food products that contain eggs, but it can be found in other food commodities. For example, it is used in the wine clarification process to eliminate the excess suspended matter, without altering the character of the drink. Ovalbumin is also used in many food products as an emulsifying agent or to bind ingredients together, thanks to its ability to thermally coagulate. Furthermore, the widespread use of OVA poses significant risks of unintended food contamination during food processing procedures. All these considerations call for the development of analytical tools that are able to rapidly detect OVA in a variety of products for human use. The detection of allergens in food products can be pursued through different analytical approaches, the main being immunoanalytical, mass-spectrometry, nucleic – acid – based methods, and

biosensors [6, 7]. Laboratory methods are generally very sensitive and accurate; however, they are often laborious, time – consuming, expensive, and require experienced personnel and well – equipped laboratories. To enable fast and convenient point – of – use analyses, in recent decades, many efforts have been directed towards the development of simple – to – use devices for on – site analysis, thus allowing real – time measurement of allergens [2, 8, 9]. The conventional enzyme – linked immunosorbent assays (ELISAs), which employ antibodies for the highly specific analyte recognition and enzyme catalysts for sensitive detection, provide good analytical performance, especially when coupled with chemiluminescence (CL) detection [10]. However, they are not suited for point – of – use applications, as they need a large volume of reagents, time – consuming manipulations, and tedious washing steps. Lateral flow immunochromatographic assays (LFIAs) are routinely used for the on – site detection of allergen traces in finished products, due to their ease of use and competitive prices. However, most of them rely on colorimetric detection, exploiting colloidal gold as a tracer; thus, they only provide qualitative yes/no results [11, 12]. Microfluidic paper – based analytical devices (μ PADs) have recently attracted much attention due to their ease of use, low consumption of reagents, low cost, rapidity, portability, and disposability [13, 14, 15, 16]. These devices use paper as a substrate to create microfluidic structures (e.g., channels, reagent mixers, reaction chambers) by patterning hydrophobic materials on hydrophilic paper. The use of origami (paper folding) and kirigami (paper cutting) techniques in the fabrication of μ PADs has given researchers the opportunity to fabricate 3D paper – based devices, which provide high flexibility of application and allow us to conduct complex multistep analytical procedures, such as full immunoassays, on paper [17, 18, 19, 20]. Indeed, in contrast to the simplest μ PADs, such as LFIAs, in which fluids are only drawn horizontally through the device, 3D devices sustain the flow both horizontally and vertically. In addition to higher versatility, these devices often possess superior analytical performance, since the vertical flow provides higher assay rapidity and sensitivity [21]. Coupling this format with CL detection also takes advantage of CL's specific features [22], such as amenability to miniaturization as well as high sensitivity and specificity of detection, even though only a

few examples have been published up to now [23, 24, 25, 26]. Furthermore, μ PAD – based assays enable the immobilization of biospecific recognition molecules (such as enzymes, antigens, antibodies, aptamers, or nucleic acids) on paper. Bioprobes can be directly immobilized onto paper surfaces; however, this has the limitations of providing a limited surface area for the subsequent reactions and poor coating efficiency, and requiring complex procedures for substrate modification and surface functionalization [21]. On the contrary, particle – modified μ PADs allow easy and efficient biomolecule immobilization in defined device areas, therefore improving the overall assay performance [27, 28, 29]. However, previously published particle – modified μ PADs involve complex analytical protocols and in most cases, only the final signal detection is performed in the μ PAD, thus compromising their amenability for point – of – use application. Herein, we report an origami paper – based device, which employs magnetic microbeads (MBs) for paper substrate functionalization and is used to perform a competitive CL immunoassay for OVA in food samples. In this assay, OVA in the sample competes with OVA immobilized on MBs for a limited amount of HRP – labelled anti – OVA antibody (anti – OVA – HRP). The use of MBs enables easy and efficient OVA immobilization, as well as the production of a device in which the MBs are contained in well – defined reaction areas on paper, providing an increased surface area for immunoreaction. By exploiting the origami approach, all the steps of the immunoassay procedure (i.e., immunoreaction, washing, detection) were carried out by appropriately folding/unfolding the device. All the reagents required for assay execution are preloaded in dried form in the μ PAD, so that only sample and buffer applications were required to complete the assay, with no need for handling chemicals or conducting complex procedures. Finally, as the washing step is critical for obtaining accurate analyte detection in immunoassays and because effective washing is quite challenging in μ PAD-based formats, we designed and implemented multiple washing layers in the μ PAD to solve this issue.

5.2 Materials and methods

5.2.1 Chemicals

SPHEROTM Carboxyl magnetic particles (MBs, 2.5% w/v, 3.90 μm diameter) were obtained from Spherotech Inc (Lake Forest, IL, USA). Ovalbumin from chicken egg white (lyophilized powder, $\geq 98\%$), bovine serum albumin (lyophilized powder, $\geq 96\%$), rabbit serum albumin (lyophilized powder, $\geq 99\%$), lysozyme from chicken egg white (lyophilized powder, protein $\geq 90\%$), horseradish peroxidase (HRP, lyophilized powder, $\geq 250 \text{ U mg}^{-1}$), casein from bovine milk (purified powder), N-hydroxysulfosuccinimide sodium salt (sulfo-NHS, $\geq 98\%$), 1-ethyl-3-(3-dimethylaminopropyl)carbodiimide hydrochloride (EDC, $\geq 98\%$), sorbitol ($\geq 99\%$), 2-(N-morpholino)ethanesulfonic acid (MES, $\geq 99\%$), tris(hydroxymethyl)aminomethane (TRIS, $\geq 99.8\%$) and Tween 20 were purchased from Sigma – Aldrich (St Louis, MO, USA). HRP – labelled anti – ovalbumin polyclonal rabbit antibody (anti – OVA – HRP) and SuperSignalTM ELISA Femto Maximum Sensitivity Substrate (a two – component luminol – based CL cocktail, composed of a luminol/enhancer solution and a stable peroxide solution) were obtained from Thermo-Fisher Scientific (Fair Lawn, NJ, USA). All the other chemicals were of the highest purity available. The Whatman CHR 1 chromatographic paper (200 \times 200 mm sheets) was bought from Sigma – Aldrich. The following buffers were used in the functionalization of MBs and in the assay procedure: PBS (10 mmol L^{-1} phosphate buffer, pH 7.4, containing 137 mmol L^{-1} NaCl), PBST (PBS containing 0.05% v/v Tween 20), MES (25 mmol L^{-1} MES, pH 5.0), and TRIS (25 mmol L^{-1} TRIS, pH 7.0, containing 250 mmol L^{-1} NaCl). For assay validation, a commercial colorimetric microtiter plate – based ELISA kit for the quantitative detection of OVA in food samples (AgraQuant® Ovalbumin, Romer Labs Division Holding GmbH, Getzersdorf, Austria) has been used. Samples have been extracted following the procedure described in Section 2.6 and assayed according to the manufacturer’s instructions.

5.2.2 Fabrication of the origami μ PAD device

The origami μ PAD was produced by drawing the layout of the hydrophobic areas on PowerPoint (*Figure 1a*) and printing the areas on a 200×200 mm Whatman CHR 1 chromatography paper sheet using a commercial solid ink Phaser 8560DN printer (Xerox Co., Norwalk, CN, USA). The folding lines were created by a manual rotary perforating blade and the μ PAD was cut from the paper sheet and heated at 120 °C for 10 min in an oven to melt the wax-based solid ink, which diffused into the paper, generating the hydrophobic barriers. Then, the reagents were loaded into the origami μ PAD by dispensing the solutions onto the four hydrophilic areas of levels A (first 10 μ L of 3.5 mg mL^{-1} OVA – MBs suspension in PBS was added in each area and then, after drying, 15 μ L of 1% w/v casein solution in PBS was added to saturate the paper surface), C (5 μ L of 1 $\mu\text{g mL}^{-1}$ anti – OVA – HRP conjugate solution in PBS containing 1 mg mL^{-1} sorbitol in each area), E1 (20 μ L of the luminol/enhancer solution of the SuperSignalTM substrate in each area), and E2 (20 μ L of 10 mmol L^{-1} sodium perborate solution in PBS in each area); the solutions in layers E1 and E2 were loaded through four successive 5 - μ L additions, each after complete evaporation of the liquid. After air – drying at room temperature in the dark for 1 h, the biosensor was vacuum sealed in a plastic bag and stored at 4 °C and in the dark until use (*Figure 1b*).

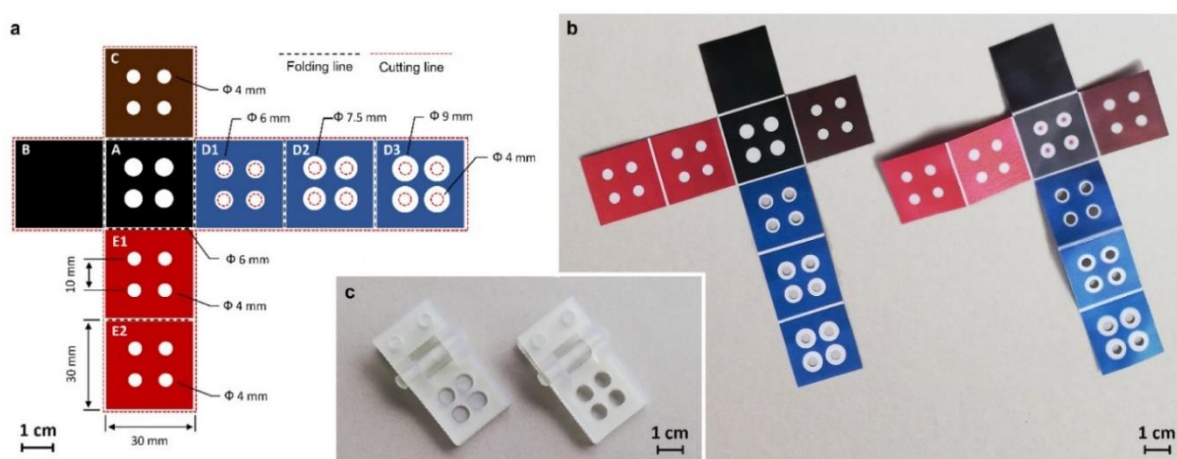


Figure 1. (a) Design of the hydrophobic areas of the origami μ PAD. Black and red dashed lines represent folding lines (created by a manual rotary perforating blade) and cutting lines, respectively. A: base layer; B: anti-leaching layer; C: immunoreaction layer; D: washing layers; E: CL detection layers. (b) Images of the origami

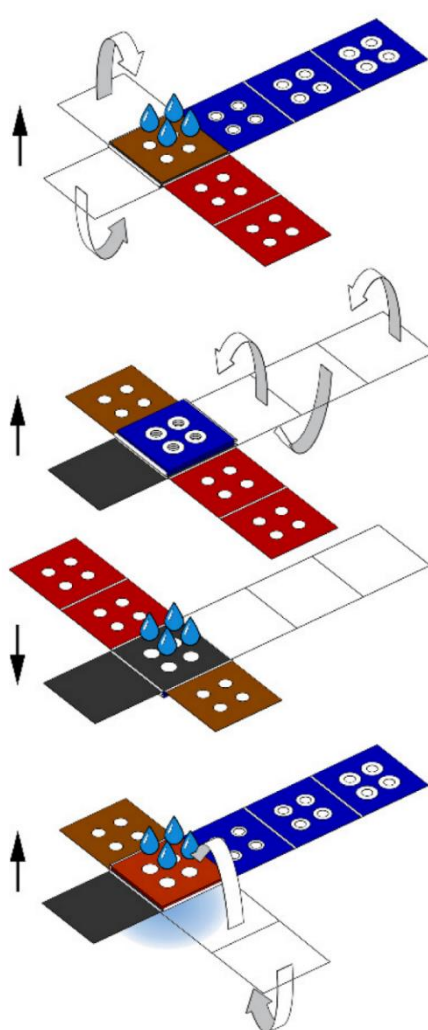
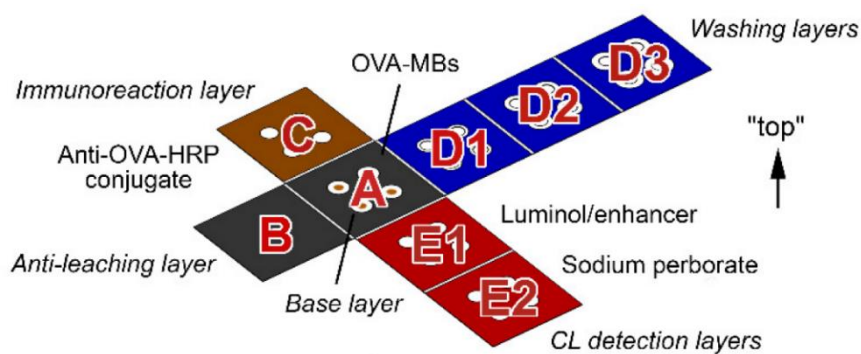
μ PAD just after cutting of excess paper (left) and upon loading and air – drying of reagents and OVA-MBs (right). (c) Images of the spring – loaded 3D – printed holding clips one equipped with magnets and used for loading of OVA – MBs in the μ PAD (left) and one without magnets and employed in the assay procedure (right). The scale bars represent 1 cm.

To facilitate the preparation of the biosensor and the assay procedure, we used two spring – loaded holding clips (*Figure 1c*). The clips were designed and produced in clear resin by stereolithography (SLA) 3D – printing with a Form 2 desktop 3D printer (Formlabs Inc, Somerville, MA, USA). One clip, equipped with four small NdFeB magnets (N45 grade, 8 mm diameter, 3 mm height) located in the bottom half in the correspondence of the four hydrophilic areas of the μ PAD, was used during the loading of OVA – MBs to avoid their excessive dispersion over the hydrophilic area. The second one had four holes in both halves and was used in the assay procedure to guarantee the contact between the layers in the folded origami μ PAD, still permitting the addition of buffers and imaging of the CL signal.

5.2.3 Assay procedure

The overall assay procedure is outlined in *Figure 2* and shown in the Supplementary Materials (Video S1: Assay procedure). The origami μ PAD was removed from the sealed plastic bag. To configure the origami for the first assay step, layer C was folded over layer A and layer B was folded under layer A. The folded origami was inserted in the holding clip with layer C upwards, then 10 μ L of the solutions to be assayed, namely OVA – free solution (PBS), low (0.003 μ g mL⁻¹) and high (1 μ g mL⁻¹) OVA standard solutions in PBS, and the sample, was deposited on each hydrophilic area of layer C to solubilize the anti-OVA – HRP conjugate and start the immunological reaction. Upon 20 min of incubation at room temperature, the origami was unfolded, then the stack of layers D1 – D3 was folded over layer A. The folded origami was inserted in the holding clip with layer A upwards and three 15 μ L – aliquots of washing buffer were deposited at 5 min – time intervals on each hydrophilic area of layer A to remove all unbound species from the MBs in this layer. Finally, after 20 min, the origami was unfolded and the stack of layers E1 – E2 was folded over layer A. The folded origami was inserted in the

holding clip with layer E2 upwards and 10 μL of PBS was added on each hydrophilic area of layer E2, to dissolve the components of the luminol – based CL cocktail required to perform CL detection of the anti – OVA – HRP conjugate bound to the MBs. The CL emission produced by the MBs in layer A was then measured, employing a portable, battery – operated, two – stage Peltier cooled charge coupled device (CCD) camera (ATIK 11000, ATIK Cameras, New Road, Norwich) adapted to perform contact imaging detection, as previously described [30].



Step 1: immunoreaction

- Fold layer B below layer A
- Fold layer C over layer A
- Insert the folded origami in the clip
- Dispense OVA standard solutions or samples on layer C (10 μL for each hydrophilic area)
- Wait 20 min
- Unfold the origami

Step 2: washing

- Fold the stack of layers D1 - D3 over layer A
- Reverse the folded origami
- Insert the folded origami in the clip
- Dispense washing buffer on layer A (3 \times 15 μL for each hydrophilic area at 5-min time intervals)
- Wait 20 min
- Unfold the origami

Step 3: CL detection

- Fold the stack of layers E1 - E2 over layer A
- Insert the folded origami in the clip
- Dispense buffer on layer E2 (10 μL for each hydrophilic area)
- Measure the CL emission

Figure 2. Scheme of the analytical procedure for the determination of OVA using the origami μ PAD. In each assay step, upon folding, the origami μ PAD was inserted into the 3D – printed holding clip (not shown).

A sequence of 100 consecutive images with exposure time of 15 s was acquired, starting immediately after the addition of the buffer. The CL images were analyzed using the freeware ImageJ v.1.53h software (National Institutes of Health, Bethesda, MD). Regions of interest (ROIs) corresponding to the four OVA – MBs deposition areas of layer A were defined and for each image, the CL emission intensities were evaluated by integrating the CL emissions on the ROI areas. Finally, the analytical CL signals were obtained by reconstructing the CL emission intensity kinetic profiles and evaluating the total CL emission as the area under the curve. The ratios between the CL signals of the OVA standards or of the sample and the CL signal of the OVA-free solution were calculated. Finally, the logit of the CL signal ratios of the two OVA standards was plotted against the logarithm of OVA concentration to obtain a two-point linear calibration curve and the amount of OVA in the unknown sample was evaluated by interpolation of its CL signal ratio logit on the calibration curve.

5.2.4 Data elaboration and statistics

All measurements were performed at least in three replicates. All data analysis and statistical data elaboration were performed using GraphPad Prism, version 8.0 (GraphPad Software, Inc., La Jolla, CA, USA). The program was also used to obtain immunoassay calibration curves by fitting experimental data with both a four-parameter logistic equation (sigmoidal curve) and a logit-log function (linear curve).

5.2.5 Real sample processing

The method applicability for the analysis of real samples was assessed by analyzing chocolate chip cookies from different market brands bought in local stores. Sample preparation was carried out according to a previously published procedure [31, 32]. Briefly, about 10 g of cookies were grounded with a cooking blender and 1 g of powder was extracted with 10 mL of TRIS buffer. After homogenization by manual shaking, the

suspension was shaken for 30 min, then let settle for 5 min. Any upper fat layer was discarded, and the clear supernatant was collected, diluted 1:10 (v/v) with TRIS buffer and stored at 4 °C in the dark until analyzed.

5.2.6 In silico simulations

The molecular modelling of the anti – OVA antibody was based on homology modelling that exploits abYsis, a web-based antibody research system [33, 34], and Abymod, an antibody model building tool [35]. In silico binding affinities of proteins with the anti-OVA antibody were calculated by protein – protein molecular docking using HDOCK [36, 37] and PRODIGY webservers [38, 39]. GROMACS [35, 40] was used for structural refinement based on molecular dynamics and energy minimization, while templates for modelling anti – OVA antibody target sequences were obtained from the RCSB Protein Data Bank [41]. The PRODIGY online tool [38] was employed to calculate the thermodynamic binding parameters of complexes between anti – OVA and proteins. The images of complexes were generated by the pyMOL tool [42].

5.3 Results

5.3.1 Synthesis of OVA-MBs

The bioconjugation between MBs and OVA was performed following a previously reported synthetic protocol [43], with slight modifications. Briefly, the surface carboxyl groups of the MBs were activated by a reaction with EDC/sulfo – NHS to produce primary amine – reactive sulfo – NHS esters, which then reacted with OVA to obtain OVA – MBs. The synthetic procedure was optimized to maximize the amount of OVA bound to the MBs, which translated to higher CL signals in the assay. First, the concentration of sulfo – NHS and EDC for the activation of the MBs' carboxyl groups was selected. Different EDC/sulfo – NHS mixtures (1:1 weight ratio) were used to activate the carboxyl groups of MBs. Then, the activated MBs were reacted with a large excess of HRP used as a model protein to verify the efficiency of the activation reaction

(HRP was selected as a model, since the amount of HRP bound to the MBs can be easily measured by CL, due to its enzymatic activity). As shown in *Figure 3a*, the EDC/sulfo – NHS concentration that provided the most efficient activation of carboxyl groups was 0.1 mg mL^{-1} (i.e., 0.1 mg mL^{-1} of EDC and 0.1 mg mL^{-1} of sulfo – NHS). As expected, weaker CL signals, showing an incomplete activation of carboxyl groups, were obtained at lower EDC/sulfo – NHS concentrations. The recorded CL signals were lower also at the highest EDC/sulfo – NHS concentrations, which could be ascribed to the onset of parallel secondary reactions that yielded undesired products, as previously reported by Yan et al. [44]. Then, the best concentration of OVA for the bioconjugation reaction was assessed. Activated MBs were reacted with different concentrations of OVA and the amount of OVA bound to the MBs was measured by CL after incubation of OVA – MBs, with an excess of anti – OVA – HRP.

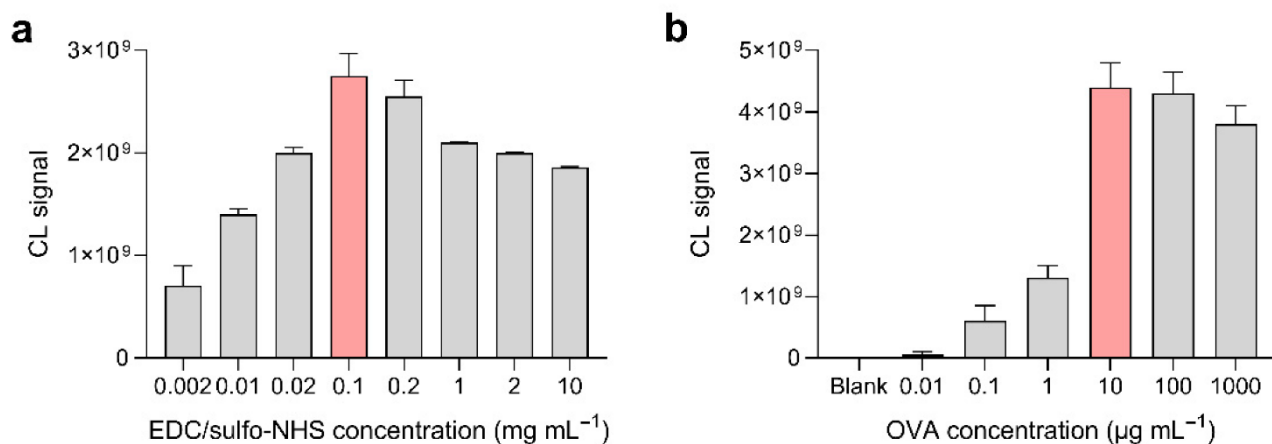


Figure 3. (a) CL signals obtained by employing different EDC/sulfo – NHS concentrations for the activation of the surface carboxyl groups of the MBs. Activated carboxyl groups were quantified by reaction with an excess of HRP, followed by CL detection of the bound enzyme. **(b)** CL signals obtained by employing different OVA concentrations in the coating of activated MBs to obtain OVA – MBs. Ovalbumin bound to MBs was quantified by reaction with an excess of anti – OVA – HRP, followed by CL detection of the conjugate. The optimal experimental conditions are highlighted in red. Each of the data are the mean \pm SD of three measurements.

As shown in *Figure 3b*, which reported the CL signal as a function of the OVA concentration used in the coating of MBs, 10 µg mL^{-1} OVA allowed us to achieve the highest CL signals (i.e., the highest amount of OVA bound to MBs and recognized by

anti – OVA – HRP). In the absence of OVA, no detectable CL signal was obtained, which confirmed the efficacy of the saturation procedures in avoiding any non-specific binding of immunoreagents to MBs. As can be also observed in *Figure 3b*, a slight decrease in the CL signal was also observed for the highest OVA concentrations, which should correspond to the greatest OVA loadings. This effect can be attributed to the worse recognition of OVA by the anti – OVA – HRP antibody due to steric hindrance, when a large amount of OVA is immobilized on the MBs surface [45, 46].

5.3.2 Design of the origami μ PAD

The origami μ PAD consisted of a chromatographic paper sheet in which hydrophilic areas are delimited by wax-printed hydrophobic barriers (the layout of the μ PAD allowed four different analyses to be carried out simultaneously). It included the following five functional layers (i.e., A, B, C, D1–D3, E1–E2), each one with a specific function in the assay procedure:

- A: base layer containing OVA – MBs (all (bio)chemical reactions took place in this layer);
- B: anti – leaching layer (a wax – coated sheet that reduced evaporation and prevented solution leaching during incubation);
- C: immunoreaction layer containing the anti – OVA – HRP immunoreagent;
- D1 – D3: washing layers (collected the buffer in the washing step);
- E1 – E2: CL detection layers containing the luminol/enhancer and sodium perborate CL detection reagents, respectively.

Layers B – E are arranged in a cross shape around the base layer A, thus facilitating their sequential folding during the execution of the steps of the immunoassay protocol (except the first one, each step required folding of only one layer on the base layer). To simplify the assay protocol and eliminate the need for the user to prepare and handle chemicals, all the reagents were preloaded in a dried form on the proper layer. By adding buffers (the only chemicals required for the assay), the dried reagents were dissolved and

transported in the base layer, where the (bio)chemical reactions took place. To guarantee fast and uniform migration of solutions between different layers, a holding clip was produced by 3D-printing and used to keep the origami μ PAD folded, ensuring close contact between the adjacent layers (a second clip equipped with magnets was used during the loading of OVA – MBs in the origami to avoid their excessive dispersion over the hydrophilic areas). Incubation and washing steps are more challenging in μ PADs as compared with conventional (e.g., microtiter plate – based) immunoassay formats, thus requiring specific design and optimization of the device. The assay relies on binding equilibria that involve both species in solution (i.e., OVA and anti – OVA – HRP) and bound to MBs (OVA) and the incubation step is crucial for obtaining accurate quantitative results. Due to small amounts of reagents and the quite long incubation time, evaporation could significantly reduce the volume of solution during incubation, thus altering the concentration of chemicals and affecting the binding equilibria. The stacking of layers C, A and B (from top to bottom) of the origami μ PAD during the incubation created a well-like structure, in which the hydrophilic areas of layers A and C constituted the “well” volume, and the hydrophobic layer B acted as the “well” bottom. This accommodated the solution, avoiding leaking and reducing evaporation, which could only take place at the surface of layer C. Effective washing is also critical in immunoassays because incomplete removal of excess reagents and of non – specifically bound species greatly affects assay sensitivity and reproducibility. The latter phenomenon is particularly important in μ PAD – based formats, since the interaction between biomolecules and cellulose fiber can lead to nonspecific adsorption phenomena, especially for polar or charged molecules [21]. Furthermore, due to capillarity effects of paper, the complete removal of the washing solution is difficult; thus, for efficient washing, a high and sustained flow of liquid across paper is needed. It has been previously shown that this can be obtained in a μ PAD geometry that would provide a steady increase in the available wettable volume. This approach, which was described for a 2D planar configuration [47], was adapted in this work to a 3D geometry by designing a device in which three paper layers (D1 – D3) provided, once folded over layer A, circular hydrophilic crowns with increasing diameter (from 6 to 9 mm). With

this configuration, the washing buffer flows both vertically across the different folded layers and radially towards the boundary hydrophilic zone [48, 49, 50]. In addition, the layers D1 – D3 had a central hole (4 mm diameter) to avoid any mechanical loss of OVA – MBs when unfolding the origami due to the contact with the layer D1. Theoretical approaches for modelling flow in the paper substrate have been proposed to accelerate development of μ PADs [51]. The most applied ones rely on the Lucas – Washburn equation [52] or the Darcy’s law [53]. However, they only are suited for nearly bidimensional paper-based systems (e.g., single – layer paper devices) and simple geometries [54, 55]. Fluid dynamics in a 3D paper – based device is of greater complexity and its theoretical treatment requires understanding of the physics that regulates microfluidics, as well as of the influence of several variables, in addition to the fluidics geometry, such as the characteristics of porous material and the type, ionic strength, and viscosity of the fluid [56, 57]. In this paper, we adopted a simple approach to investigate the effect of D1 – D3 layers’ geometry on the fluid motion. We used a mathematical model that described the trajectory of the liquid flow from the detection zone in layer A towards the washing layers as a function of their geometry, considering only the direction of the contours of each layer. This model is based on the following hypotheses, which described an ideal behaviour [58, 59]: (a) the fluid is assumed to be non – viscous, neglecting internal friction; (b) the fluid is incompressible; (c) the motion of the flow is stationary (i.e., its velocity at each point does not change); (d) the flow is irrotational (i.e., the angular momentum of the fluid is zero at any point). The three – dimensional trajectory of the liquid was described according to a system of parametric equations in polar coordinates of the general form $h = f(u,t)$ ($h = i$ -th component of the position vector; $u, t =$ polar coordinates).

$$\begin{cases} x(t, u) = (n_1 + nt^{0.7})\cos(2u) \\ y(t, u) = (n_1 + nt^{0.7})\sin(2u) \\ z(u) = -n_2 \sin(n_3 t) \end{cases} \quad n_i > 0; 0 < t < 2\pi; 0 < u < \pi \quad (1)$$

The results reported in Figure 4 showed that the flow of the liquid passing from layer A to the washing layers D1 – D3 followed a bell-shaped trajectory, assuming the shape of crowns with rays of increasing size for the successive layers. Therefore, the design of the μ PAD with an increasing radius of the hydrophilic zones of layers D1 – D3, which made available a larger wettable volume for the fluid when it moved vertically through the layers, eased the flow of liquid (thus the removal of unbound species) from the hydrophilic areas of layer A.

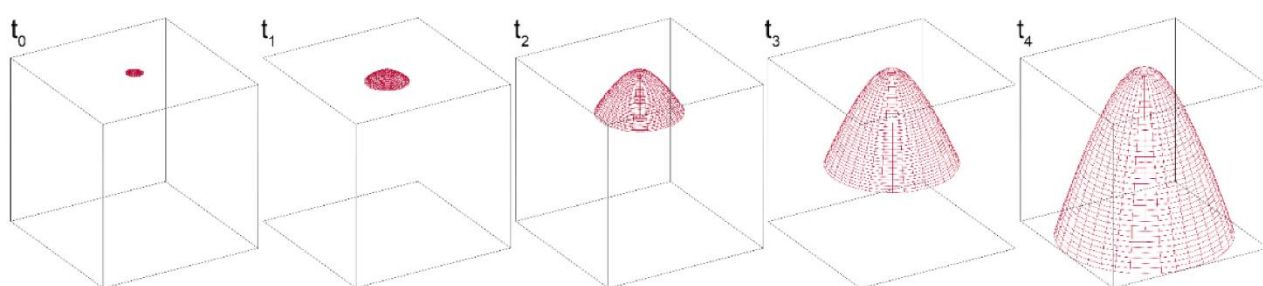


Figure 4. Simulation of 3D trajectory of fluid across the washing layers D1 – D3 at various times ($t_0 > t_1 > t_2 > t_3 > t_4$). The fluid trajectory was described according to a system of parametric equations in polar coordinates (Equation (1)), considering only the direction of the contours of the fluid in each layer. A bell – shaped trajectory is obtained for the fluid front moving across the D layers, characterized by the increasing diameter of the hydrophilic area. This can be ascribed to the combination of a radial movement towards the boundary of the hydrophilic zone of a given D layer and a vertical movement between the adjacent D layers.

5.3.3 Optimization of the origami μ PAD and assay procedure

While the CL detection reagents should be present in large excess, the amount of anti – OVA – HRP conjugate loaded in the origami μ PAD is crucial for assay performance. Indeed, to achieve the best assay performance in terms of limit of detection (LOD), the anti – OVA – HRP should be just sufficient to saturate the binding sites on MBs (an excess of anti – OVA – HRP shifted the assay calibration curve towards higher concentrations, thus increasing the LOD). To determine the best amount of anti – OVA – HRP, we analyzed OVA – free solutions (PBS) in origami μ PADs, prepared by loading anti – OVA – HRP solutions at different concentrations, and measured the resulting CL

signals. *Figure 5* showed that the CL signal (thus the amount of anti – OVA – HRP bound to the MBs) increased for anti – OVA – HRP solution concentrations up to $1 \mu\text{g mL}^{-1}$, then remained nearly constant. Based on this result, this concentration was selected for the preparation of the μPADs .

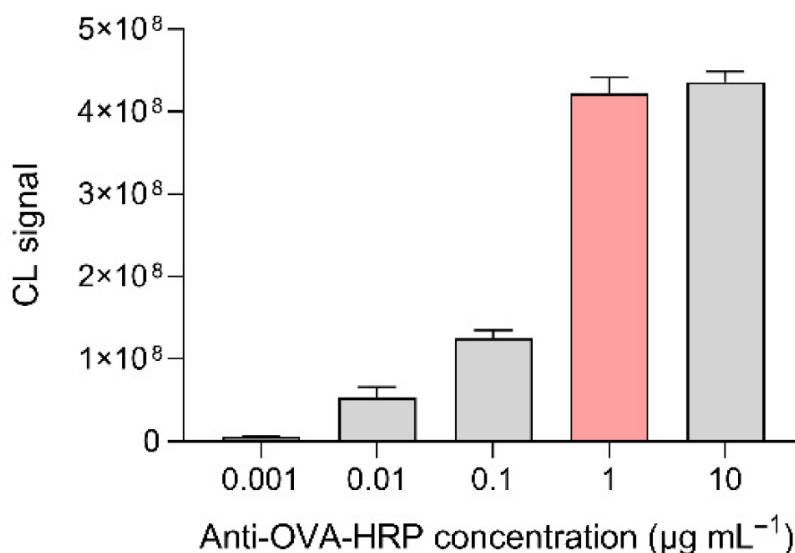


Figure 5. CL signals obtained by analyzing OVA – free solutions (PBS) in origami μPADs prepared using anti – OVA – HRP solutions at different concentrations. The optimal anti – OVA – HRP concentration is highlighted in red. Each of the data are the mean \pm SD of three measurements.

Figure 6 shows the calibration curve generated in the optimized experimental conditions, obtained by plotting the ratios between the CL signals measured for different OVA standard solutions and the signal measured in the absence of OVA (i.e., the immunoassay B/B_0 parameter) against the logarithm of OVA concentration. Since the number of samples that can be analyzed in an origami is limited, the calibration curve has been obtained by combining the results of several biosensors (three OVA standard solutions were assayed in each μPAD , together with an OVA – free sample, then the B/B_0 parameter for each standard solution was calculated and the data from different μPADs were joined). A four – parameter logistic equation was used to fit the experimental data and obtain the calibration curve parameters. According to the equation of the calibration curve, the LOD of the assay (calculated as the concentration

of OVA corresponding to the CL signal of the OVA – free sample, minus three times its standard deviation) was 1 ng mL^{-1} , while the assay working range (estimated as the range of OVA concentrations that correspond to the 10 – to – 90% change in the CL signal ratio) was from 0.003 to $1 \text{ } \mu\text{g mL}^{-1}$ of OVA.

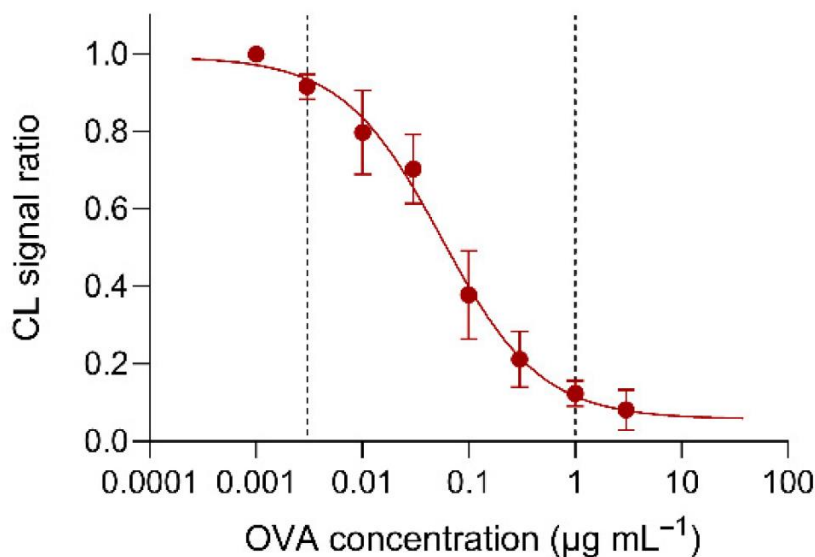


Figure 6. Calibration curve generated by combining the results obtained by analysing OVA standard solutions with different biosensors. A four – parameter logistic equation was used to fit the experimental data and the equation of the resulting calibration curve was $Y = 0.925/(1 + 10(0.932(1.257 + X))) + 0.057$ ($R^2 = 0.994$), where Y and X were the CL signal ratio and the logarithm of concentration of OVA standard solutions. The dashed lines show the assay range (see text). Each of the data are the mean \pm SD of three measurements.

5.3.4 Measurement of OVA with the origami μ PAD

Since the number of samples that can be analyzed in a single origami μ PAD is limited, an analytical procedure that relies on a multiple-point calibration curve could be only performed using several origami devices, which would complicate assay execution. To perform the assay in a single μ PAD, we developed a procedure that requires the analysis of the sample and of three standards, i.e., an OVA-free solution (PBS) and two OVA standards in PBS at concentrations that correspond to the upper ($1 \text{ } \mu\text{g mL}^{-1}$) and lower ($0.003 \text{ } \mu\text{g mL}^{-1}$) limits of the assay working range. After evaluation of the ratios between the CL signals of the OVA standards and of the OVA – free solution, a two – point

linear calibration curve was obtained by plotting the logit of the CL signal ratios of the OVA standards against the logarithm of OVA concentrations (such a procedure is often used to linearize the central portion of the sigmoidal calibration curves of competitive immunoassays) and the amount of OVA in the unknown sample was evaluated by interpolation of its CL signal ratio logit on the linear calibration curve. No blank was needed for this procedure, since the non-specific binding of anti – OVA – HRP was negligible (we verified this in origami μ PADs prepared with MBs conjugated with BSA, instead of OVA). In case many samples need to be analyzed, the assay could be also conducted by using an origami to produce the calibration curve and then employing other origami μ PADs to analyze four samples at the same time (the inter – origami variability in the CL signals measured in origami μ PADs from the same production lot was less than 5%). *Figure 7a,b* show, respectively, a representative CL image of the origami μ PAD and the CL emission intensity kinetic profiles, obtained by the quantitative analysis of the sequence of CL images acquired during the assay. To demonstrate the feasibility of the two – standard calibration approach, we applied such an approach to the data of the calibration curve of *Figure 6*. *Figure 7c* shows the two – point linear calibration curve obtained from the points at the upper and lower limits of the assay working range, while the other points within the working range were simply plotted on the graph. All the intermediate calibration points are on the calibration curve; therefore, this approach can be used to calculate the OVA concentration of unknown samples within the assay working range.

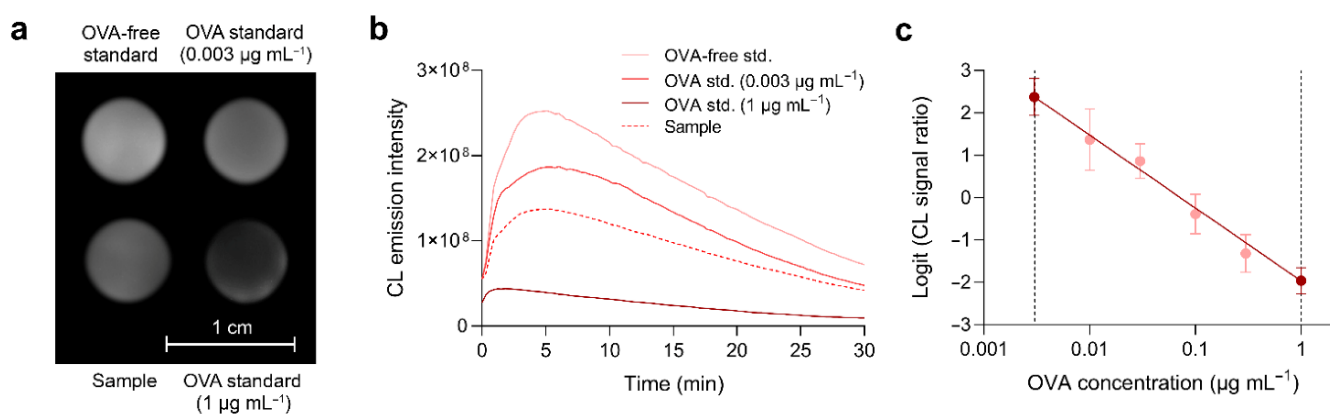


Figure 7. (a) CL image of the origami μ PAD acquired during the assay. The scale bar represents 1 cm. (b) CL emission intensity kinetic profiles obtained by the analysis of the CL images acquired during the assay. (c) Application of the two – standard calibration approach to the calibration data of Figure 6. The readings obtained for concentrations that correspond to the upper and lower limits of the assay working range (dark points) were used to obtain the two-point calibration curve, while the other readings (light points) were simply plotted on the graph.

5.3.5 Assay specificity

To evaluate assay specificity, standard solutions of other proteins commonly found in food, such as bovine serum albumin (BSA), rabbit serum albumin (RSA), and lysozyme from chicken egg white (Lys), were analyzed with origami μ PADs. *Figure 8* shows the comparison between the CL signals measured for $10 \mu\text{g mL}^{-1}$ standard solutions of the potentially interfering proteins and an OVA-free standard solution (i.e., PBS), for which the largest amount of anti – OVA – HRP was bound to the OVA – MBs. The results showed that, even at such relatively high concentrations, Lys, RSA, and BSA did not significantly interfere with the binding of anti – OVA – HRP to OVA – MBs (for comparison, a $10 \mu\text{g mL}^{-1}$ OVA standard solution displaced about 95% of the anti – OVA – HRP conjugate from the OVA – MBs).

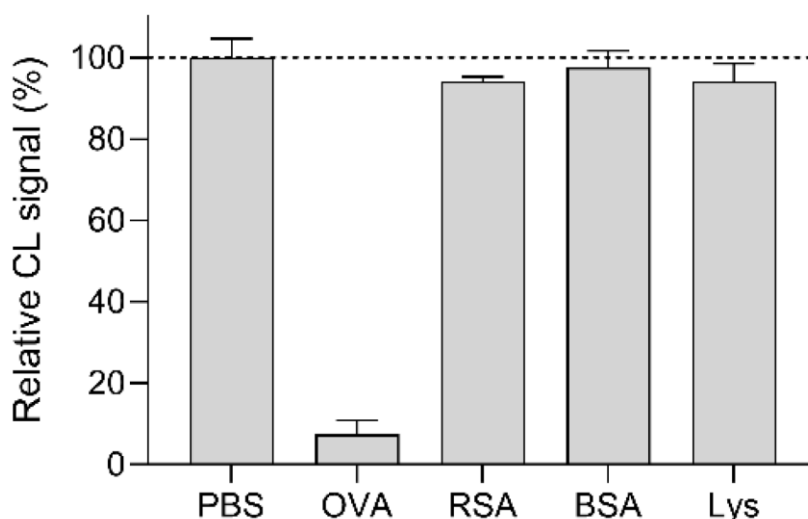


Figure 8. CL signals measured in the origami μ PAD for an OVA – free standard solution (PBS) and $10 \mu\text{g mL}^{-1}$ standard solutions of the potentially interfering proteins RSA, BSA, and Lys. For comparison, the CL signal

measured for a $10 \mu\text{g mL}^{-1}$ OVA standard solution is reported. Each of the data are the mean \pm SD of three measurements.

For a better comprehension of assay specificity, an in – silico model was used to compare the experimental results with computational data. Computational modelling methods for the in – silico construction of the 3D structure of monoclonal antibodies (mAbs) have been already developed and applied in drug discovery [60, 61], while their exploitation to support immunosensor development is not yet widespread. Furthermore, many immunosensors employ polyclonal antibodies (pAbs) rather than mAbs, taking advantage of their higher binding avidity and affinity [62, 63]. However, pAbs are heterogeneous mixtures; thus, developing a theoretical model of antigen – antibody interaction in the case of pAbs would require high computational effort. To overcome this limitation, the in – silico model proposed in this manuscript used complementary computational techniques to simulate approximate models of antibody – antigen complexes. In our opinion, the use of an approximate model that is capable of simulating, in a simple manner, an ideal case in which the interaction between biological macromolecules is optimal does not represent a limitation. In fact, theoretical models based on mathematical approximations are commonly employed in other fields of chemistry, such as investigation of reaction mechanisms [64, 65, 66] or simulation of spectroscopy experiments [67]. In detail, the model was used to calculate the thermodynamic stability parameters of the antibody – antigen complexes formed between the anti – OVA antibody and either OVA or the tested interfering proteins. Due to the absence of a crystallographic structure for the anti – OVA antibody, its modelling was performed starting from sequences obtained from the abYsis webserver [33, 68]. In particular, the sequences of the variable regions in the heavy (VH) and light (VL) chains of the Fab fragment of anti – OVA mAbs produced by a hybridoma were employed. The chosen sequences were subjected to homology modelling in the AbYmod webserver, which automatically selected the most suitable PDB templates from the Protein Data Bank for modelling the target sequence. Structural refinement based on molecular dynamics and energy minimization were performed in GROMACS,

which provided the 3D molecular structure of the Fab fragment of anti – OVA. The final model was employed in ab initio protein-protein molecular docking simulations in the presence of either the target protein (1OVA.pdb) or interfering proteins [36, 69] to generate the most plausible, lower – energy complexes, based on topological and electrostatic complementarity (*Figure 9*). Finally, the binding stability of the complexes anti – OVA – OVA, anti – OVA – Lys, and anti – OVA – BSA was evaluated using the PRODIGY online tool to obtain the corresponding value of ΔG_{bind} . The results of the molecular docking simulations (*Table 1*) showed that, in agreement with the experimental results, the antibody has a higher affinity for OVA. The stability of the anti – OVA – Lys complex is much lower and the anti – OVA – BSA complex is even less stable, thus confirming the antibody specificity. We suggest that in – silico modelling of biomolecule interaction can be a useful tool for supporting biosensor development and, when needed, aid in the optimization of experimental parameters, such as buffer, pH, and ionic strength, to improve assay analytical performance.

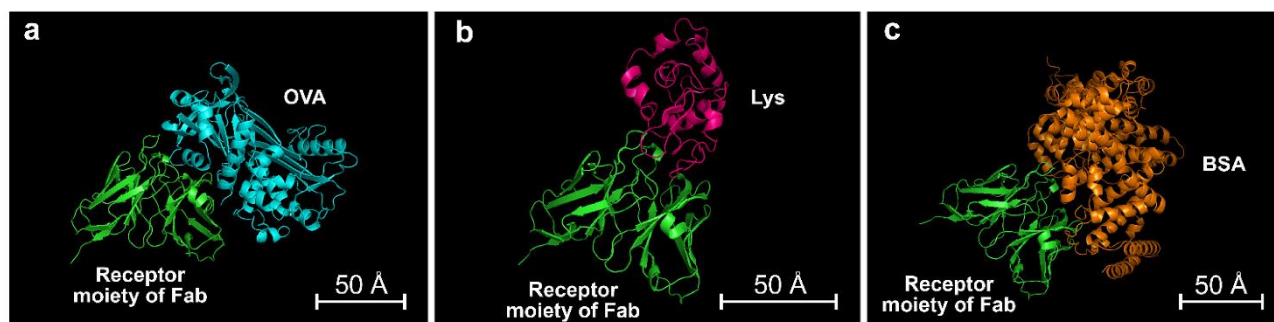


Figure 9. Most probable 3D structures obtained by molecular docking simulations for the complexes of (a) OVA, (b) Lys, and (c) BSA with anti – OVA. The scale bars represent 50 Å.

Table 1. Predicted binding affinities and dissociation constants of complexes between anti – OVA and target proteins 1.

Target Protein	Binding Affinity (ΔG_{bind}) (kcal mol ⁻¹)	Dissociation Constant (K_d) (mol L ⁻¹)
OVA	-12.3	8.9×10^{-10}
Lys	-10.9	1.1×10^{-8}

Target Protein	Binding Affinity (ΔG_{bind}) (kcal mol ⁻¹)	Dissociation Constant (K_d) (mol L ⁻¹)
BSA	-9.1	2.1×10^{-7}

¹ RSA was highly similar (> 90%) in sequence with BSA; thus, its binding affinity to anti – OVA was not evaluated.

5.3.6 Accuracy and quantification of Ovalbumin in real samples

The accuracy of the origami μ PAD biosensor for OVA was evaluated by comparison of measurements obtained for real samples (chocolate chip cookies from different market brands bought in local stores). All samples were analyzed both with the origami μ PAD and with a colorimetric ELISA kit reference method, based on a non-competitive sandwich immunoassay using anti – OVA – HRP. The results reported in *Figure 10* showed a good correlation between the two methods ($R^2 > 0.98$).

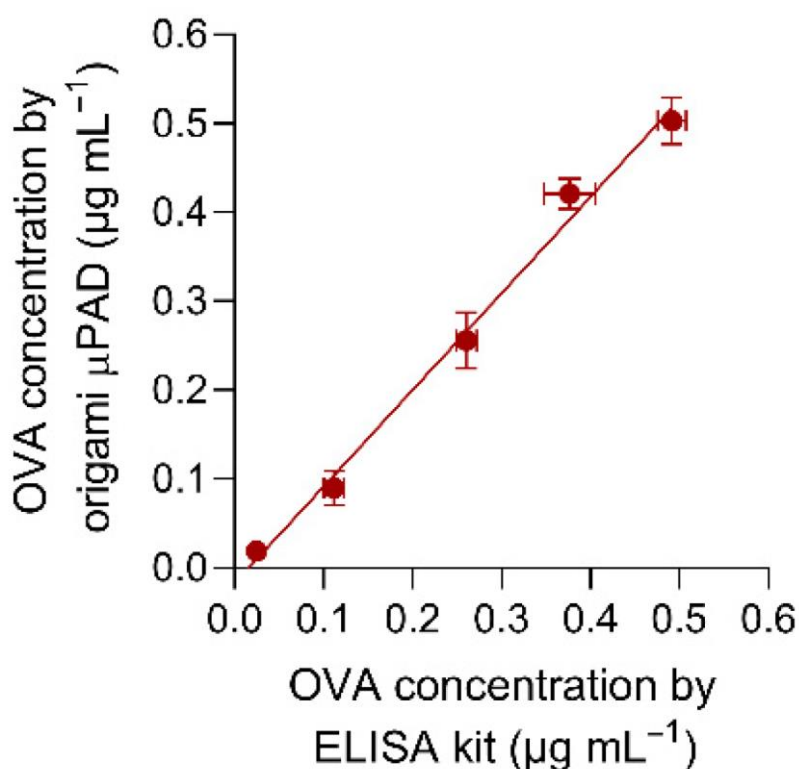


Figure 10. Comparison between OVA concentrations measured in real samples by using the origami μ PAD and the colorimetric ELISA kit reference method. The equation of the linear regression curve is $Y = 1.087 X - 0.018$

($R^2 = 0.992$), where Y and X are the OVA concentrations measured with the origami μ PAD and the colorimetric ELISA kit reference method, respectively. Each of the data are the mean \pm SD of three measurements.

We also investigated the potential interference of a real sample matrix by performing a recovery study. An extract of chocolate chip cookies (obtained as described in Section 2.6) with OVA content below the LOD of the assay was spiked with known amounts of OVA and analyzed using the origami μ PAD. A previously reported procedure for sample extraction was employed, in which a 0.025 M TRIS buffered solution was employed to ensure analyte recovery from the matrix at controlled pH. In case of highly acidic food samples, a TRIS buffer with higher buffering capacity might be employed for sample extraction. As shown in *Table 2*, we obtained good correspondence between the OVA concentrations measured in spiked extracts and the added OVA. Recovery ranged from 83 to 133%, which can be considered adequate for a point – of – use immunosensor, as compared with the 80 – 120% recovery commonly accepted for laboratory immunoassays [70]. The assay precision for the real samples was also found to be satisfactory for a point – of – use assay, with a coefficient of variation below 15%. Overall, these results proved the effectiveness of the origami μ PAD for the analysis of OVA in the real samples tested.

Table 2. Results of the recovery study of the origami μ PAD biosensor performed on a blank extract of biscuit sample spiked with known amounts of OVA.

	Concentration of OVA Spiked ($\mu\text{g mL}^{-1}$)	Concentration of OVA Measured ($\mu\text{g mL}^{-1}$)	Recovery (%)
Sample 1	0.003	0.004	133
Sample 2	0.010	0.009	89.2
Sample 3	0.020	0.025	124
Sample 4	0.100	0.083	82.6
Sample 5	0.400	0.383	95.8

5.3.7 Stability of the origami μ PAD

The stability over time of the reagents (OVA – MBs, anti – OVA – HRP, luminol/enhancer, and sodium perborate) loaded in the origami μ PAD has been investigated. A series of origami μ PADs loaded only with the reagent under study was sealed under a vacuum in plastic bags and stored at 4 °C. After a given storage time (up to 6 weeks), the remaining reagents were loaded in the μ PAD, then the CL signals obtained for the analysis of an OVA – free standard were measured. The comparison of the CL signals with that obtained in a freshly prepared μ PAD allowed us to assess the degradation over time of the investigated reagent.

As shown in *Figure 11*, OVA – MBs, luminol/enhancer, and sodium perborate displayed good stability, with a CL signal decrease of less than 10% after 6 weeks of storage. On the other hand, the anti – OVA – HRP conjugate markedly decreased its bioactivity (up to 40% after only 3 weeks of storage, data not shown). To improve the stability of the conjugate, we added the low molecular weight polyol sorbitol to the anti – OVA – HRP solution loaded in the μ PAD [71]. This significantly increased the stability of the conjugate and made it possible to use the ready – to – use μ PAD after up to 4 weeks of storage. We also investigated the use of other protein protecting agents, such as pullulan, a polysaccharide that ensures high protein stability upon drying [72]. Unfortunately, pullulan negatively affected the re – solubilization of anti – OVA – HRP upon addition of the buffer, thus making the assay unfeasible.

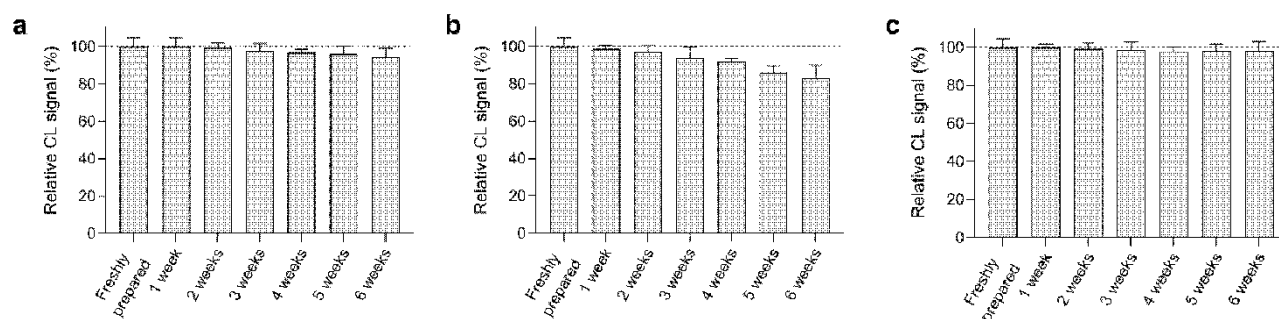


Figure 11. Decrease in the CL signal measured upon storage at 4 °C for origami μ PADs containing the reagents (a) OVA – MBs, (b) anti – OVA – HRP, and (c) luminol/enhancer and sodium perborate. The remaining reagents were loaded in the μ PADs just before the measurement. Each of the data are the mean \pm SD of three measurements.

5.4 Conclusions

This article describes an origami μ PAD for the quantitative determination of OVA in food samples that displayed improved performance and were suitable for on – site application. The assay relied on a competitive immunoassay, followed by CL detection by a luminol/hydrogen peroxide system. The use of magnetic microbeads allowed easy and efficient immobilization of immunoreagents in the μ PAD. Due to the origami approach, it was possible to fully implement on paper a multi – step analytical procedure and to avoid chemical handling by the operator, as all the reagents were preloaded in the μ PAD. The assay proved to be suitable for the detection of OVA traces in real samples in a relatively short period of time (i.e., approximately 1 h). The same approach could be used for other allergens or clinical protein markers. Future work is foreseen to evaluate the use of a smartphone’s camera and a detector in the substitution of the portable CCD and dedicated application for data elaboration, to further improve assay portability and widespread applicability [73].

Supplementary Materials

The following supporting information can be downloaded at: <https://www.mdpi.com/article/10.3390/bios12100825/s1>, Video S1: Assay procedure.

Funding

This research was funded by the Italian Ministry of University and Research (PRIN2017 project “Development of novel DNA – based analytical platforms for the rapid, point – of – use quantification of multiple hidden allergens in food samples”, Prot. 2017YER72K).

References

- [1] Gargano, D.; Appanna, R.; Santonicola, A.; De Bartolomeis, F.; Stellato, C.; Cianferoni, A.; Casolaro, V.; Iovino, P. Food Allergy and Intolerance: A Narrative Review on Nutritional Concerns. *Nutrients* **2021**, *13* (5), 1638. <https://doi.org/10.3390/nu13051638>.
- [2] Sena-Torralba, A.; Pallás-Tamarit, Y.; Morais, S.; Maquieira, Á. Recent Advances and Challenges in Food-Borne Allergen Detection. *TrAC Trends in Analytical Chemistry* **2020**, *132*, 116050. <https://doi.org/10.1016/j.trac.2020.116050>.
- [3] Zhu, Y.; Vanga, S. K.; Wang, J.; Raghavan, V. Impact of Food Processing on the Structural and Allergenic Properties of Egg White. *Trends in Food Science & Technology* **2018**, *78*, 188–196. <https://doi.org/10.1016/j.tifs.2018.06.005>.
- [4] Abeyrathne, E. D. N. S.; Lee, H. Y.; Ahn, D. U. Egg White Proteins and Their Potential Use in Food Processing or as Nutraceutical and Pharmaceutical Agents—A Review. *Poultry Science* **2013**, *92* (12), 3292–3299. <https://doi.org/10.3382/ps.2013-03391>.
- [5] Feng, X.-L.; Ren, H.-L.; Li, Y.-S.; Hu, P.; Zhou, Y.; Liu, Z.-S.; Yan, D.-M.; Hui, Q.; Liu, D.; Lin, C.; Liu, N.-N.; Liu, Y.-Y.; Lu, S.-Y. A Magnetic Particles-Based Chemiluminescence Enzyme Immunoassay for Rapid Detection of Ovalbumin. *Analytical Biochemistry* **2014**, *459*, 12–17. <https://doi.org/10.1016/j.ab.2014.04.016>.
- [6] Dong, X.; Raghavan, V. A Comprehensive Overview of Emerging Processing Techniques and Detection Methods for Seafood Allergens. *Comprehensive Reviews in Food Science and Food Safety* **2022**, *21* (4), 3540–3557. <https://doi.org/10.1111/1541-4337.12987>.
- [7] Shin, J. H.; Reddy, Y. V. M.; Park, T. J.; Park, J. P. Recent Advances in Analytical Strategies and Microsystems for Food Allergen Detection. *Food Chemistry* **2022**, *371*, 131120. <https://doi.org/10.1016/j.foodchem.2021.131120>.
- [8] Xu, J.; Ye, Y.; Ji, J.; Sun, J.; Sun, X. Advances on the Rapid and Multiplex Detection Methods of Food Allergens. *Critical Reviews in Food Science and Nutrition* **2022**, *62* (25), 6887–6907. <https://doi.org/10.1080/10408398.2021.1907736>.

- [9] Calabria, D.; Zangheri, M.; Pour, S. R. S.; Trozzi, I.; Pace, A.; Lazzarini, E.; Calabretta, M. M.; Mirasoli, M.; Guardigli, M. Luminescent Aptamer-Based Bioassays for Sensitive Detection of Food Allergens. *Biosensors* **2022**, *12* (8), 644. <https://doi.org/10.3390/bios12080644>.
- [10] Xiao, X.; Hu, S.; Lai, X.; Peng, J.; Lai, W. Developmental Trend of Immunoassays for Monitoring Hazards in Food Samples: A Review. *Trends in Food Science & Technology* **2021**, *111*, 68–88. <https://doi.org/10.1016/j.tifs.2021.02.045>.
- [11] Calabria, D.; Calabretta, M. M.; Zangheri, M.; Marchegiani, E.; Trozzi, I.; Guardigli, M.; Michelini, E.; Di Nardo, F.; Anfossi, L.; Baggiani, C.; Mirasoli, M. Recent Advancements in Enzyme-Based Lateral Flow Immunoassays. *Sensors* **2021**, *21* (10), 3358. <https://doi.org/10.3390/s21103358>.
- [12] Di Nardo, F.; Chiarello, M.; Cavallera, S.; Baggiani, C.; Anfossi, L. Ten Years of Lateral Flow Immunoassay Technique Applications: Trends, Challenges and Future Perspectives. *Sensors* **2021**, *21* (15), 5185. <https://doi.org/10.3390/s21155185>.
- [13] Ozer, T.; McMahon, C.; Henry, C. S. Advances in Paper-Based Analytical Devices. *Annual Review of Analytical Chemistry* **2020**, *13* (1), 85–109. <https://doi.org/10.1146/annurev-anchem-061318-114845>.
- [14] Calabretta, M. M.; Zangheri, M.; Calabria, D.; Lopreside, A.; Montali, L.; Marchegiani, E.; Trozzi, I.; Guardigli, M.; Mirasoli, M.; Michelini, E. Paper-Based Immunosensors with Bio-Chemiluminescence Detection. *Sensors* **2021**, *21* (13), 4309. <https://doi.org/10.3390/s21134309>.
- [15] Qin, X.; Liu, J.; Zhang, Z.; Li, J.; Yuan, L.; Zhang, Z.; Chen, L. Microfluidic Paper-Based Chips in Rapid Detection: Current Status, Challenges, and Perspectives. *TrAC Trends in Analytical Chemistry* **2021**, *143*, 116371. <https://doi.org/10.1016/j.trac.2021.116371>.
- [16] Das, S.; Gagandeep; Bhatia, R. Paper-Based Microfluidic Devices: Fabrication, Detection, and Significant Applications in Various Fields. *Reviews in Analytical Chemistry* **2022**, *41* (1), 112–136. <https://doi.org/10.1515/revac-2022-0037>.

- [17] Singh, A. T.; Lantigua, D.; Meka, A.; Taing, S.; Pandher, M.; Camci-Unal, G. Paper-Based Sensors: Emerging Themes and Applications. *Sensors* **2018**, *18* (9), 2838. <https://doi.org/10.3390/s18092838>.
- [18] Roda, A.; Zangheri, M.; Calabria, D.; Mirasoli, M.; Caliceti, C.; Quintavalla, A.; Lombardo, M.; Trombini, C.; Simoni, P. A Simple Smartphone-Based Thermochemiluminescent Immunosensor for Valproic Acid Detection Using 1,2-Dioxetane Analogue-Doped Nanoparticles as a Label. *Sensors and Actuators B: Chemical* **2019**, *279*, 327–333. <https://doi.org/10.1016/j.snb.2018.10.012>.
- [19] Chen, C.-A.; Yeh, W.-S.; Tsai, T.-T.; Li, Y.-D.; Chen, C.-F. Three-Dimensional Origami Paper-Based Device for Portable Immunoassay Applications. *Lab on a Chip* **2019**, *19* (4), 598–607. <https://doi.org/10.1039/C8LC01255E>.
- [20] Colozza, N.; Caratelli, V.; Moscone, D.; Arduini, F. Origami Paper-Based Electrochemical (Bio)Sensors: State of the Art and Perspective. *Biosensors* **2021**, *11* (9), 328. <https://doi.org/10.3390/bios11090328>.
- [21] Noviana, E.; Ozer, T.; Carrell, C. S.; Link, J. S.; McMahon, C.; Jang, I.; Henry, C. S. Microfluidic Paper-Based Analytical Devices: From Design to Applications. *Chem. Rev.* **2021**, *121* (19), 11835–11885. <https://doi.org/10.1021/acs.chemrev.0c01335>.
- [22] Roda, A.; Arduini, F.; Mirasoli, M.; Zangheri, M.; Fabiani, L.; Colozza, N.; Marchegiani, E.; Simoni, P.; Moscone, D. A Challenge in Biosensors: Is It Better to Measure a Photon or an Electron for Ultrasensitive Detection? *Biosensors and Bioelectronics* **2020**, *155*, 112093. <https://doi.org/10.1016/j.bios.2020.112093>.
- [23] Ge, L.; Wang, S.; Song, X.; Ge, S.; Yu, J. 3D Origami-Based Multifunction-Integrated Immunodevice: Low-Cost and Multiplexed Sandwich Chemiluminescence Immunoassay on Microfluidic Paper-Based Analytical Device. *Lab on a Chip* **2012**, *12* (17), 3150–3158. <https://doi.org/10.1039/C2LC40325K>.
- [24] Liu, F.; Zhang, C. A Novel Paper-Based Microfluidic Enhanced Chemiluminescence Biosensor for Facile, Reliable and Highly-Sensitive Gene Detection of *Listeria Monocytogenes*. *Sensors and Actuators B: Chemical* **2015**, *209*, 399–406. <https://doi.org/10.1016/j.snb.2014.11.099>.

- [25] Chu, W.; Chen, Y.; Liu, W.; Zhao, M.; Li, H. Paper-Based Chemiluminescence Immunodevice with Temporal Controls of Reagent Transport Technique. *Sensors and Actuators B: Chemical* **2017**, *250*, 324–332. <https://doi.org/10.1016/j.snb.2017.04.126>.
- [26] Calabria, D.; Zangheri, M.; Trozzi, I.; Lazzarini, E.; Pace, A.; Mirasoli, M.; Guardigli, M. Smartphone-Based Chemiluminescent Origami μ PAD for the Rapid Assessment of Glucose Blood Levels. *Biosensors* **2021**, *11* (10), 381. <https://doi.org/10.3390/bios11100381>.
- [27] Evans, E.; Gabriel, E. F. M.; E. Benavidez, T.; Coltro, W. K. T.; D. Garcia, C. Modification of Microfluidic Paper-Based Devices with Silica Nanoparticles. *Analyst* **2014**, *139* (21), 5560–5567. <https://doi.org/10.1039/C4AN01147C>.
- [28] C. Cunningham, J.; Scida, K.; R. Kogan, M.; Wang, B.; D. Ellington, A.; M. Crooks, R. Paper Diagnostic Device for Quantitative Electrochemical Detection of Ricin at Picomolar Levels. *Lab on a Chip* **2015**, *15* (18), 3707–3715. <https://doi.org/10.1039/C5LC00731C>.
- [29] A. Ortega, G.; Pérez-Rodríguez, S.; Reguera, E. Magnetic Paper – Based ELISA for IgM-Dengue Detection. *RSC Advances* **2017**, *7* (9), 4921–4932. <https://doi.org/10.1039/C6RA25992H>.
- [30] Zangheri, M.; Mirasoli, M.; Guardigli, M.; Di Nardo, F.; Anfossi, L.; Baggiani, C.; Simoni, P.; Benassai, M.; Roda, A. Chemiluminescence-Based Biosensor for Monitoring Astronauts' Health Status during Space Missions: Results from the International Space Station. *Biosensors and Bioelectronics* **2019**, *129*, 260–268. <https://doi.org/10.1016/j.bios.2018.09.059>.
- [31] Trashin, S. A.; Cucu, T.; Devreese, B.; Adriaens, A.; De Meulenaer, B. Development of a Highly Sensitive and Robust Cor a 9 Specific Enzyme-Linked Immunosorbent Assay for the Detection of Hazelnut Traces. *Analytica Chimica Acta* **2011**, *708* (1), 116–122. <https://doi.org/10.1016/j.aca.2011.09.036>.
- [32] Anfossi, L.; Di Nardo, F.; Russo, A.; Cavallera, S.; Giovannoli, C.; Spano, G.; Baumgartner, S.; Lauter, K.; Baggiani, C. Silver and Gold Nanoparticles as Multi-Chromatic Lateral Flow Assay Probes for the Detection of Food Allergens. *Anal*

- Bioanal Chem* **2019**, *411* (9), 1905–1913. <https://doi.org/10.1007/s00216-018-1451-6>.
- [33] Swindells, M. B.; Porter, C. T.; Couch, M.; Hurst, J.; Abhinandan, K. R.; Nielsen, J. H.; Macindoe, G.; Hetherington, J.; Martin, A. C. R. abYsis: Integrated Antibody Sequence and Structure—Management, Analysis, and Prediction. *Journal of Molecular Biology* **2017**, *429* (3), 356–364. <https://doi.org/10.1016/j.jmb.2016.08.019>.
- [34] *AbYsis*. <http://www.abysis.org>.
- [35] *Abymod*. <http://abymod.abysis.org>.
- [36] Yan, Y.; Zhang, D.; Zhou, P.; Li, B.; Huang, S.-Y. HDOCK: A Web Server for Protein–Protein and Protein–DNA/RNA Docking Based on a Hybrid Strategy. *Nucleic Acids Research* **2017**, *45* (W1), W365–W373. <https://doi.org/10.1093/nar/gkx407>.
- [37] HDOCK Server. <http://hdock.phys.hust.edu.cn>.
- [38] Xue, L. C.; Rodrigues, J. P.; Kastriitis, P. L.; Bonvin, A. M.; Vangone, A. PRODIGY: A Web Server for Predicting the Binding Affinity of Protein–Protein Complexes. *Bioinformatics* **2016**, *32* (23), 3676–3678. <https://doi.org/10.1093/bioinformatics/btw514>.
- [39] *Prodigy Webservice*. <https://wenmr.science.uu.nl/prodigy/>.
- [40] Van Der Spoel, D.; Lindahl, E.; Hess, B.; Groenhof, G.; Mark, A. E.; Berendsen, H. J. C. GROMACS: Fast, Flexible, and Free. *Journal of Computational Chemistry* **2005**, *26* (16), 1701–1718. <https://doi.org/10.1002/jcc.20291>.
- [41] *RCSB Protein Data Bank*. <https://www.rcsb.org/>.
- [42] DeLano, W. L. *The PyMOL Molecular Graphics System*; <http://www.pymol.org>.
- [43] Ruiz-Valdepeñas Montiel, V.; Torrente-Rodríguez, R. M.; Campuzano, S.; Pellicanò, A.; Reviejo, Á. J.; Cosio, M. S.; Pingarrón, J. M. Simultaneous Determination of the Main Peanut Allergens in Foods Using Disposable Amperometric Magnetic Beads-Based Immunosensing Platforms. *Chemosensors* **2016**, *4* (3), 11. <https://doi.org/10.3390/chemosensors4030011>.

- [44] Yan, Q.; Zheng, H.-N.; Jiang, C.; Li, K.; Xiao, S.-J. EDC/NHS Activation Mechanism of Polymethacrylic Acid: Anhydride versus NHS-Ester. *RSC Advances* **2015**, *5* (86), 69939–69947. <https://doi.org/10.1039/C5RA13844B>.
- [45] Valverde, A.; Montero-Calle, A.; Barderas, R.; Calero, M.; Yáñez-Sedeño, P.; Campuzano, S.; Pingarrón, J. M. Electrochemical Immunoplatfom to Unravel Neurodegeneration and Alzheimer's Disease through the Determination of Neurofilament Light Protein. *Electrochimica Acta* **2021**, *371*, 137815. <https://doi.org/10.1016/j.electacta.2021.137815>.
- [46] Pidal, J. M. G.; Valverde, A.; Benedé, S.; Molina, E.; Moreno-Guzmán, M.; Ángel López, M.; M. Pingarrón, J.; Escarpa, A.; Campuzano, S. Rapid Diagnosis of Egg Allergy by Targeting Ovalbumin Specific IgE and IgG4 in Serum on a Disposable Electrochemical Immunoplatfom. *Sensors & Diagnostics* **2022**, *1* (1), 149–159. <https://doi.org/10.1039/D1SD00040C>.
- [47] Mendez, S.; Fenton, E. M.; Gallegos, G. R.; Petsev, D. N.; Sibbett, S. S.; Stone, H. A.; Zhang, Y.; López, G. P. Imbibition in Porous Membranes of Complex Shape: Quasi-Stationary Flow in Thin Rectangular Segments. *Langmuir* **2010**, *26* (2), 1380–1385. <https://doi.org/10.1021/la902470b>.
- [48] Deegan, R. D.; Bakajin, O.; Dupont, T. F.; Huber, G.; Nagel, S. R.; Witten, T. A. Capillary Flow as the Cause of Ring Stains from Dried Liquid Drops. *Nature* **1997**, *389* (6653), 827–829. <https://doi.org/10.1038/39827>.
- [49] Kyoung Oh, Y.; Joung, H.-A.; Kim, S.; Kim, M.-G. Vertical Flow Immunoassay (VFA) Biosensor for a Rapid One-Step Immunoassay. *Lab on a Chip* **2013**, *13* (5), 768–772. <https://doi.org/10.1039/C2LC41016H>.
- [50] Liu, M.; Wu, J.; Gan, Y.; Hanaor, D. A. H.; Chen, C. Q. Evaporation Limited Radial Capillary Penetration in Porous Media. *Langmuir* **2016**, *32* (38), 9899–9904. <https://doi.org/10.1021/acs.langmuir.6b02404>.
- [51] Modha, S.; Castro, C.; Tsutsui, H. Recent Developments in Flow Modeling and Fluid Control for Paper-Based Microfluidic Biosensors. *Biosensors and Bioelectronics* **2021**, *178*, 113026. <https://doi.org/10.1016/j.bios.2021.113026>.

- [52] Washburn, E. W. The Dynamics of Capillary Flow. *Phys. Rev.* **1921**, *17* (3), 273–283. <https://doi.org/10.1103/PhysRev.17.273>.
- [53] Darcy, H. *Les fontaines publiques de la ville de Dijon: Exposition et Application*, 1st ed.; Victor Dalmont Libraire des Corps imperiaux des ponts et chaussées et des mines: Paris, France, 1856.
- [54] Gasperino, D.; Baughman, T.; Hsieh, H. V.; Bell, D.; Weigl, B. H. Improving Lateral Flow Assay Performance Using Computational Modeling. *Annual Review of Analytical Chemistry* **2018**, *11* (1), 219–244. <https://doi.org/10.1146/annurev-anchem-061417-125737>.
- [55] Kumar, S.; Bhushan, P.; Bhattacharya, S. Fluid Transport Mechanisms in Paper-Based Microfluidic Devices. In *Paper Microfluidics: Theory and Applications*; Bhattacharya, S., Kumar, S., Agarwal, A. K., Eds.; Advanced Functional Materials and Sensors; Springer: Singapore, 2019; pp 7–28. https://doi.org/10.1007/978-981-15-0489-1_2.
- [56] Das, D.; Singh, T.; Ahmed, I.; Masetty, M.; Priye, A. Effects of Relative Humidity and Paper Geometry on the Imbibition Dynamics and Reactions in Lateral Flow Assays. *Langmuir* **2022**, *38* (32), 9863–9873. <https://doi.org/10.1021/acs.langmuir.2c01017>.
- [57] Kordorwu, V.; Tegladza, I.; Okoampah, E. A Simple Two-Dimensional Convective-Diffusive Based Modelling Study of a Biosensor for Glucose Detection. *Journal of Chemistry Studies* **2022**, *1* (2), 01–08. <https://doi.org/10.32996/jcs.2022.1.2.1>.
- [58] Chow, C. Y. *An Introduction to Computational Fluid Mechanics*, 1st ed.; John Wiley & Sons Inc.: New York, NY, USA, 1979.
- [59] O’Neill, M. E.; Chorlton, F. *Ideal and Incompressible Fluid Dynamics*, 1st ed.; Ellis Horwood series in mathematics and its applications; Halsted Press: Chichester, UK, 1986.
- [60] Khetan, R.; Curtis, R.; Deane, C. M.; Hadsund, J. T.; Kar, U.; Krawczyk, K.; Kuroda, D.; Robinson, S. A.; Sormanni, P.; Tsumoto, K.; Warwicker, J.; Martin, A. C. R. Current Advances in Biopharmaceutical Informatics: Guidelines, Impact and

- Challenges in the Computational Developability Assessment of Antibody Therapeutics. *mAbs* **2022**, *14* (1), 2020082. <https://doi.org/10.1080/19420862.2021.2020082>.
- [61] Hummer, A. M.; Abanades, B.; Deane, C. M. Advances in Computational Structure-Based Antibody Design. *Current Opinion in Structural Biology* **2022**, *74*, 102379. <https://doi.org/10.1016/j.sbi.2022.102379>.
- [62] Wu, A. H. B. Immunochemical Techniques. In *Clinical Chemistry: Principles, Techniques, and Correlations, Enhanced Edition: Principles, Techniques, and Correlations*; Lippincott Williams & Wilkins: Philadelphia, PA, USA, 2017; pp 160–178.
- [63] He, J. Practical Guide to ELISA Development. In *The Immunoassay Handbook: Theory and Applications of Ligand Binding, ELISA and Related Techniques*; Elsevier Ltd: Amsterdam, The Netherlands, 2013; pp 381–393.
- [64] Leelananda, S. P.; Lindert, S. Computational Methods in Drug Discovery. *Beilstein J. Org. Chem.* **2016**, *12* (1), 2694–2718. <https://doi.org/10.3762/bjoc.12.267>.
- [65] Feng, F.; Lai, L.; Pei, J. Computational Chemical Synthesis Analysis and Pathway Design. *Frontiers in Chemistry* **2018**, *6*.
- [66] Nakliang, P.; Yoon, S.; Choi, S. Emerging Computational Approaches for the Study of Regio- and Stereoselectivity in Organic Synthesis. *Organic Chemistry Frontiers* **2021**, *8* (18), 5165–5181. <https://doi.org/10.1039/D1QO00531F>.
- [67] Barone, V.; Alessandrini, S.; Biczysko, M.; Cheeseman, J. R.; Clary, D. C.; McCoy, A. B.; DiRisio, R. J.; Neese, F.; Melosso, M.; Puzzarini, C. Computational Molecular Spectroscopy. *Nat Rev Methods Primers* **2021**, *1* (1), 1–27. <https://doi.org/10.1038/s43586-021-00034-1>.
- [68] Dattamajumdar, A. K.; Jacobson, D. P.; Hood, L. E.; Osman, G. E. Rapid Cloning of Any Rearranged Mouse Immunoglobulin Variable Genes. *Immunogenetics* **1996**, *43* (3), 141–151. <https://doi.org/10.1007/BF00176675>.
- [69] Yan, Y.; Tao, H.; He, J.; Huang, S.-Y. The HDock Server for Integrated Protein–Protein Docking. *Nat Protoc* **2020**, *15* (5), 1829–1852. <https://doi.org/10.1038/s41596-020-0312-x>.

- [70] Andreasson, U.; Perret-Liaudet, A.; van Waalwijk van Doorn, L. J. C.; Blennow, K.; Chiasserini, D.; Engelborghs, S.; Fladby, T.; Genc, S.; Kruse, N.; Kuiperij, H. B.; Kulic, L.; Lewczuk, P.; Mollenhauer, B.; Mroczko, B.; Parnetti, L.; Vanmechelen, E.; Verbeek, M. M.; Winblad, B.; Zetterberg, H.; Koel-Simmelink, M.; Teunissen, C. E. A Practical Guide to Immunoassay Method Validation. *Frontiers in Neurology* **2015**, *6*.
- [71] Nicoud, L.; Cohrs, N.; Arosio, P.; Norrant, E.; Morbidelli, M. Effect of Polyol Sugars on the Stabilization of Monoclonal Antibodies. *Biophysical Chemistry* **2015**, *197*, 40–46. <https://doi.org/10.1016/j.bpc.2014.12.003>.
- [72] Jahanshahi-Anbuhi, S.; Kannan, B.; Leung, V.; Pennings, K.; Liu, M.; Carrasquilla, C.; White, D.; Li, Y.; H. Pelton, R.; D. Brennan, J.; M. Filipe, C. D. Simple and Ultrastable All-Inclusive Pullulan Tablets for Challenging Bioassays. *Chemical Science* **2016**, *7* (3), 2342–2346. <https://doi.org/10.1039/C5SC04184H>.
- [73] Zangheri, M.; Di Nardo, F.; Calabria, D.; Marchegiani, E.; Anfossi, L.; Guardigli, M.; Mirasoli, M.; Baggiani, C.; Roda, A. Smartphone Biosensor for Point-of-Need Chemiluminescence Detection of Ochratoxin A in Wine and Coffee. *Analytica Chimica Acta* **2021**, *1163*, 338515. <https://doi.org/10.1016/j.aca.2021.338515>.

Smartphone-Based Chemiluminescence Glucose Biosensor Employing a Peroxidase- Mimicking, Guanosine-Based Self-Assembled Hydrogel

Reproduced from: "Smartphone-Based Chemiluminescence Glucose Biosensor Employing a Peroxidase-Mimicking, Guanosine-Based Self-Assembled Hydrogel"

Donato Calabria, Andrea Pace, Elisa Lazzarini, Ilaria Trozzi, Martina Zangheri, Massimo Guardigli, Silvia Pieraccini, Stefano Masiero, Mara Mirasoli

Biosensors, 2023, 13(6), 650

<https://doi.org/10.3390/bios13060650>

Reproduced by permission of MDPI (Open Access Article)

<https://creativecommons.org/licenses/by/4.0/>

6.1 Introduction

The monitoring of health – related biomarkers at the point of care (POC) by means of simple, cost-effective, and easy – to – use diagnostic tests could revolutionize screening procedures, reducing the incidence of chronic pathologies, and improve patient survival rates and people’s life quality. In particular, the availability of instrument – free and rapid diagnostic devices is considered a fundamental step to reduce healthcare costs and to enlarge the screening scale, thus providing a real breakthrough in the diagnostic field [1]. A recent major development for the decentralization and democratization of clinical laboratory tests has been the combination of smartphones and (bio)sensors [2]. To this end, optical biosensors are particularly advantageous because their interfacing with smartphones can be quite simple and straightforward, while electrochemical ones require dedicated equipment and a power supply for signal generation and measurement at the electrodes [2, 3]. Hydrogen peroxide is involved in many physiological processes, such as metabolic processes, apoptosis, and immune – cell activation [4, 5, 6, 7]. Owing to its roles as an oxidative stress marker, defense agent, and aging promoter [8], it is recognized as a crucial biomarker of various diseases including diabetes [9], cancer [10], Parkinson’s, cardiovascular, Alzheimer’s, and neurodegenerative disorders [11]. Moreover, H_2O_2 is produced by oxidase enzymes (e.g., glucose oxidase, alcohol oxidase, cholesterol oxidase, lactate oxidase, and glutamate oxidase). This allows us to develop bioassays relying on H_2O_2 detection for the quantification of such enzymes, as well as of their substrates [12]. Therefore, the development of (bio)sensors for H_2O_2 based on peroxidase activity is an active research field, finding applications in medical diagnostics, clinical research, food chemistry, environmental investigations, and industrial process monitoring [13, 14, 15, 16, 17, 18, 19, 20, 21]. The use of natural enzymes in biosensor technology has some drawbacks, such as their limited stability and high cost, especially when multiple enzymes are required [1]. However, advances in materials science and nanotechnology have led to several strategies for obtaining synthetic enzymes as substitutes for natural ones [22, 23]. Even though synthetic enzymes sometimes show reduced catalytic activity with respect to their natural counterparts, they offer high

stability in the surrounding environment, low cost, simple synthesis, easy chemical modification, long – term storage without a decrease in catalytic activity, and the possibility to recover the enzyme after reaction. All these properties make them promising candidates as non – biological recognition elements in electrochemical and optical biosensors [24, 25, 26, 27]. In recent years, hydrogels have gained great interest in the development of biosensors. Taking advantage of their ability to incorporate foreign substances while preserving a benign environment for biosensing events, hydrogels have been exploited as functional materials in biosensing [28, 29, 30, 31]. Their 3D porous structure implies a wide surface area of the material, allowing the loading of large amounts of recognition elements (ranging from small molecules to proteins and even cells), which remain easily accessible to substrates or analytes. Furthermore, hydrogels provide a biocompatible environment thanks to their flexible and highly water – swellable nature. Indeed, the preservation of the native structure of biomolecules is a crucial requirement for feasibility, specificity, and sensitivity in biosensing applications. DNA represents an ideal candidate for supramolecular gelation because of its reversible hybridization reaction via non – covalent interactions [32, 33]. However, the large amount of material required for their preparation makes DNA – based hydrogels expensive, and the utilization of nucleosides and their analogs as alternative starting materials becomes an effective solution [34]. Recently, the self – assembly reactions of guanosine (G) and its derivatives served as an inspirational approach for the design of functional soft materials displaying enzyme – like catalytic activity [35]. In this approach, the G – quartets (G4) formed by the self – assembly of four guanosine bases via Hoogsteen – type hydrogen bond networks produced nanofibrous G – quadruplex structures in the presence of metal ions, such as K^+ (*Figure 1*). The ability of guanosine derivatives to form stable supramolecular architectures has been widely studied by some of us [36–37]. In particular, the assembly of the G4 subunits offers unique possibilities for generating functional materials such as gels, cross – linked polymers, and synthetic ion channels [35, 36, 37, 38, 39, 40, 41]. In addition, the incorporation of hemin into G4 columnar structures gives rise to a synthetic enzyme showing peroxidase – like activity

and good biocompatibility [35, 41]. Consequently, G4 – based enzyme – like hydrogels are excellent functional materials for biosensor development.

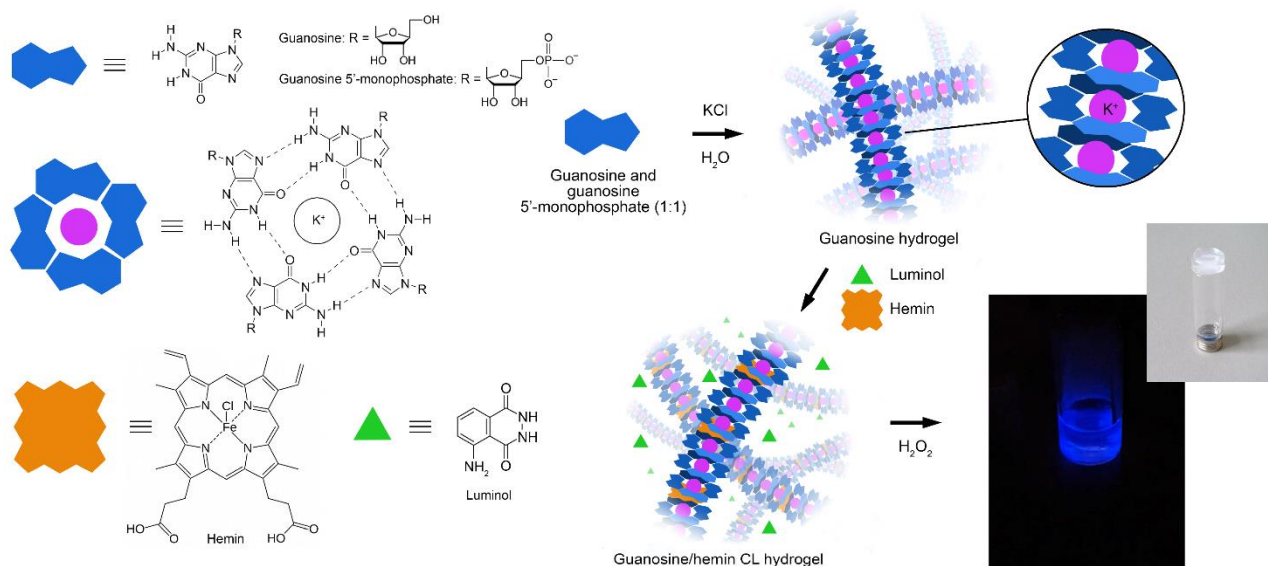


Figure 1. Scheme of the formation of the guanosine/hemin CL hydrogel, by supramolecular self – assembly of guanosine and guanosine 5'-monophosphate in the presence of K⁺, hemin, and luminol.

Herein, we propose a smartphone – based chemiluminescence (CL) biosensor for the detection of H₂O₂ and glucose. Glucose is an important source of carbon and energy and a biomarker of many diseases. Glucose monitoring in blood is of great significance in clinical practice, particularly in the diagnosis and management of diabetes. To this end, the development of improved biosensors for measuring blood glucose levels at the POC is an active research field, aiming at providing a significant improvement in the management of diabetes [42, 43, 44, 45]. In this paper, a binary guanosine hydrogel prepared using a mixture of guanosine and guanosine 5'-monophosphate in the presence of K⁺ ions [46, 47] is loaded with a CL reagent (luminol) and a catalytic cofactor (hemin), to produce a functional material showing peroxidase – like activity to the CL reaction of luminol with H₂O₂. The hydrogel is then functionalized with glucose oxidase (GOD) enzyme to enable glucose biosensing: the hydrogen peroxide produced by GOD (or, in principle, by any other oxidase enzyme) reacts, in the presence of the self – assembled guanosine/hemin gel mixture, with luminol to produce photon emission

(*Figure 1*). The biosensor takes advantage of both the features of CL detection, offering high detectability and amenability to miniaturization [15, 17, 21, 48], and of the 3D porous structure of hydrogel, as providing increased stability to incorporated enzymes [42, 49]. To provide assay POC applicability, photon emission was detected by means of a portable device employing a smartphone's CMOS (complementary metal oxide semiconductor) camera for the detection of the CL emission.

6.2 Materials and methods

6.2.1 Reagents

Hemin, luminol sodium salt, glucose oxidase (GOD) enzyme from *Aspergillus niger*, human serum albumin (HSA), glucose, glucose-6-phosphate, sucrose, galactose, trehalose, mannose, hydrogen peroxide, and guanosine 5'-monophosphate disodium salt hydrate were purchased from Merck KGaA (Darmstadt, Germany). Guanosine was purchased from TCI (Portland, OR). The following buffers, prepared in Milli – Q Plus ultra – pure water, were used in the preparation of the hydrogel and in the enzymatic assays: carbonate buffer (0.1 mol L⁻¹ carbonate buffer, pH 10.8), phosphate buffered saline (PBS, 0.01 mol L⁻¹ phosphate buffer containing 137 mmol L⁻¹ NaCl and 2.7 mmol L⁻¹ KCl, pH 7.4), Tris buffer (50 mmol L⁻¹ Tris buffer containing 100 mmol L⁻¹ NaCl and 2.7 mmol L⁻¹ KCl, pH 7.4). The single – stranded DNA (ssDNA) designed DNAzyme was obtained by mixing a ssDNA sequence (5'-TTTTGGGTGGGTGGGTGGGT-3') purchased from Integrated DNA Technologies (Coralville, IA, USA) with hemin in Tris buffer to reach a final 200 mmol L⁻¹ concentration for both species and incubating the mixture for 30 min at room temperature. The CL measurements in microplates were performed in black 96 – well microtiter plates using a Varioskan LUX microtiter plate luminometer (Thermo Scientific, Waltham, MA, USA). The enzymatic glucose colorimetric assay (Glucose Colorimetric Detection Kit) in the 96 – well microplate format used as a reference

method for assessing glucose concentration of real samples was bought from Life Technologies Corporation (Thermo Fisher Scientific, Frederick, MD, USA).

6.2.2 Preparation of the Guanosine/Hemin CL hydrogel

A binary 100 mmol L⁻¹ guanosine hydrogel was prepared by following a previously published procedure with modifications [46]. Guanosine (0.25 mmol) and guanosine 5'-monophosphate disodium salt (0.25 mmol) were added with 5 mL of 50 mM aqueous KCl in a glass tube. The vial was heated at 95 °C in a water bath for 10 min. The resulting clear solution was then left to cool down at room temperature in the dark and a transparent gel formed in 15–20 min. After 1h, the gel phase was heated again at 95 °C for 5 min, then 200 µL of hemin (100 µmol L⁻¹ in carbonate buffer) and 500 µL of luminol (10 mmol L⁻¹ in 0.1 M NaOH) were sequentially added to the hot isotropic solution [50]. The thus-obtained guanosine/hemin CL hydrogel (*Figure 1*) was stored for one night at room temperature in the dark before further use. A pH of 9.2 was detected in the final gel phase.

6.2.3 Measurement of H₂O₂ and Glucose in the Microtiter Plate Format

For the measurement of H₂O₂ in the microtiter plate format, the guanosine/hemin CL hydrogel was heated to 80 °C on a heating plate to be converted to the liquid state, then dispensed into the wells of a microplate (80 µL for each well) and allowed to cool to room temperature. To generate a H₂O₂ calibration curve, 100 µL of H₂O₂ solutions in PBS buffer at different concentrations (ranging from 0.1 µmol L⁻¹ to 1.0 mmol L⁻¹) or PBS buffer for the blank were added to each well and the CL emission was immediately measured by the microtiter plate luminometer. The emission was recorded for 1h to obtain the CL kinetic profiles for each well, then the analytical CL signals were calculated as the area under the curves. For measuring glucose, the GOD enzyme – loaded CL hydrogel was prepared as follows. The guanosine/hemin CL hydrogel was heated to about 90 °C, then, upon letting it cool down to about 60 °C, a 5 mg mL⁻¹ (500

U mL⁻¹) GOD enzyme solution in PBS was added in a hydrogel: enzyme solution in a 8:1 (v/v) ratio. Following this, the mixture was immediately dispensed into the wells of a black 96 – well microtiter plate (90 μL for each well) and allowed to cool to room temperature. The calibration curve was generated using glucose standard solutions in PBS buffer (0.1 μmol L⁻¹ – 1.0 mmol L⁻¹ concentration range) or PBS buffer as blank.

6.2.4 Smartphone – based CL detection with 3D printed device

To enable POC applicability of the hydrogel – based biosensor, a portable analytical device was developed allowing the measurement of the CL signal using a Samsung Galaxy S20 Plus smartphone (Samsung Group, Seoul, Republic of Korea). The analytical device consisted of two 3D printed components: a disposable analytical cartridge and a dark box. Both components were designed using Fusion 360 CAD software (Autodesk Inc., San Rafael, CA, USA) and produced in black resin employing a commercial Form 2 stereolithography (SLA) 3D printer (Formlabs Inc., Somerville, MA, USA). The analytical cartridge contained four wells (diameter 8 mm, volume 250 μL), thus providing a convenient portable assay format for a limited number of standard solutions and/or samples. To perform the CL measurement, the cartridge was inserted into the dark box that, after being connected to the smartphone, eliminated the interference of the ambient light in the measurement, also assuring the reproducible positioning of the analytical cartridge in front of the smartphone's CMOS camera and the correct focal distance for acquisition of CL images. To produce the analytical cartridges, the GOD enzyme – loaded CL hydrogel, prepared as described in Section 5.2.3, was dispensed into the wells of the cartridge (90 μL for each well) and allowed to cool to room temperature. Analytical cartridges could be prepared in advance, sealed in plastic bags, and stored in the dark at +4 °C for up to four weeks. To perform the measurement, the bag containing the analytical cartridge was retrieved from cold stowage and allowed to reach room temperature. Following this, the cartridge was removed from the bag and 100 μL of three glucose standard solutions in PBS (0.5 mmol L⁻¹, 1.5 mmol L⁻¹, and 2.5 mmol L⁻¹) and the sample were dispensed in the wells. The cartridge was inserted into the dark box, and after a 30 – min incubation the CL emission was measured. The CL image of

the cartridge was acquired with the following parameters: sensitivity ISO (International Organization for Standardization) 3200 and integration time 60 s. The Android Camera FV – 5 app, available on Google Play, was employed (other camera apps enabling long exposure times and automated acquisition of image sequences could be also employed).

6.2.5 Real sample analysis

The applicability of the smartphone – based biosensor for the analysis of real samples was assessed by analyzing glucose – spiked artificial serum samples. Artificial serum (containing NaCl 6.8 mg mL⁻¹, CaCl₂ 0.2 mg mL⁻¹, KCl 0.4 mg mL⁻¹, MgSO₄ 0.1 mg mL⁻¹, NaHCO₃ 2.2 mg mL⁻¹, Na₂HPO₄ 0.126 mg mL⁻¹, NaH₂PO₄ 0.026 mg mL⁻¹, and HSA 35 g L⁻¹) was prepared following a published procedure with slight modifications [51, 52] and spiked with known amounts of glucose (in the range 0.5 – 10.0 mmol L⁻¹). The samples were diluted 1:4 (v/v) with PBS buffer prior to the analysis with both the biosensing device and the reference enzymatic glucose colorimetric assay.

6.2.6 Data analysis

The freeware ImageJ software (v.1.53 h, National Institutes of Health, Bethesda, MD, USA) was employed for the quantitative analysis of the CL images. First, regions of interest (ROIs) corresponding to the well areas of the disposable cartridge of the biosensor were defined, then for each image the CL signals were evaluated by integrating the CL emissions over the ROI areas. Data graphing and analysis were performed using GraphPad Prism (version 8.0, GraphPad Software, Inc., La Jolla, CA, USA).

6.3 Results and discussion

6.3.1 Design of the G-quadruplex hydrogel – based biosensor

In this work, a self – assembled nanofibrous G4-based hydrogel was exploited for developing a smartphone – based CL biosensor for detecting H₂O₂ and glucose (through its GOD – catalyzed oxidation reaction) at the POC. The supramolecular gel

phase, exhibiting thermal reversible sol – gel transition, consisted of K^+ stabilized G – quadruplex structures [46, 53] and showed, upon hemin incorporation, peroxidase – like activity to the oxidation of luminol by H_2O_2 . Owing to its nanofibrous entangled structure, the hydrogel constituted an optimal matrix for loading enzymes, providing increased enzyme stability and catalytic activity even in highly alkaline and oxidizing conditions [49, 52]. Indeed, the alkaline pH of the hydrogel used in the biosensor (pH \sim 9) was optimal for obtaining intense CL emission by the luminol - H_2O_2 system, but it was far from the pH value providing the maximum activity of GOD from *Aspergillus niger* (pH 5.5) [54]. The ability of hydrogel to preserve enzyme activity even in an alkaline environment was very advantageous, as it enabled us to simplify the analytical protocol by carrying out all the reactions in a single compartment and at a basic pH. As previously reported, the compatibility of the different reaction environments is a common drawback encountered in the use of coupled enzyme reactions, for which, in most cases, the two enzyme – catalyzed reactions must be performed in sequence, each in its optimal milieu [17, 21]. The proposed hydrogel displayed additional positive features, such as simple, low – cost, and rapid synthesis [46], thermos – reversible gelation, environmental friendliness [50], good biocompatibility [55], and inertness towards the analyte and the reagents. In addition, it was highly transparent in the visible range [50] and permeable to hydrogen peroxide and glucose by diffusion, thus providing a uniform and reproducible light emission in the whole hydrogel volume.

6.3.2 G-quadruplex hydrogel performance for H_2O_2 quantitative detection

To ensure the optimal analytical conditions, the CL response of the hydrogel in the presence of different concentrations of H_2O_2 (from $0.5 \mu\text{mol L}^{-1}$ to 1.0mmol L^{-1}) was evaluated in the 96 – well microtiter plate format (*Figure 2a*). The calibration curve (*Figure 2b*) showed a CL signal increase with the amount of H_2O_2 . A good linear correlation between the CL signal and the concentration of H_2O_2 ($R^2 = 0.98$) was found in the $5 – 250 \mu\text{mol L}^{-1}$ concentration range and the limit of detection (calculated as the H_2O_2 concentration corresponding to the blank signal plus three times its standard deviation)

was $7.0 \mu\text{mol L}^{-1}$ (corresponding to 700 pmol of H_2O_2). The working range of the calibration curve appears to be adequate for distinguishing between physiological and pathological H_2O_2 levels in plasma. Indeed, while reference values are still under debate in the scientific community, a recent literature survey [56] suggested physiological ranges below $10 \mu\text{M}$ and higher levels ($30 - 50 \mu\text{M}$) in certain pathological conditions, such as inflammatory diseases. Overall, these results confirmed the enzyme – like activity of the guanosine/hemin CL hydrogel towards the oxidation of luminol by H_2O_2 .

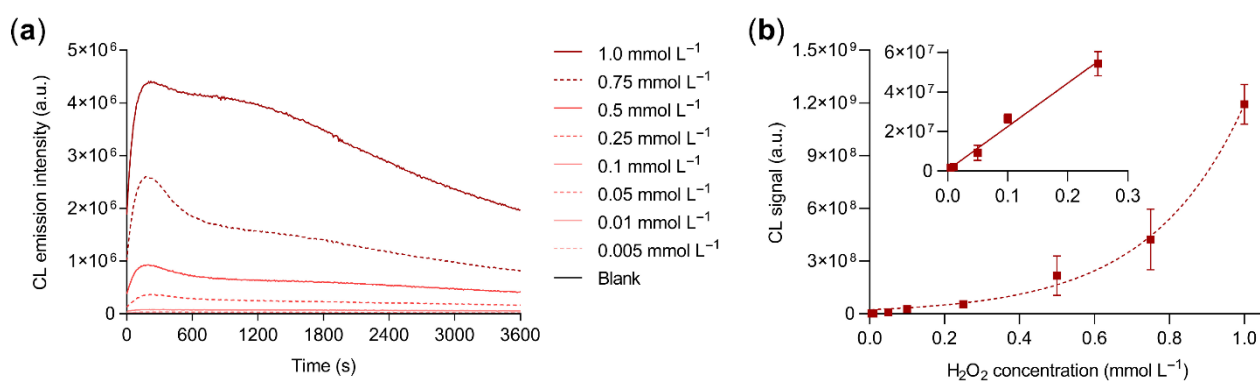


Figure 2. (a) CL kinetic profiles obtained for different concentrations of H_2O_2 ; (b) CL calibration curve for the quantification of H_2O_2 obtained from the quantitative analysis of the CL kinetic profiles. The inset of (b) shows the linear part of the calibration curve (i.e., between 5 and $250 \mu\text{mol L}^{-1}$ of H_2O_2). The equation of the linear calibration curve is $Y = (2.2 \times 10^8 \pm 4 \times 10^7)X + (6 \times 10^5 \pm 5.4 \times 10^6)$, $R^2 = 0.98$, where Y is the CL signal and X is the concentration of H_2O_2 in mmol L^{-1} . Each datum is the mean \pm SD of three independent experiments; a.u.: arbitrary units.

To further investigate the CL response of the hydrogel to H_2O_2 , we compared its CL kinetic profile to that of a ssDNA designed hemin/G – quadruplex DNAzyme. Indeed, hemin/DNA – based G – quadruplex structures prepared employing guanine – rich ssDNA sequences are widely used as peroxidase – like DNAzymes in CL biosensors [57]. As shown in *Figure 3*, upon addition of a CL cocktail containing 10 mmol L^{-1} luminol and 1.0 mmol L^{-1} H_2O_2 in carbonate buffer, the ssDNA designed DNAzyme displayed a fast photon emission kinetics, in which the CL emission reached its maximum intensity in few seconds, then decayed to background signal in about ten minutes. Therefore, the measurement of its CL emission would require automatic

sample injection, which complicates the design of a portable analytical device. Conversely, the guanosine/hemin CL hydrogel provided glow – type, long – lasting photon – emission kinetics and the maximum CL was observed several minutes after the addition of the H₂O₂ solution. The ability to stabilize the CL signal over time by means of slow diffusion – controlled penetration of H₂O₂ into the gel facilitated the design of simple and cheap smartphone – based biosensing devices. In addition, the overall photon emission observed with the guanosine/hemin CL hydrogel was at least one order of magnitude higher with respect to that of the ssDNA designed DNAzyme, when tested with the same amounts of luminol and H₂O₂, thus suggesting a higher efficiency for the luminol/H₂O₂ CL reaction. It must be also noted that an increased structural stability was expected for the guanosine – based hydrogel due to the absence of lateral loops composed of one or more nucleotides that have been reported to modify its topology upon conformational changes [58]. Deeper investigation of these aspects will be the subject of future studies.

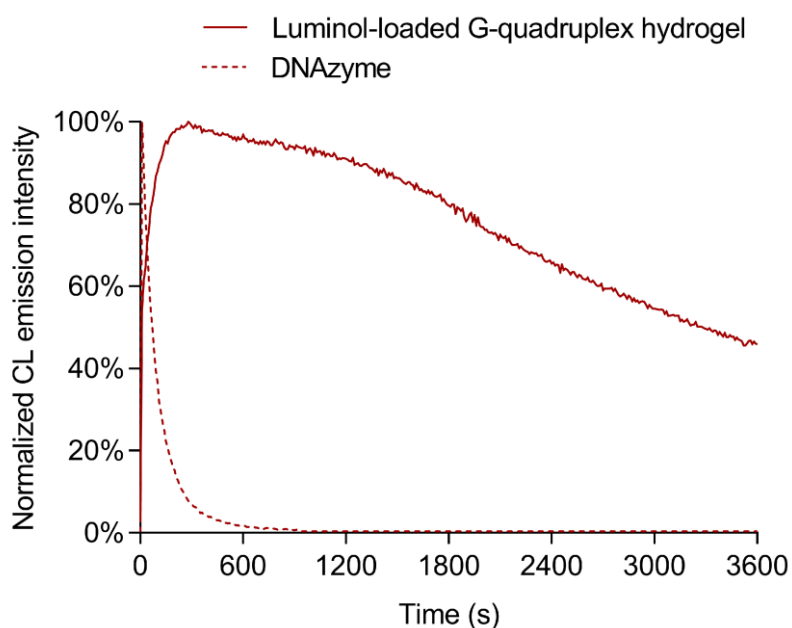


Figure 3. Comparison between the kinetic profiles of the CL emissions obtained with the luminol – loaded G – quadruplex hydrogel (upon addition of hydrogen peroxide) and a reference ssDNA designed DNAzyme (upon addition of luminol and hydrogen peroxide). To facilitate the comparison of the kinetic profiles, each profile has been normalized to its maximum intensity.

6.3.3 G-quadruplex hydrogel performance for glucose quantitative detection

The 3D porous structure of the guanosine/hemin CL hydrogel was exploited to incorporate GOD enzyme, thus enabling the quantitative detection of glucose. Upon sample addition, glucose diffuses into the hydrogel and is oxidized by the enzyme with production of H_2O_2 , which then triggers photon emission. *Figure 4a* shows the CL kinetic profiles recorded upon addition of standard glucose solutions in PBS in the range 0.1 to 5.0 mmol L^{-1} . The kinetics are slower than those obtained in the presence of H_2O_2 , which is consistent with the two-step nature of the CL production process (i.e., the intensity of CL emission now also depends on the rate of glucose oxidation to H_2O_2). A linear calibration curve was obtained over the whole calibration concentration range (*Figure 4b*) with an estimated limit of detection of $50 \mu\text{mol L}^{-1}$ (corresponding to 5 nmol of glucose).

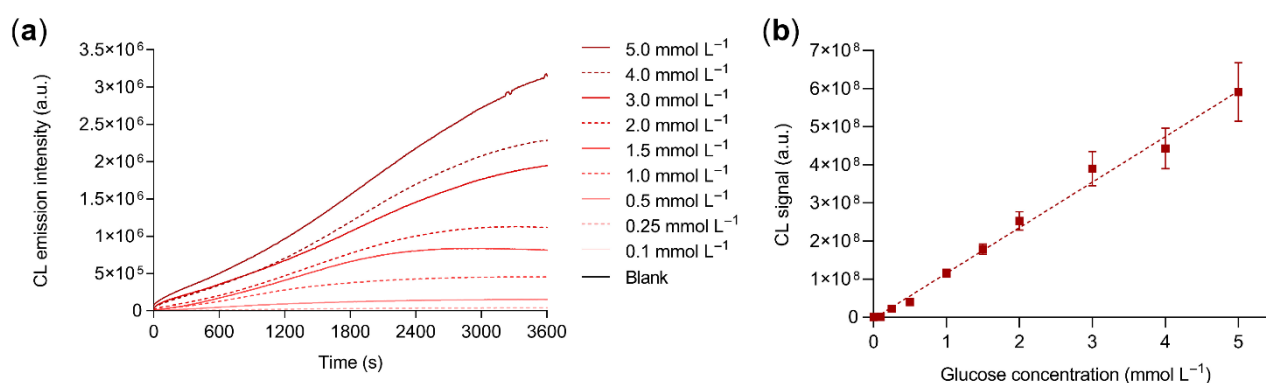


Figure 4. (a) CL kinetic profiles obtained for different concentrations of glucose and (b) calibration curve for the quantification of glucose obtained from the quantitative analysis of the CL kinetic profiles. The equation of the linear calibration curve is $Y = (1.19 \times 10^8 \pm 8 \times 10^6)X + (-4 \times 10^6 \pm 2.0 \times 10^7)$, $R^2 = 0.99$, where Y is the blank – subtracted CL signal and X is the glucose concentration in mmol L^{-1} . Each datum is the mean \pm SD of three independent experiments; a.u.: arbitrary units.

6.3.4 Smartphone – based glucose biosensing device

The hydrogel – based glucose bioassay was integrated into a portable device, taking advantage of the peculiar characteristics of CL measurements, such as high sensitivity

(i.e., high signal – to – noise ratio) and simplicity of instrumental requirements (no light sources, wavelength selection systems, specific geometry of the sample container are required). Moreover, thanks to the intense and long – lasting photon emission, the CL measurement could be successfully performed by the built – in CMOS camera of a commercial smartphone. Stereolithography (SLA) 3D printing was exploited to produce device components with a complex shape, which includes an analytical cartridge with four wells to be loaded with the GOD enzyme – loaded CL hydrogel (90 μ L per well) and a mini dark box (*Figure 5*). In the assembled device, the dark box has the role of positioning the cartridge at the correct distance from the smartphone CMOS camera and, upon being connected to the smartphone, to prevent interference from ambient light during the measurement. A critical issue in the design of smartphone – based optical biosensors is the distance between the smartphone’s built – in camera and the detection zone. Modern smartphones’ built – in camera technology enables focusing at as close as a 4 – 5 cm distance, or even less if the smartphone is equipped with a macro camera. Exploiting this feature, very compact devices can be designed without the need to add focusing lenses [17, 59]. The app used for image acquisition should also be considered, since in addition to the app provided by the producer, many others (either free or commercial) are available. The selection should be mainly based on the maximum image exposure time allowed by the software. Indeed, to acquire the weak CL emission, the sensitivity of the camera should be improved either by lengthening image exposure time, or by increasing sensor sensitivity (i.e., using higher ISO numbers) [17, 59]. Nevertheless, longer exposure time (e.g., up to 60 s) should be preferred to higher sensor sensitivity because the latter also increases the noise in the acquired CL image.

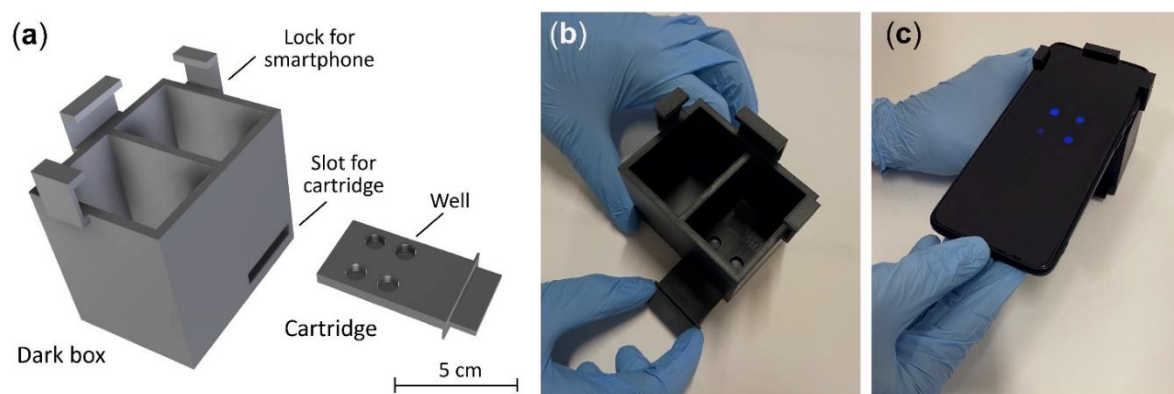


Figure 5. (a) Scheme of the 3D – printed cartridge and the dark box used for the glucose bioassay employing smartphone – based CL detection; (b,c) Images taken during the measurement of the CL emission in a cartridge containing three glucose standards and an unknown sample.

Figure 6a shows representative CL images of the wells of the analytical cartridge acquired upon addition of glucose standard solutions in PBS in the range 0.1 – 2.5 mmol L⁻¹ of glucose. The corresponding calibration curve (Figure 6b) was linear in the whole concentration range and the estimated limit of detection was 120 μmol L⁻¹ of glucose (i.e., about 2.5 times the value found in the 96 – well microtiter analytical format).

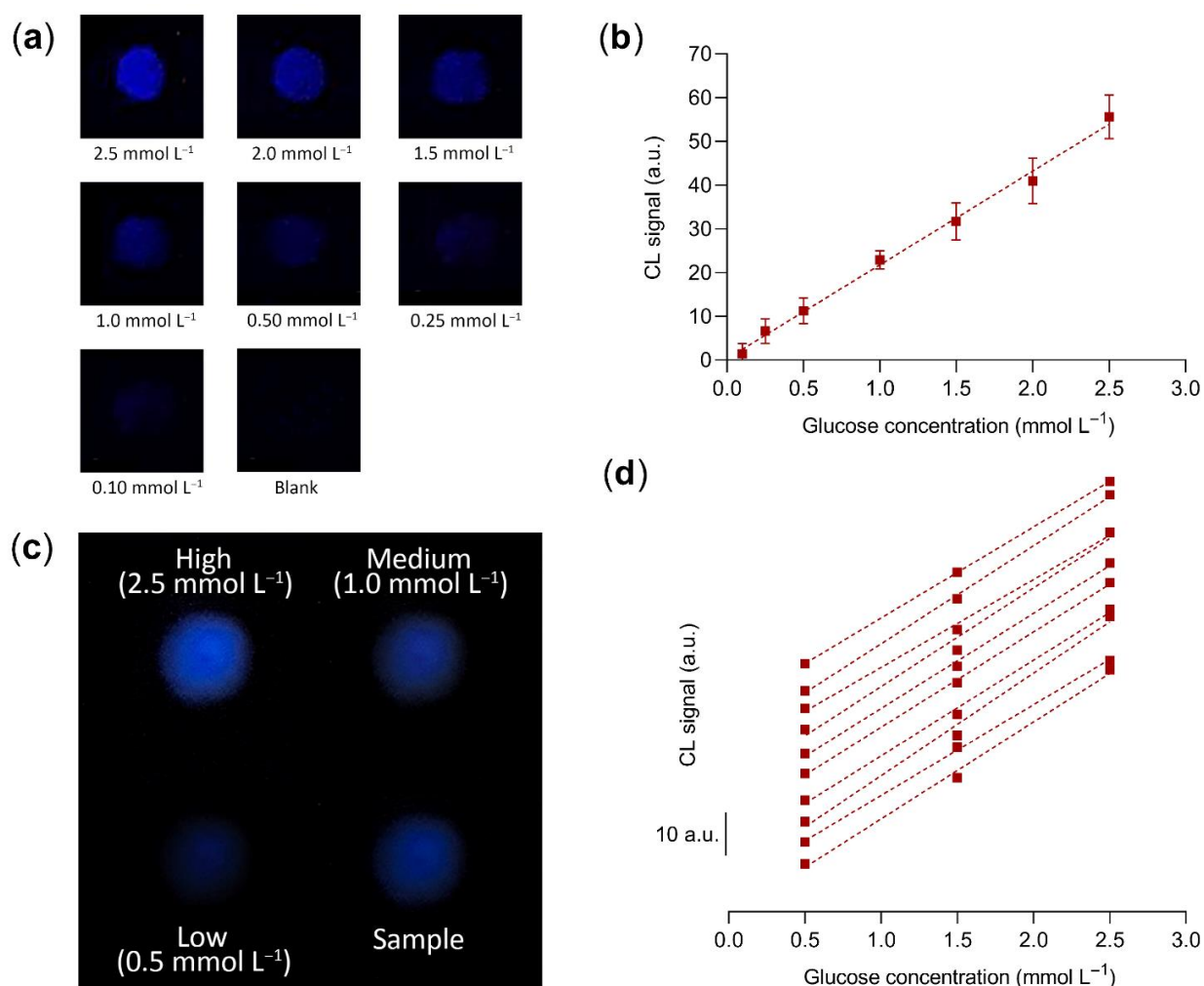


Figure 6. (a) CL images obtained for the analysis of solutions containing different concentrations of glucose using the smartphone – based assay device and (b) calibration curve for the quantification of glucose obtained from the quantitative analysis of the CL images. The equation of the linear calibration curve is $Y = (21.4 \pm 1.7)X$

+ (0.3 ± 1.4) , $R^2 = 0.99$, where Y is the blank – subtracted CL signal and X is the glucose concentration in mmol L^{-1} . Each datum is the mean \pm SD of three independent experiments. **(c)** CL image of a cartridge with the three glucose standard solutions and a sample acquired during the assay. **(d)** Set of ten three – point calibration curves for the quantification of glucose obtained from the quantitative analysis of the CL images of different cartridges (the curves have been shifted along the Y axis to avoid overlapping). The slopes of the curves were in the range 20.2–23.5 (mean value 21.8 ± 1.0), while the Y – intercepts ranged from -2.3 to 1.5 (mean value -0.3 ± 1.2); a.u.: arbitrary units.

Since the number of samples that can be analyzed in a single cartridge is limited, an analytical procedure that relies on a calibration curve obtained by analyzing several standards in replicate could be only performed using many analytical cartridges. To perform the assay in a single cartridge, we evaluated a simpler procedure that requires the analysis in the same cartridge of the sample and of three glucose standards, i.e., corresponding to low (0.5 mmol L^{-1}), intermediate (1.5 mmol L^{-1}), and high (2.5 mmol L^{-1}) glucose concentrations (a blank measurement was not performed, thus avoiding the requirement of an additional blank well in the cartridge). A three – point linear calibration curve was obtained using the standards' CL signals, then the sample's concentration of glucose was evaluated by interpolation of its CL signal on the calibration curve. To prove the feasibility of the three – standard calibration approach, we used analysis of covariance (ANCOVA) [60, 61] to compare a set of ten three – point calibration curves obtained in different cartridges (*Figure 6d*) with the calibration curve of *Figure 6b* (*Figure 6c* shows the CL image of a cartridge acquired during the assay). The comparison test showed that, for each three – point curve, both slope and intercept were not significantly different ($p > 0.05$) from those of the reference calibration curve. This demonstrated that reliable calibration curves can be generated in the analytical cartridge using a limited number of standards. In addition, as shown in Section 3.6, using the three – point calibration curve a good accuracy was obtained in the analysis of real samples.

6.3.5 Assay selectivity

The selectivity of the hydrogel – based CL glucose biosensor was verified by comparing the response to glucose to those obtained for interferents such as glucose 6-phosphate, sucrose, galactose, trehalose, and mannose (glucose and interferents were assayed at a concentration of 1.25 mmol L^{-1}). As shown in *Figure 7*, there is no significant interference by the other sugars considered. The highest cross – reactivity (with a CL signal corresponding to about 0.9% of that of glucose) was observed for galactose, while for the other interferents the CL signals were almost negligible, thus demonstrating the high specificity of the biosensor for glucose.

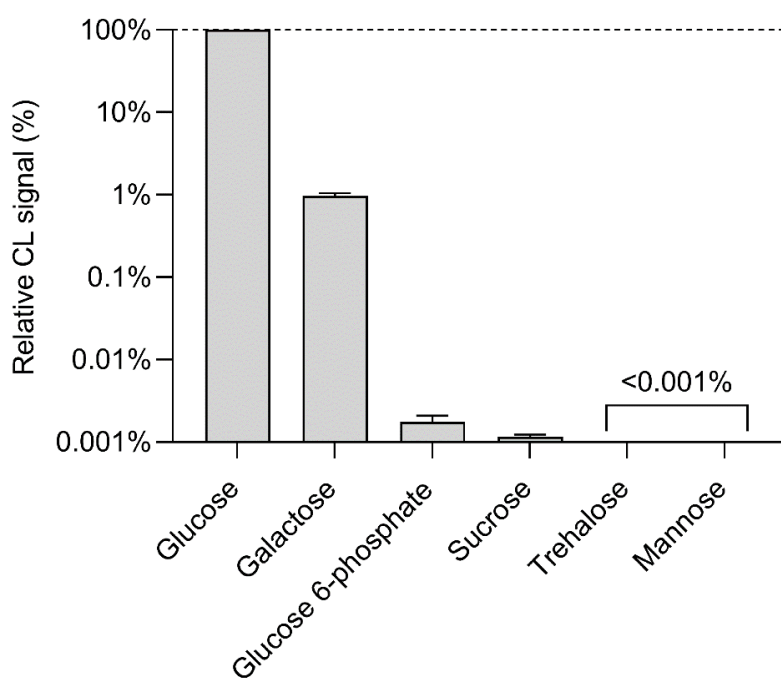


Figure 7. Comparison of the CL signals obtained by analyzing 1.25 mmol L^{-1} solutions in PBS of glucose and potentially interferent sugars (the CL signals obtained for the interferents have been normalized to that of glucose). Each datum is the mean \pm SD of three independent experiments.

6.3.6 Application to real samples

To evaluate the assay accuracy of the smartphone – based biosensor on real samples, recovery experiments were performed by analyzing artificial serum samples spiked with

known amounts of glucose. The samples, spiked with glucose concentrations ranging from 0.5 to 10.0 mmol L⁻¹, were analyzed in 1:4 (v/v) dilution with PBS to comprise the assay calibration range (in addition, the samples' dilution with PBS allowed us to reduce a possible matrix effect). The spiked concentrations were selected to comply with the physiological levels of glucose in blood, also including hypoglycemic and hyperglycemic samples (blood glucose levels in fasting healthy subjects are in the range 70 – 130 mg dL⁻¹, corresponding to 3.9 – 7.1 mmol L⁻¹ [62]). The assay results were compared to those obtained with a commercial enzymatic glucose colorimetric assay in the standard 96 – well microtiter plate format (*Table 1*). The recovery values (in the range 92 – 110%) and the good correlation observed between the results of both methods demonstrates the ability of the assay to provide accurate quantification of glucose in serum samples, either at physiological or hypo- and hyperglycemic levels.

Table 1. Glucose concentrations measured in glucose – spiked artificial serum samples using the smartphone – based glucose biosensor and the reference enzymatic glucose colorimetric assay. ¹

Glucose Concentration (mmol L ⁻¹)	Smartphone – Based CL Biosensor ²			Colorimetric Reference Method ²		
	Found (mmol L ⁻¹)	Recovery (%)	RSD (%)	Found (mmol L ⁻¹)	Recovery (%)	RSD (%)
0.5	0.55 ± 0.05	110	9.1	0.45 ± 0.10	90	22.2
3.0	3.25 ± 0.15	108	4.6	2.90 ± 0.15	97	5.2
5.0	4.80 ± 0.30	96	6.3	5.25 ± 0.40	105	7.6
6.5	6.00 ± 0.50	92	8.3	6.50 ± 0.50	100	7.7
8.0	8.20 ± 1.00	103	12.2	7.40 ± 0.65	93	8.8
10.0	10.7 ± 0.80	107	7.4	9.45 ± 0.55	95	5.8

¹ Samples were analyzed after 1:4 (v/v) dilution with PBS.

² Each datum represents the mean ± SD of three replicates.

6.3.7 Stability of the glucose biosensor

The guanosine/hemin CL hydrogel was macroscopically stable for at least one year, as confirmed by a tube – inversion test and CL emission intensity, when stored at 4 °C in

the dark and in a sealed container to avoid water evaporation. The stability of the cartridges containing the GOD enzyme – loaded CL hydrogel was evaluated by measuring the CL signal obtained upon addition of glucose standard solutions using cartridges stored for various times in sealed plastic bags at +4 °C and in the dark. The response of the biosensor was maintained for at least four weeks (i.e., after a four – week storage, the CL signal decreased not more than 10%), showing, as previously reported [52], the ability of the guanosine – based hydrogel to preserve enzyme activity.

6.3.8 Hydrogel 3D printing

Guanosine – derived hydrogels have been shown to possess good thixotropic properties [41, 55] and consequently they can be used as injectable materials [34, 41, 46, 55]. In a typical injection 3D printing experiment, the guanosine/hemin CL hydrogel (“ink”) was extruded from a medical syringe (“pen”) to write 3D – shaped patterns on a glass substrate (*Figure 8a*). Upon addition of a H₂O₂ solution, the CL emission of the 3D printed biosensor could be imaged employing a smartphone’s camera coupled with a custom dark box (*Figure 8b*). Therefore, the guanosine/hemin CL hydrogel has been demonstrated to be a promising candidate for syringe – injectable, flexible, and patternable biosensors and bioelectronics.

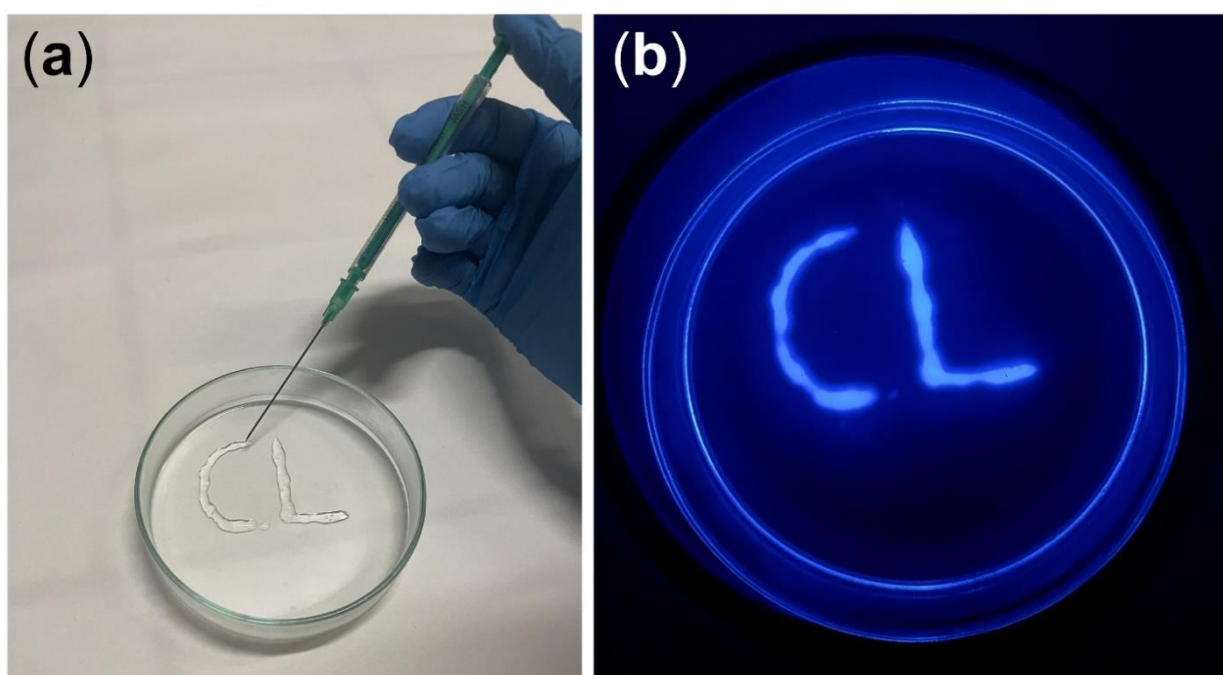


Figure 8. (a) 3D printing of the guanosine/hemin CL hydrogel with a syringe by exploiting its thixotropic property. **(b)** CL image of the 3D – printed hydrogel upon addition of H₂O₂.

6.4 Conclusions

In this work, a simple and instrument – free biosensor for glucose measurement in serum has been developed exploiting a smartphone’s CMOS camera technology. The system is ideally suited for widespread POC applicability, as it employs a ready – to – use analytical cartridge that only requires the addition of a sample. Furthermore, unlike electrochemical glucose biosensors, no electronics, power supply, or dedicated equipment is required, other than the smartphone’s built – in camera. To this end, a CL self – assembled guanosine – derived hydrogel was prepared in the presence of hemin and luminol. Thanks to its good biocompatibility, biodegradability, optical transparency, and injectability, the guanosine/hemin CL hydrogel is ideally suited for the development of biosensors based on H₂O₂ detection. Upon addition of the GOD enzyme, the hydrogel could be used as responsive biomaterial for the detection of glucose. Indeed, the sol – gel interconversion of the biomaterial allowed the encapsulation of the enzyme inside the structure of the hydrogel, enhancing its stability and catalytic activity even in non – optimal conditions (i.e., in an alkaline pH environment) and generating an intense, long – lasting CL emission, which could be conveniently detected employing a smartphone’s built – in CMOS camera. An analytical cartridge and a mini dark box produced by 3D printing technology provided an easy – to – use, rapid, and sensitive analytical device that can be applied at the POC for the measurement of glucose serum levels. The analysis of glucose – spiked artificial serum samples demonstrated the selectivity and accuracy of the biosensor, which allowed measurement of both hyper- and hypoglycemic samples. This approach could be applied to other oxidases, thus enabling the development of other specific bioassays to quantify several biomarkers of clinical interest, such as cholesterol, ethanol, cortisol, and bilirubin.

Funding

This research was funded by the Italian Ministry of University and Research: PRIN2017 project “Cutting edge analytical chemistry methodologies and bio – tools to boost precision medicine in hormone-related diseases”, Prot. 2017Y2PAB8; and PRIN2017 project “Development of novel DNA-based analytical platforms for the rapid, point – of – use quantification of multiple hidden allergens in food samples”, Prot. 2017YER72K; S.M. thanks the EU funding within the MUR PNRR “National Center for Gene Therapy and Drugs based on RNA Technology” (Project No. CN00000041 CN3 RNA).

References

- [1] Boselli, L.; Pomili, T.; Donati, P.; Pompa, P. P. Nanosensors for Visual Detection of Glucose in Biofluids: Are We Ready for Instrument-Free Home-Testing? *Materials* **2021**, *14* (8), 1978. <https://doi.org/10.3390/ma14081978>.
- [2] Chen, W.; Yao, Y.; Chen, T.; Shen, W.; Tang, S.; Lee, H. K. Application of Smartphone-Based Spectroscopy to Biosample Analysis: A Review. *Biosensors and Bioelectronics* **2021**, *172*, 112788. <https://doi.org/10.1016/j.bios.2020.112788>.
- [3] Hernández-Neuta, I.; Neumann, F.; Brightmeyer, J.; Ba Tis, T.; Madaboosi, N.; Wei, Q.; Ozcan, A.; Nilsson, M. Smartphone-Based Clinical Diagnostics: Towards Democratization of Evidence-Based Health Care. *Journal of Internal Medicine* **2019**, *285* (1), 19–39. <https://doi.org/10.1111/joim.12820>.
- [4] Pravda, J. Hydrogen Peroxide and Disease: Towards a Unified System of Pathogenesis and Therapeutics. *Molecular Medicine* **2020**, *26* (1), 41. <https://doi.org/10.1186/s10020-020-00165-3>.
- [5] Lennicke, C.; Rahn, J.; Lichtenfels, R.; Wessjohann, L. A.; Seliger, B. Hydrogen Peroxide – Production, Fate and Role in Redox Signaling of Tumor Cells. *Cell Communication and Signaling* **2015**, *13* (1), 39. <https://doi.org/10.1186/s12964-015-0118-6>.
- [6] Giorgio, M.; Trinei, M.; Migliaccio, E.; Pelicci, P. G. Hydrogen Peroxide: A Metabolic by-Product or a Common Mediator of Ageing Signals? *Nat Rev Mol Cell Biol* **2007**, *8* (9), 722–728. <https://doi.org/10.1038/nrm2240>.
- [7] Miller, E. W.; Dickinson, B. C.; Chang, C. J. Aquaporin-3 Mediates Hydrogen Peroxide Uptake to Regulate Downstream Intracellular Signaling. *Proceedings of the National Academy of Sciences* **2010**, *107* (36), 15681–15686. <https://doi.org/10.1073/pnas.1005776107>.
- [8] Sies, H. Hydrogen Peroxide as a Central Redox Signaling Molecule in Physiological Oxidative Stress: Oxidative Eustress. *Redox Biology* **2017**, *11*, 613–619. <https://doi.org/10.1016/j.redox.2016.12.035>.

- [9] Pi, J.; Bai, Y.; Zhang, Q.; Wong, V.; Floering, L. M.; Daniel, K.; Reece, J. M.; Deeney, J. T.; Andersen, M. E.; Corkey, B. E.; Collins, S. Reactive Oxygen Species as a Signal in Glucose-Stimulated Insulin Secretion. *Diabetes* **2007**, *56* (7), 1783–1791. <https://doi.org/10.2337/db06-1601>.
- [10] Liou, G.-Y.; Storz, P. Reactive Oxygen Species in Cancer. *Free Radical Research* **2010**, *44* (5), 479–496. <https://doi.org/10.3109/10715761003667554>.
- [11] Barnham, K. J.; Masters, C. L.; Bush, A. I. Neurodegenerative Diseases and Oxidative Stress. *Nat Rev Drug Discov* **2004**, *3* (3), 205–214. <https://doi.org/10.1038/nrd1330>.
- [12] Patel, V.; Kruse, P.; Selvaganapathy, P. R. Solid State Sensors for Hydrogen Peroxide Detection. *Biosensors* **2021**, *11* (1), 9. <https://doi.org/10.3390/bios11010009>.
- [13] Chen, S.; Yuan, R.; Chai, Y.; Hu, F. Electrochemical Sensing of Hydrogen Peroxide Using Metal Nanoparticles: A Review. *Microchim Acta* **2013**, *180* (1), 15–32. <https://doi.org/10.1007/s00604-012-0904-4>.
- [14] Meier, J.; M Hofferber, E.; A Stapleton, J.; M Iverson, N. Hydrogen Peroxide Sensors for Biomedical Applications. *Chemosensors* **2019**, *7* (4), 64. <https://doi.org/10.3390/chemosensors7040064>.
- [15] Roda, A.; Arduini, F.; Mirasoli, M.; Zangheri, M.; Fabiani, L.; Colozza, N.; Marchegiani, E.; Simoni, P.; Moscone, D. A Challenge in Biosensors: Is It Better to Measure a Photon or an Electron for Ultrasensitive Detection? *Biosensors and Bioelectronics* **2020**, *155*, 112093. <https://doi.org/10.1016/j.bios.2020.112093>.
- [16] Calabria, D.; Guardigli, M.; Mirasoli, M.; Punzo, A.; Porru, E.; Zangheri, M.; Simoni, P.; Pagnotta, E.; Ugolini, L.; Lazzeri, L.; Caliceti, C.; Roda, A. Selective Chemiluminescent TURN-ON Quantitative Bioassay and Imaging of Intracellular Hydrogen Peroxide in Human Living Cells. *Analytical Biochemistry* **2020**, *600*, 113760. <https://doi.org/10.1016/j.ab.2020.113760>.
- [17] Calabria, D.; Zangheri, M.; Trozzi, I.; Lazzarini, E.; Pace, A.; Mirasoli, M.; Guardigli, M. Smartphone-Based Chemiluminescent Origami μ PAD for the Rapid

- Assessment of Glucose Blood Levels. *Biosensors* **2021**, *11* (10), 381. <https://doi.org/10.3390/bios11100381>.
- [18] Giaretta, J. E.; Duan, H.; Oveissi, F.; Farajikhah, S.; Dehghani, F.; Naficy, S. Flexible Sensors for Hydrogen Peroxide Detection: A Critical Review. *ACS Appl. Mater. Interfaces* **2022**, *14* (18), 20491–20505. <https://doi.org/10.1021/acsami.1c24727>.
- [19] Gupta, U.; Gupta, V.; Arun, R. K.; Chanda, N. Recent Advances in Enzymatic Biosensors for Point-of-Care Detection of Biomolecules. *Biotechnology and Bioengineering* **2022**, *119* (12), 3393–3407. <https://doi.org/10.1002/bit.28251>.
- [20] Yu, Y.; Pan, M.; Peng, J.; Hu, D.; Hao, Y.; Qian, Z. A Review on Recent Advances in Hydrogen Peroxide Electrochemical Sensors for Applications in Cell Detection. *Chinese Chemical Letters* **2022**, *33* (9), 4133–4145. <https://doi.org/10.1016/j.ccllet.2022.02.045>.
- [21] Calabria, D.; Trozzi, I.; Lazzarini, E.; Pace, A.; Zangheri, M.; Iannascoli, L.; Maipan Davis, N.; Gosikere Matadha, S. S.; Baratto De Albuquerque, T.; Pirrotta, S.; Del Bianco, M.; Impresario, G.; Popova, L.; Lovecchio, N.; de Cesare, G.; Caputo, D.; Brucato, J.; Nascetti, A.; Guardigli, M.; Mirasoli, M. AstroBio-CubeSat: A Lab-in-Space for Chemiluminescence-Based Astrobiology Experiments. *Biosensors and Bioelectronics* **2023**, *226*, 115110. <https://doi.org/10.1016/j.bios.2023.115110>.
- [22] Neumann, B.; Wollenberger, U. Electrochemical Biosensors Employing Natural and Artificial Heme Peroxidases on Semiconductors. *Sensors* **2020**, *20* (13), 3692. <https://doi.org/10.3390/s20133692>.
- [23] Gao, Y.; Wang, Y.; Wang, Y.; Magaud, P.; Liu, Y.; Zeng, F.; Yang, J.; Baldas, L.; Song, Y. Nanocatalysis Meets Microfluidics: A Powerful Platform for Sensitive Bioanalysis. *TrAC Trends in Analytical Chemistry* **2023**, *158*, 116887. <https://doi.org/10.1016/j.trac.2022.116887>.
- [24] Tummala, S.; Bandi, R.; Ho, Y.-P. Synthesis of Cu-Doped Carbon Dot/Chitosan Film Composite as a Catalyst for the Colorimetric Detection of Hydrogen

- Peroxide and Glucose. *Microchim Acta* **2022**, *189* (8), 284. <https://doi.org/10.1007/s00604-022-05386-3>.
- [25] Huang, W.; Xu, Y.; Wang, Z.; Liao, K.; Zhang, Y.; Sun, Y. Dual Nanozyme Based on Ultrathin 2D Conductive MOF Nanosheets Intergraded with Gold Nanoparticles for Electrochemical Biosensing of H₂O₂ in Cancer Cells. *Talanta* **2022**, *249*, 123612. <https://doi.org/10.1016/j.talanta.2022.123612>.
- [26] Wang, M.; Zhang, J.; Zhou, X.; Sun, H.; Su, X. Fluorescence Sensing Strategy for Xanthine Assay Based on Gold Nanoclusters and Nanozyme. *Sensors and Actuators B: Chemical* **2022**, *358*, 131488. <https://doi.org/10.1016/j.snb.2022.131488>.
- [27] Smutok, O.; Kavetsky, T.; Prokopiv, T.; Serkiz, R.; Šauša, O.; Novák, I.; Švajdlenková, H.; Mat'ko, I.; Gonchar, M.; Katz, E. Biosensor Based on Peroxidase-Mimetic Nanozyme and Lactate Oxidase for Accurate L-Lactate Analysis in Beverages. *Biosensors* **2022**, *12* (11), 1042. <https://doi.org/10.3390/bios12111042>.
- [28] Herrmann, A.; Haag, R.; Schedler, U. Hydrogels and Their Role in Biosensing Applications. *Advanced Healthcare Materials* **2021**, *10* (11), 2100062. <https://doi.org/10.1002/adhm.202100062>.
- [29] Völlmecke, K.; Afroz, R.; Bierbach, S.; Brenker, L. J.; Frücht, S.; Glass, A.; Giebelhaus, R.; Hoppe, A.; Kanemaru, K.; Lazarek, M.; Rabbe, L.; Song, L.; Velasco Suarez, A.; Wu, S.; Serpe, M.; Kuckling, D. Hydrogel-Based Biosensors. *Gels* **2022**, *8* (12), 768. <https://doi.org/10.3390/gels8120768>.
- [30] Calabria, D.; Guardigli, M.; Severi, P.; Trozzi, I.; Pace, A.; Cinti, S.; Zangheri, M.; Mirasoli, M. A Smartphone-Based Chemosensor to Evaluate Antioxidants in Agri-Food Matrices by In Situ AuNP Formation. *Sensors* **2021**, *21* (16), 5432. <https://doi.org/10.3390/s21165432>.
- [31] Shafique, H.; de Vries, J.; Strauss, J.; Khorrami Jahromi, A.; Siavash Moakhar, R.; Mahshid, S. Advances in the Translation of Electrochemical Hydrogel-Based Sensors. *Advanced Healthcare Materials* **2023**, *12* (1), 2201501. <https://doi.org/10.1002/adhm.202201501>.

- [32] Gačanin, J.; Synatschke, C. V.; Weil, T. Biomedical Applications of DNA-Based Hydrogels. *Advanced Functional Materials* **2020**, *30* (4), 1906253. <https://doi.org/10.1002/adfm.201906253>.
- [33] Wang, D.; Duan, J.; Liu, J.; Yi, H.; Zhang, Z.; Song, H.; Li, Y.; Zhang, K. Stimuli-Responsive Self-Degradable DNA Hydrogels: Design, Synthesis, and Applications. *Advanced Healthcare Materials* **2023**, *12* (16), 2203031. <https://doi.org/10.1002/adhm.202203031>.
- [34] Zhang, J.; Lu, N.; Peng, H.; Li, J.; Yan, R.; Shi, X.; Ma, P.; Lv, M.; Wang, L.; Tang, Z.; Zhang, M. Multi-Triggered and Enzyme-Mimicking Graphene Oxide/Polyvinyl Alcohol/G-Quartet Supramolecular Hydrogels. *Nanoscale* **2020**, *12* (8), 5186–5195. <https://doi.org/10.1039/C9NR10779G>.
- [35] Bhattacharyya, T.; Kumar, Y. P.; Dash, J. Supramolecular Hydrogel Inspired from DNA Structures Mimics Peroxidase Activity. *ACS Biomater. Sci. Eng.* **2017**, *3* (10), 2358–2365. <https://doi.org/10.1021/acsbio.7b00563>.
- [36] Lena, S.; Masiero, S.; Pieraccini, S.; Spada, G. P. Guanosine Hydrogen-Bonded Scaffolds: A New Way to Control the Bottom-Up Realisation of Well-Defined Nanoarchitectures. *Chemistry – A European Journal* **2009**, *15* (32), 7792–7806. <https://doi.org/10.1002/chem.200802506>.
- [37] Pieraccini, S.; Campitiello, M.; Carducci, F.; T. Davis, J.; Mariani, P.; Masiero, S. Playing Supramolecular Dominoes with Light: Building and Breaking a Photoreversible G-Quadruplex Made from Guanosine, Boric Acid and an Azobenzene. *Organic & Biomolecular Chemistry* **2019**, *17* (10), 2759–2769. <https://doi.org/10.1039/C9OB00193J>.
- [38] Peters, G. M.; Skala, L. P.; Plank, T. N.; Hyman, B. J.; Manjunatha Reddy, G. N.; Marsh, A.; Brown, S. P.; Davis, J. T. A G4·K⁺ Hydrogel Stabilized by an Anion. *J. Am. Chem. Soc.* **2014**, *136* (36), 12596–12599. <https://doi.org/10.1021/ja507506c>.
- [39] Peters, G. M.; Skala, L. P.; Plank, T. N.; Oh, H.; Manjunatha Reddy, G. N.; Marsh, A.; Brown, S. P.; Raghavan, S. R.; Davis, J. T. G4-Quartet·M⁺ Borate Hydrogels. *J. Am. Chem. Soc.* **2015**, *137* (17), 5819–5827. <https://doi.org/10.1021/jacs.5b02753>.

- [40] N. Plank, T.; T. Davis, J. A G 4 ·K + Hydrogel That Self-Destructs. *Chemical Communications* **2016**, 52 (28), 5037–5040. <https://doi.org/10.1039/C6CC01494A>.
- [41] Zhong, R.; Tang, Q.; Wang, S.; Zhang, H.; Zhang, F.; Xiao, M.; Man, T.; Qu, X.; Li, L.; Zhang, W.; Pei, H. Self-Assembly of Enzyme-Like Nanofibrous G-Molecular Hydrogel for Printed Flexible Electrochemical Sensors. *Advanced Materials* **2018**, 30 (12), 1706887. <https://doi.org/10.1002/adma.201706887>.
- [42] Hassan, M. H.; Vyas, C.; Grieve, B.; Bartolo, P. Recent Advances in Enzymatic and Non-Enzymatic Electrochemical Glucose Sensing. *Sensors* **2021**, 21 (14), 4672. <https://doi.org/10.3390/s21144672>.
- [43] Adeel, M.; Rahman, Md. M.; Caligiuri, I.; Canzonieri, V.; Rizzolio, F.; Daniele, S. Recent Advances of Electrochemical and Optical Enzyme-Free Glucose Sensors Operating at Physiological Conditions. *Biosensors and Bioelectronics* **2020**, 165, 112331. <https://doi.org/10.1016/j.bios.2020.112331>.
- [44] Hwang, D.-W.; Lee, S.; Seo, M.; Chung, T. D. Recent Advances in Electrochemical Non-Enzymatic Glucose Sensors – A Review. *Analytica Chimica Acta* **2018**, 1033, 1–34. <https://doi.org/10.1016/j.aca.2018.05.051>.
- [45] Chen, Q.; Zhao, Y.; Liu, Y. Current Development in Wearable Glucose Meters. *Chinese Chemical Letters* **2021**, 32 (12), 3705–3717. <https://doi.org/10.1016/j.ccllet.2021.05.043>.
- [46] Yoneda, J. S.; de Araujo, D. R.; Sella, F.; Liguori, G. R.; Liguori, T. T. A.; Moreira, L. F. P.; Spinozzi, F.; Mariani, P.; Itri, R. Self-Assembled Guanosine-Hydrogels for Drug-Delivery Application: Structural and Mechanical Characterization, Methylene Blue Loading and Controlled Release. *Materials Science and Engineering: C* **2021**, 121, 111834. <https://doi.org/10.1016/j.msec.2020.111834>.
- [47] Yu, Y.; Nakamura, D.; DeBoyace, K.; Neisius, A. W.; McGown, L. B. Tunable Thermoassociation of Binary Guanosine Gels. *J. Phys. Chem. B* **2008**, 112 (4), 1130–1134. <https://doi.org/10.1021/jp709613p>.
- [48] Zangheri, M.; Di Nardo, F.; Calabria, D.; Marchegiani, E.; Anfossi, L.; Guardigli, M.; Mirasoli, M.; Baggiani, C.; Roda, A. Smartphone Biosensor for Point-of-Need

- Chemiluminescence Detection of Ochratoxin A in Wine and Coffee. *Analytica Chimica Acta* **2021**, *1163*, 338515. <https://doi.org/10.1016/j.aca.2021.338515>.
- [49] Pierre, A. C. The Sol-Gel Encapsulation of Enzymes. *Biocatalysis and Biotransformation* **2004**, *22* (3), 145–170. <https://doi.org/10.1080/10242420412331283314>.
- [50] Ye, J.; Zhu, L.; Yan, M.; Xiao, T.; Fan, L.; Xue, Y.; Huang, J.; Yang, X. An Intensive and Glow-Type Chemiluminescence of Luminol-Embedded, Guanosine-Derived Hydrogel. *Talanta* **2021**, *230*, 122351. <https://doi.org/10.1016/j.talanta.2021.122351>.
- [51] Basiaga, M.; Paszenda, Z.; Walke, W.; Karasiński, P.; Marciniak, J. Electrochemical Impedance Spectroscopy and Corrosion Resistance of SiO₂ Coated CpTi and Ti-6Al-7Nb Alloy. In *Information Technologies in Biomedicine, Volume 4*; Piętka, E., Kawa, J., Wieclawek, W., Eds.; Advances in Intelligent Systems and Computing; Springer International Publishing: Cham, 2014; pp 411–420. https://doi.org/10.1007/978-3-319-06596-0_39.
- [52] Calabria, D.; Lazzarini, E.; Pace, A.; Trozzi, I.; Zangheri, M.; Cinti, S.; Difonzo, M.; Valenti, G.; Guardigli, M.; Paolucci, F.; Mirasoli, M. Smartphone-Based 3D-Printed Electrochemiluminescence Enzyme Biosensor for Reagentless Glucose Quantification in Real Matrices. *Biosensors and Bioelectronics* **2023**, *227*, 115146. <https://doi.org/10.1016/j.bios.2023.115146>.
- [53] Baldassarri, E. J.; Ortore, M. G.; Spinozzi, F.; Round, A.; Ferrero, C.; Mariani, P. K⁺ vs. Na⁺ Effects on the Self-Assembly of Guanosine 5'-Monophosphate: A Solution SAXS Structural Study. *Nanomaterials* **2020**, *10* (4), 629. <https://doi.org/10.3390/nano10040629>.
- [54] Weibel, M. K.; Bright, H. J. The Glucose Oxidase Mechanism: Interpretation of the pH Dependence. *Journal of Biological Chemistry* **1971**, *246* (9), 2734–2744. [https://doi.org/10.1016/S0021-9258\(18\)62246-X](https://doi.org/10.1016/S0021-9258(18)62246-X).
- [55] Ghosh, T.; Biswas, A.; Gavel, P. K.; Das, A. K. Engineered Dynamic Boronate Ester-Mediated Self-Healable Biocompatible G-Quadruplex Hydrogels for

- Sustained Release of Vitamins. *Langmuir* **2020**, *36* (6), 1574–1584. <https://doi.org/10.1021/acs.langmuir.9b03837>.
- [56] Forman, H. J.; Bernardo, A.; Davies, K. J. A. What Is the Concentration of Hydrogen Peroxide in Blood and Plasma? *Archives of Biochemistry and Biophysics* **2016**, *603*, 48–53. <https://doi.org/10.1016/j.abb.2016.05.005>.
- [57] Guan, Y.; Ma, J.; Neng, J.; Yang, B.; Wang, Y.; Xing, F. A Novel and Label-Free Chemiluminescence Detection of Zearalenone Based on a Truncated Aptamer Conjugated with a G-Quadruplex DNzyme. *Biosensors* **2023**, *13* (1), 118. <https://doi.org/10.3390/bios13010118>.
- [58] Cheng, M.; Cheng, Y.; Hao, J.; Jia, G.; Zhou, J.; Mergny, J.-L.; Li, C. Loop Permutation Affects the Topology and Stability of G-Quadruplexes. *Nucleic Acids Research* **2018**, *46* (18), 9264–9275. <https://doi.org/10.1093/nar/gky757>.
- [59] Calabria, D.; Mirasoli, M.; Guardigli, M.; Simoni, P.; Zangheri, M.; Severi, P.; Caliceti, C.; Roda, A. Paper-Based Smartphone Chemosensor for Reflectometric on-Site Total Polyphenols Quantification in Olive Oil. *Sensors and Actuators B: Chemical* **2020**, *305*, 127522. <https://doi.org/10.1016/j.snb.2019.127522>.
- [60] McDonald, J. H. *Handbook of Biological Statistics*, 3rd ed.; Sparky House Publishing: Baltimore, MA, USA, 2014.
- [61] Snedecor, G. W.; Cochran, W. G. *Statistical Methods*, 8th ed.; Iowa State University Press: Ames, IA, USA, 1989.
- [62] Danaei, G.; Finucane, M. M.; Lu, Y.; Singh, G. M.; Cowan, M. J.; Paciorek, C. J.; Lin, J. K.; Farzadfar, F.; Khang, Y.-H.; Stevens, G. A.; Rao, M.; Ali, M. K.; Riley, L. M.; Robinson, C. A.; Ezzati, M. National, Regional, and Global Trends in Fasting Plasma Glucose and Diabetes Prevalence since 1980: Systematic Analysis of Health Examination Surveys and Epidemiological Studies with 370 Country-Years and 2.7 Million Participants. *The Lancet* **2011**, *378* (9785), 31–40. [https://doi.org/10.1016/S0140-6736\(11\)60679-X](https://doi.org/10.1016/S0140-6736(11)60679-X).

Conclusions and future perspectives

In an effort to advance knowledge in the field of biosensors, this doctoral research has delved deep into the intricacies of immunosensors and enzyme – based biosensors. These remarkable analytical tools have shown tremendous potential in various applications, ranging from clinical diagnostics to food monitoring. Indeed, the research in the field of biosensors requires an interdisciplinary approach, in which chemists, engineers, biologists and physicists work together to tackle important problems [1]. Since the 1980s, the remarkable achievements in biosensing, exemplified by the development of glucose sensors and lateral flow devices such as pregnancy test kits, led to a shift in research focus towards the development of portable devices for non-specialist use [2]. Through a comprehensive exploration of the principles, development strategies, and practical implementations, this thesis has aimed to contribute to the ever-evolving landscape of biosensor technology. Primarily, it has provided a comprehensive overview of immunosensors and enzyme-based biosensors, elucidating their underlying mechanisms and highlighting their strengths and limitations. In addition, this research has focused on the design and optimisation of new biosensing devices. The development of novel sensing platforms, the integration of advanced materials such as paper and hydrogel, and exploration of cutting-edge signal transduction techniques (i.e. chemiluminescence) have been key to improving the sensitivity, selectivity, and overall performance of the developed devices. The insights gained from these endeavors

contribute to the ongoing efforts to improve the capabilities of biosensors for real – world applications.

Despite the many steps forward in this field, there are still many avenues for future research. The ever-evolving landscape of nanotechnology, materials science, and biotechnology opens up exciting opportunities to further enhance the performance of biosensors [3, 4]. Moreover, the integration of biosensors into emerging fields such as the Internet of Things (IoT) [5] and wearable technology [6] offers new opportunities for real – time, continuous monitoring in various applications. In addition, the translation of biosensor technologies from the laboratory to the market requires overcoming practical challenges related to miniaturisation, reproducibility, and cost-effectiveness [7, 8]. Future research should focus on bridging this gap to ensure that promising innovations get into the hands of end users and have a meaningful impact on society. As we move forward, let us remember that biosensors are not just scientific tools but instruments of progress and positive change for a healthier, safer, and more sustainable future.

References

- [1] Bollella, P.; Katz, E. Biosensors—Recent Advances and Future Challenges. *Sensors* **2020**, *20* (22), 6645. <https://doi.org/10.3390/s20226645>.
- [2] Wu, Y.; Tilley, R. D.; Gooding, J. J. Challenges and Solutions in Developing Ultrasensitive Biosensors. *J. Am. Chem. Soc.* **2019**, *141* (3), 1162–1170. <https://doi.org/10.1021/jacs.8b09397>.
- [3] Zhang, X.; Guo, Q.; Cui, D. Recent Advances in Nanotechnology Applied to Biosensors. *Sensors* **2009**, *9* (2), 1033–1053. <https://doi.org/10.3390/s90201033>.
- [4] Jianrong, C.; Yuqing, M.; Nongyue, H.; Xiaohua, W.; Sijiao, L. Nanotechnology and Biosensors. *Biotechnology Advances* **2004**, *22* (7), 505–518. <https://doi.org/10.1016/j.biotechadv.2004.03.004>.
- [5] Pateraki, M.; Fysarakis, K.; Sakkalis, V.; Spanoudakis, G.; Varlamis, I.; Maniadakis, M.; Lourakis, M.; Ioannidis, S.; Cummins, N.; Schuller, B.; Loutsetis, E.; Koutsouris, D. Biosensors and Internet of Things in Smart Healthcare Applications: Challenges and Opportunities. In *Wearable and Implantable Medical Devices*; Dey, N., Ashour, A. S., James Fong, S., Bhatt, C., Eds.; Advances in ubiquitous sensing applications for healthcare; Academic Press, 2020; Vol. 7, pp 25–53. <https://doi.org/10.1016/B978-0-12-815369-7.00002-1>.
- [6] Kim, J.; Campbell, A. S.; de Ávila, B. E.-F.; Wang, J. Wearable Biosensors for Healthcare Monitoring. *Nat Biotechnol* **2019**, *37* (4), 389–406. <https://doi.org/10.1038/s41587-019-0045-y>.
- [7] Luong, J. H. T.; Male, K. B.; Glennon, J. D. Biosensor Technology: Technology Push versus Market Pull. *Biotechnology Advances* **2008**, *26* (5), 492–500. <https://doi.org/10.1016/j.biotechadv.2008.05.007>.
- [8] Vashist, S. K.; Venkatesh, A. G.; Mitsakakis, K.; Czilwik, G.; Roth, G.; von Stetten, F.; Zengerle, R. Nanotechnology-Based Biosensors and Diagnostics: Technology Push versus Industrial/Healthcare Requirements. *BioNanoSci.* **2012**, *2* (3), 115–126. <https://doi.org/10.1007/s12668-012-0047-4>.